

Spring 5-15-2019

Development of Novel Tumor-Targeted Compounds for Boron Neutron Capture Therapy

Micah John Luderer

Washington University in St. Louis

Follow this and additional works at: https://openscholarship.wustl.edu/art_sci_etds



Part of the [Cell Biology Commons](#), and the [Chemistry Commons](#)

Recommended Citation

Luderer, Micah John, "Development of Novel Tumor-Targeted Compounds for Boron Neutron Capture Therapy" (2019). *Arts & Sciences Electronic Theses and Dissertations*. 1782.

https://openscholarship.wustl.edu/art_sci_etds/1782

This Dissertation is brought to you for free and open access by the Arts & Sciences at Washington University Open Scholarship. It has been accepted for inclusion in Arts & Sciences Electronic Theses and Dissertations by an authorized administrator of Washington University Open Scholarship. For more information, please contact digital@wumail.wustl.edu.

WASHINGTON UNIVERSITY IN ST. LOUIS

Division of Biology and Biomedical Sciences
Molecular Cell Biology

Dissertation Examination Committee:

Abdel Kareem Azab, Chair

Hong Chen

Dennis Hallahan

Buck Rogers

Joshua Rubin

Monica Shokeen

Development of Novel Tumor-Targeted Compounds for Boron Neutron Capture Therapy

by

Micah John Luderer

A dissertation presented to
The Graduate School
of Washington University in
partial fulfillment of the
requirements for the degree
of Doctor of Philosophy

May 2019

St. Louis, Missouri

© 2019, Micah John Luderer

Table of Contents

List of Figures	v
List of Tables	vii
List of Abbreviations	viii
Acknowledgments	x
Abstract	xii
Chapter 1: Introduction to Neutron Capture Therapy	1
1.1 Mechanism of Boron Neutron Capture Therapy	1
1.2 Alternative Isotopes for Neutron Capture Therapy	3
1.3 Neutron Beam Sources: from Nuclear Reactor to Linear Accelerator	4
1.4 Early BNCT Clinical Trials	6
1.5 Current BNCT Agents: BPA and BSH	7
1.5.1 Boronophenylalanine (BPA).....	8
1.5.2 Sodium borocaptate (BSH)	10
1.5.3 Techniques to Improve BPA and BSH Uptake in Cancer Cells	10
1.6 Development of Novel BNCT Agents	12
1.6.1 Nucleoside and Carbohydrate Analogs.....	13
1.6.2 Unnatural Amino Acids	15
1.6.3 Porphyrins.....	16
1.6.4 Antibody-Dendrimer Conjugates.....	17
1.6.5 Cationic Polymers.....	19
1.6.6 Cell-Membrane Penetrating Peptides.....	20
1.6.7 Liposomes	21
1.6.8 Nanoparticles	24
1.7 Summary of Current BNCT Agents	26
Chapter 2: Development of a Hypoxia Targeted Agent for BNCT	27
2.1 Introduction	27
2.1.1 Background on BNCT Treatment of Glioblastoma Multiforme.....	28
2.1.2 Role of Tumor Hypoxia in Radiation and Chemotherapy Resistance	30
2.1.3 Molecular Probes of Tumor Hypoxia	34

2.2 Hypothesis – Targeting Hypoxic Microenvironment	39
2.3 Materials and Methods	40
2.3.1 Reagents and Cell Culture.....	40
2.3.2 Synthesis of Boronated 2-nitroimidazole Derivative B-381	41
2.3.3 Cell Viability Assay	41
2.3.4 HPLC Assay for Detection of B-381	42
2.3.5 Cellular uptake of B-381 in vitro	42
2.3.6 Cellular uptake of BPA in vitro	43
2.3.7 Tumor Retention of BPA and B-381 in vivo	43
2.3.8 B-381 in vivo Biodistribution	44
2.3.9 B-381 Plasma half-life	44
2.4 Results	45
2.4.1 Synthesis and characterization of boronated nitroimidazole derivative B-381.....	45
2.4.2 The effect of B-381 and BPA on viability of normoxic and hypoxic cells in vitro	46
2.4.3 Cellular uptake of B-381 and BPA in normoxic and hypoxic cells in vitro	48
2.4.4 In vitro mechanistic study of B-381 accumulation in hypoxic cells	50
2.4.5 Tumor retention, biodistribution and pharmacokinetics of B-381 in vivo.....	51
2.5 Discussion	53
2.6 Conclusions	57
2.7 Future Directions - Synthesis of multi-boronated derivatives B-346 and B-403	57
Chapter 3: Investigation of Thermal Sensitive Liposomes for improving delivery of boronated agents	64
3.1 Introduction	64
3.1.1 History of Thermal Sensitive Liposomes.....	64
3.1.2 Mechanism of TSL Drug Release	65
3.1.3 Passive and Active Drug Loading of TSLs.....	67
3.2 Hypothesis - First Application of TSLs in BNCT	68
3.3 Materials and Methods	69
3.3.1 Reagents.....	69
3.3.2 Liposome Synthesis and Characterization	69
3.3.3 Determining Doxorubicin TSL Content.....	71
3.3.4 Determining Boron Content in TSLs or Tissue	72

3.3.5 Water bath release experiments	72
3.3.6 HIFU release experiments.....	73
3.3.7 In Vivo Tumor Implantation	73
3.3.8 In Vivo Comparison of BPA-f, BPA-f-TSL and BPA-f-Non-TSL with or without hyperthermia	74
3.3.9 In Vivo Retention of BPA-f and B-381 TSL Formulations	75
3.4 Results & Discussion	75
3.4.1 Drug release from Dox-TSL	75
3.4.2 Passive Loading of B-381 into TSL Lipid Bilayer	77
3.4.3 Active Loading of B-381 into TSL Aqueous Core with pH gradient	78
3.4.4 Passive Loading of B-381 into TSL Aqueous Core.....	80
3.4.5 Characterization of Optimized TSLs	81
3.4.6 Temperature Dependent Release from Optimized TSLs	82
3.4.7 In Vivo Analysis of B-381 and BPA-f TSLs	84
3.5 Conclusions	87
Chapter 4: Dissertation Conclusion	89
References	91
Appendix	103
Curriculum Vitae	110

List of Figures

Figure 1. Nuclear fission reaction of ^{10}B atom	2
Figure 2. Neutron beam shaping assembly	5
Figure 3. Small molecule agents for BNCT.	9
Figure 4. Example of monoclonal antibody targeting in BNCT	18
Figure 5. Boronated copolymer for use as a BNCT agent.....	19
Figure 6. Cell-membrane penetrating peptide for BNCT.....	21
Figure 7. Illustration of boron-loaded liposome.....	22
Figure 8. Nanoparticles for BNCT applications.....	24
Figure 9. Hypoxia-mediated mechanisms of therapeutic resistance.....	31
Figure 10. Comparison of normoxia and hypoxic incubators	33
Figure 11. Chemotherapy and radiation resistance in hypoxia.....	34
Figure 12. Mechanism of 2-nitroimidazole accumulation in hypoxic cells.....	36
Figure 13. Immunohistochemical staining with pimonidazole.	37
Figure 14. Clinical PET agents for monitoring tumor hypoxia.....	38
Figure 15. Targeting hypoxic tumor microenvironment.....	39
Figure 16. Synthesis and characterization of boronated 2-nitroimidazole B-381.....	45
Figure 17. The effect of B-381 and BPA on viability of normoxic and hypoxic cells in vitro	47
Figure 18. Cellular uptake of B-381 and BPA in normoxic and hypoxic cells in vitro	49
Figure 19. In vitro cell sorting of normoxic and hypoxic glioma cells	51
Figure 20. Tumor retention, biodistribution and pharmacokinetics of B-381 in vivo	52
Figure 21. Synthesis of B-346.....	58
Figure 22. Synthetic route for B-403	59
Figure 23. Synthesis of Boc-protected linker for B-403 synthesis	60
Figure 24. Synthesis of free-amine linker for B-403 synthesis.....	61
Figure 25. Final synthetic step for B-403 synthesis.....	63
Figure 26. Benefit of ThermoDox added to radiofrequency ablation (RFA).	65
Figure 27. Temperature dependence of thermal sensitive liposome permeability	66
Figure 28. Active and passive drug loading of liposomes.....	68
Figure 29. Temperature dependent release of doxorubicin from Dox-TSL and Dox-Non-TSL formulations.....	76

Figure 30. Thermal sensitive liposome size and polydispersity stable with heating	77
Figure 31. Initial drug loading of B-381 into thermal sensitive liposome	78
Figure 32. Pilot in vivo study with B-381 thermal sensitive liposome	79
Figure 33. Drug loading efficiency of B-381 as a function of temperature	80
Figure 34. Liposome Synthesis and Characterization	82
Figure 35. Water Bath and HIFU Triggered Drug Release from TSLs	83
Figure 36. In Vivo Comparison of BPA-f, BPA-f TSL and BPA-f Non-TSL with or without hyperthermia	86

List of Tables

Table 1. Summary of novel boron delivery systems for BNCT	13
Table 2. Synthesized mono- and multi-boronated 2-nitroimidazole derivatives for BNCT studies.....	58

List of Abbreviations

σ^{th}	Neutron capture cross section
$^1\text{H-NMR}$	Proton nuclear magnetic resonance spectroscopy
^{10}B	Boron-10
$^{18}\text{F-BPA}$	4-borono-2- ^{18}F -fluoro-phenylalanine
^{157}Gd	Gadolinium-157
ABCPC	1-amino-3-boronocyclopentanecarboxylic acid
AUC	Area under curve
BBB	Blood-brain barrier
BNCT	Boron neutron capture therapy
BPA	4-borono-L-phenylalanine
BSH	Sodium borocaptate
CPP	Cell-membrane penetrating peptide
D54	Human glioblastoma multiforme cell line
DMEM	Dulbecco's modified eagle's medium
DNA	Deoxyribonucleic Acid
DPPC	1,2-dipalmitoyl-sn-glycero-3-phosphocholine (16:0 PC)
DSPC	1,2-distearoyl-sn-glycero-3-phosphocholine (18:0 PC)
DSPE-PEG ₂₀₀₀	1,2-distearoyl-sn-glycero-3-phosphoethanolamine-N-[amino(polyethylene glycol)-2000] (ammonium salt)
EGFR	Epidermal growth factor receptor
EPR	Enhanced Permeability and Retention effect
FBS	Fetal bovine serum
GBM	Glioblastoma multiforme
GdNCT	Gadolinium neutron capture therapy
H ₂ PzCOB	1-methyl- <i>o</i> -closocarboranyl-2-hexylthioporphyrine
H ₂ TCP	Tetra-(4-nido-carboranylphenyl) porphyrin
HPLC	High performance liquid chromatography
HT22	Murine hippocampal cell line
ICP-OES	Inductively coupled plasma optical emission spectrometry
<i>i.v.</i>	Intravenous
L-DOPA	L-3,4-dihydroxyphenylalanine

LCOB	<i>o</i> -closocarboranyl β -lactoside
mAbs	Monoclonal antibodies
m/z	Mass to charge (m/z)
NPs	Nanoparticles
PBMC	Peripheral blood mononuclear cells (healthy donor)
PBS	Phosphate-buffered saline
PET	Positron emission tomography
ppb	Parts per billion (nanograms per gram)
RES	Reticuloendothelial system (RES)
T_{1/2}	Half-life
T/B	Tumor/blood
T_m	melting phase transition temperature
T/N	Tumor/normal tissue
U87	Human glioma cell line
XRT	Radiation therapy

Acknowledgments

I would likely to sincerely thank my advisor Dr. Abdel Kareem Azab for providing me with the privilege to be a member of his laboratory the past 4 years. Dr. Azab has provided me invaluable mentorship, and has helped me develop as a scientist. His direction and insight with rational experimental design, grant/publication writing and presentation skills has been invaluable. My graduate studies have also been enriched by being able to assist in grant writing, paper editing and understanding the importance of intellectual property. He has furthered my development as both a chemist and a biologist. Additionally, I would like to thank his amazing team of post docs – Dr. Pilar de la Puente, Dr. Barbara Muz and Dr. Cinzia Federico. I appreciate their patience and mentorship over the years. They are responsible for refining my laboratory techniques such as cell culture, flow cytometry and liposome preparation. Without the support of my mentor and amazing lab team, none of this work would have been possible.

Next, I would like to thank my committee chair Dr. Dennis Hallahan. Both his scientific and clinical insight have been especially beneficial to the direction of the project. I hope in the future to be able to use my clinical experiences to direct my laboratory research. In addition, I appreciate the time and devotion of my committee members: Dr. Buck Rogers, Dr. Monica Shokeen, Dr. Joshua Rubin and Dr. Hong Chen. They have challenged me to have to reasonable experimental controls and provided exceptional insight on the direction of the dissertation.

I also would like to thank the Medical Scientist Training Program for this opportunity and the Nano Research Facility for assistance with ICP-OES.

Micah John Luderer

Washington University in St. Louis

May 2019

Dedicated to my family, for their unwavering support throughout the years. My wonderful wife Sarah, who is an exceptional chemist, teacher, and better mother. She has helped me troubleshoot organic syntheses, but most importantly gives meaning to my work. My wonderful children Jack and Henry are an inspiration, and I work to make them proud. I am grateful to my parents Jack and Connie, who have always supported me and instilled in me the importance of education. My step-mother Monica played an equal role in this, and her lost battle to ovarian cancer gives a special meaning to my pursuit in the field of oncology. My brothers Adam and Nate are my lifelong friends. I love you all.

ABSTRACT OF THE DISSERTATION

Development of Novel Tumor-Targeted Compounds for Boron Neutron Capture Therapy

by

Micah John Luderer

Doctor of Philosophy in Biology and Biomedical Sciences

Molecular Cell Biology

Washington University in St. Louis, 2019

Assistant Professor Abdel Kareem Azab, Chair

Glioblastoma multiforme (GBM) represents the most common primary brain tumor among adults. Despite surgical resection and aggressive chemoradiotherapy regimens, the current 2- and 5-year survival rates are only 27% and 9.8%, respectively. The low survival stems from the poor response to conventional therapy and underscores the critical need to develop new therapeutic approaches for GBM treatment. The high recurrence rate observed in GBM is in part attributed to the hypoxic (poorly oxygenated) tumor microenvironment. Hypoxic tumor conditions have been shown to increase metastasis, promote angiogenesis, and confer resistance to chemotherapy and radiation.

Hypoxic tissues are inherently radiation resistant due to a diminished oxygen enhancement effect. Additionally, limited diffusion of oxygen and small molecules to hypoxic tissues mitigates the efficacy of chemotherapeutics. Therefore, due to its unique mechanism of cell death, boron neutron capture therapy (BNCT) has the potential to become an alternative treatment modality for cancer patients where radiation and chemotherapy have fallen short. However, before the full clinical potential of BNCT is realized, there is a dire need to either develop novel tumor-targeted compounds or improve the localized delivery of existing BNCT agents. The work outlined in this

dissertation aims to address both these needs. First, a series of novel boronated compounds have been synthesized capable of targeting the hypoxic (and often therapy resistant) tumor microenvironment. Second, the local tumor delivery of several boronated agents has been improved utilizing a thermal sensitive liposome delivery system.

BNCT utilizes the nuclear fission reaction that occurs when a boron-10 isotope (^{10}B) captures a neutron. Upon ^{10}B neutron capture, the resulting unstable ^{11}B isotope undergoes a nuclear fission reaction ($^{10}\text{B}(n,\alpha,\gamma)^7\text{Li}$) to release an alpha particle (^4He), lithium-7 (^7Li) ion and gamma radiation. The generated particles have a limited path length of approximately 5-10 microns, thereby localizing the cytotoxic effect. Therefore, the biggest treatment hurdle for BNCT is the requirement to preferentially deliver boron to the tumor with minimal accumulation in the surrounding normal tissue. Therefore, we hypothesized that the hypoxic tumor microenvironment could be exploited to improve preferential delivery of boronated compounds to the tumor.

To begin the dissertation, a novel boronated 2-nitroimidazole derivative (B-381) has been synthesized in a single step reaction. It has long been recognized that 2-nitroimidazole derivatives have preferential retention in hypoxic cells compared to normoxic cells. Therefore, we hypothesized that B-381 would have preferential retention in hypoxic glioma cells by exploiting the unique metabolism and retention of 2-nitroimidazoles in hypoxia. Towards this end, the cellular uptake of B-381 in D54 glioma cells was evaluated *in vitro* and *in vivo* compared to 4-borono-L-phenylalanine (BPA), the most commonly investigated agent in BNCT clinical trials. Unlike BPA, B-381 illustrated preferential retention in hypoxic glioma cells compared to normoxic glioma cells *in vitro*. *In vivo*, B-381 illustrated significantly higher long-term tumor retention compared to BPA, with 9.5-fold and 6.5-fold higher boron levels at 24 and 48 h, respectively.

While these initial studies supported the unique retention of B-381 in hypoxic cells, it was desirable to improve the total boron content delivered to the tumor.

To further improve total boron content delivered to the tumor, thermal sensitive liposomes (TSLs) were investigated. A DPPC/DSPC/DSPE-PEG₂₀₀₀/Cholesterol TSL was designed capable of having a stable drug payload at 37°C while releasing >90% of the drug payload at 42°C. Therefore, by locally inducing mild hyperthermia *in vivo* (42-43°C), it is possible to trigger a localized release of boronated drug within the tumor vasculature. Using both B-381 and BPA, TSLs can significantly improve tumor boron delivery at 42°C compared to normal tissue temperature (37°C).

In summary, B-381 is effectively administered as both a free agent or incorporated into a thermal sensitive liposome formulation. B-381 represents a new class of BNCT agents in which their selectivity to tumors is based on a hypoxic tumor metabolism. Further studies are warranted to evaluate boronated 2-nitroimidazoles as well as boron-containing thermal sensitive liposomes for future BNCT clinical trials.

Chapter 1: Introduction to Neutron Capture Therapy

1.1 Mechanism of Boron Neutron Capture Therapy

Boron neutron capture therapy (BNCT) is an emerging cancer treatment modality that utilizes the neutron capture reaction of boron-10 (^{10}B) and subsequent nuclear fission reaction to produce cellular death (1-4). BNCT has the capability to provide the regional selectivity of radiation therapy with significantly less destruction to surrounding healthy tissue. This principle is obtainable because BNCT utilizes a lower energy neutron beam compared to the traditional higher energy x-ray or gamma particles used in ionizing-radiation therapy (4). Since the neutron beam is non-ionizing in nature, primarily only tissues that contain neutron absorbing isotopes (such as ^{10}B) will undergo nuclear fission and subsequent tissue destruction. Boron has a neutron-capture cross section that is three orders of magnitude greater than other common nuclei in the body (2). Additionally, because the neutron beam alone does not cause significant cellular death, the neutron beam field can be extended to irradiate the tissue surrounding the tumor to help eradicate micro residual disease and subsequent tumor recurrence or metastasis (5). Therefore, assuming adequate neutron beam penetration, the efficacy of BNCT is primarily limited by the selective tumor accumulation of boron containing agents.

Traditionally BNCT utilized a lower energy thermal neutron beam ($E_n < 0.5 \text{ eV}$) which facilitated the neutron capture and fission reaction of ^{10}B (6). However, in order to increase neutron beam penetration depth, clinical practice has adapted using an epithermal neutron beam ($0.5 \text{ eV} < E_n < 10 \text{ keV}$)(4, 7). The higher energy neutron beam is clinically significant because it increases neutron beam penetration through the skull and thick tissues. Upon ^{10}B neutron capture, the resulting unstable ^{11}B isotope undergoes a nuclear fission reaction ($^{10}\text{B}(n,\alpha,\gamma)^7\text{Li}$) to release an

alpha particle (^4He), lithium-7 (^7Li) ion and gamma radiation corresponding to 2.31 MeV (94% of time) or 2.79 MeV (6% of time) (**Figure 1**) (6). The breadth of cell destruction is limited by the path lengths of the aforementioned linear energy transfer particles, typically 5-9 microns (6). It is important to note that BNCT does result in a background dose of radiation administered to non-boron containing tissues. This is a direct result of low linear energy transfer gamma rays (a direct result of neutron capture by tissue hydrogen atoms) and high linear energy transfer protons (resulting from either the scattering of fast neutrons or from neutron capture by nitrogen atoms) (6).

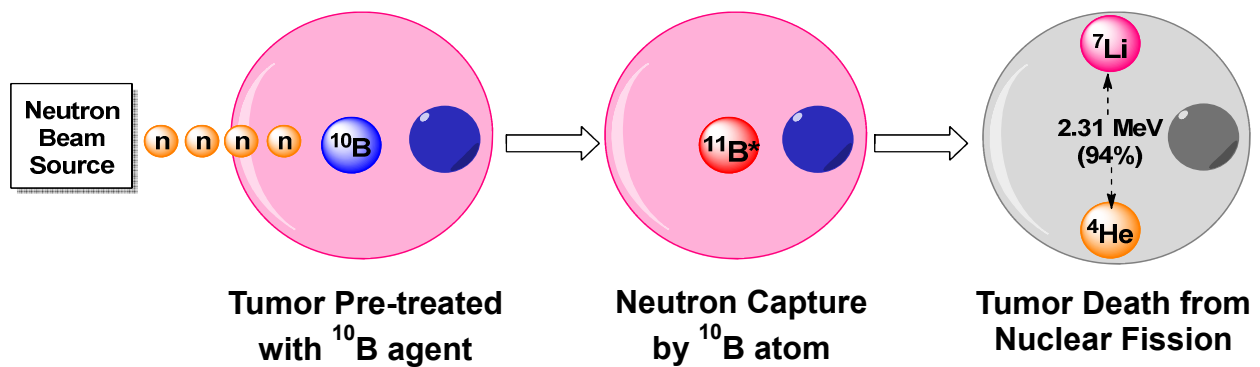


Figure 1. Nuclear fission reaction of ^{10}B atom. Schematic representation of tumor destruction by BNCT after tumor cell containing ^{10}B is irradiated with neutrons.

For BNCT to become a viable therapeutic option, the radiation dose delivered to the tumor must exceed the background radiation healthy tissue receives from non-specific neutron absorption. The efficacy of BNCT primarily depends on the selective accumulation of boron in the tumor tissue compared to the surrounding healthy tissue and blood. Generally the following requirements must be satisfied for a successful BNCT agent (1-4, 6, 8-10): (1) A tumor ^{10}B concentration of at least $10 \mu\text{g}$ boron/g of tumor; (2) Selective tumor/normal tissue (T/N) and tumor/blood (T/B) concentration ratios above 3:1; and (3) Minimal systemic cytotoxicity and rapid clearance from blood and normal tissue.

BNCT has potential to be an alternative (or adjunct) treatment modality for different cancers such as glioblastoma multiforme (GBM) (11-22), melanoma brain metastases (11, 23), adenocarcinoma liver metastases (24-29), hepatocellular carcinoma (30) and recurrent head and neck cancer patients (31-35)(9). The vast majority of patients diagnosed with the aforementioned malignancies undergo palliative care options. To put the severity of these diagnoses into perspective, consider the 2- and 5- year survival rates of newly diagnosed GBM are 27% and 9.8%, respectively (36). High grade glioma patients enrolled in recent BNCT clinical trials have demonstrated that BNCT is tolerated well, has comparable (or fewer) side effects than conventional radiation therapy, typically requires only 1-2 treatment sessions, and the median survival times are comparable to standard of care (radiation and temozolomide treatment) (14, 37). Clinical findings such as this encourage further investigation of BNCT as a therapeutic option. However, the suboptimal T/B and T/N ratios commonly achieved with BPA and BSH treatments requires development of more selective agents (2). This introduction summarizes the recent advances in boron delivery methods and reemphasizes the dire need for more selective boron delivery agents.

1.2 Alternative Isotopes for Neutron Capture Therapy

The ability to capture neutrons is not exclusive to boron. The second most commonly investigated atom for neutron capture therapy is gadolinium (^{157}Gd), with limited investigation of lithium (^6Li) and uranium (^{235}U). The probability that a given nucleus will capture thermal neutrons is known as the neutron capture cross section (σ_{th})(38)). Neutron capture cross section is measured in barns ($1 \text{ b} = 10^{-28} \text{ m}^2$). ^{10}B has a cross section $\sigma_{\text{th}} = 3,835$ whereas ^{157}Gd has a higher $\sigma_{\text{th}} = 259,000$. While it may seem more desirable to use ^{157}Gd due to its larger cross section and its dual use as MRI contrast, its biological effectiveness is limited.

Gadolinium neutron capture therapy (GdNCT) is an alternative neutron capture therapy modality which uses gadolinium-157 (^{157}Gd)(2). For the ^{157}Gd neutron capture reaction, the majority of the energy is released as long range gamma radiation, while 0.63% of the time this emission occurs as Auger and conversion electrons (39). If gadolinium is incorporated or near deoxyribonucleic acid (DNA), the generated Auger electrons can enhance the cytotoxic effect through double strand breaks. However, this represents a challenge for drug delivery as gadolinium must be delivered to the nucleus to be biologically effective. In contrast, because boron undergoes a distinct nuclear fission reaction and produces an alpha particle, boron bound to the cell surface, in the cytoplasm or in the nucleus can elicit a cytotoxic effect.

The efficacy of GdNCT and BNCT has been compared in the treatment of several canine cancer models (40). For canine oral melanoma, BNCT achieved full tumor regression in 78% of dogs (N = 14), compared to only 44% in the GdNCT treatment arm (N = 14). In the setting of osteosarcoma, both BNCT (N = 1) and GdNCT (N = 8) treatment arms illustrated full tumor progression. While further studies with GdNCT agents are clearly needed, this dissertation will focus on tumor targeting strategies for BNCT agents.

1.3 Neutron Beam Sources: from Nuclear Reactor to Linear Accelerator

As the name implies, BNCT requires a neutron source to irradiate the tumor field. Boron-containing cells at the time of treatment that fall within the irradiation field will generate high energy alpha and lithium particles *in situ*, causing localized cellular cytotoxicity. Due to the nonionizing nature of the neutron beam, the irradiation treatment field can be considerably larger than conventional radiotherapy because normal tissue will absorb neutrons less than the tumor (this assumes a modest tumor/normal tissue uptake ratio > 3 of the boronated drug)(38). Since

normal organs may also accumulate boron nonspecifically, the neutron beam is collimated to minimize nonspecific tissue injury.

One of the biggest hurdles to BNCT translation is availability of a neutron source. Neutron beams can be produced from a nuclear research reactor, particle accelerators or ^{252}Cf (Californium-252)(7, 38). Many of the clinical studies for BNCT have been restricted to a nuclear reactor facility for neutron beam production. These sites included Brookhaven and MIT in the United States, the Tsing Hua Open-pool Reactor (THOR) in Taiwan, and the RA-6 reactor at the Bariloche Atomic Center (Argentina)(38). The restriction to treat patients at a nuclear reactor facility greatly hinders its translational potential.

Traditionally, the reactor core of a nuclear reactor is the primary source of neutrons. In order to produce a suitable neutron beam for patient treatment however, neutrons exiting the reactor core must first pass through a beam shaping assembly (**Figure 2**)(41). This consists of a moderator, reflector, thermal neutron filter, gamma filter and collimator. The moderator, usually consisting of FlualentTM (Al 30% + AlF₃69% + LiF 1%) or heavy water, is used to slow fast neutrons into the epithermal region. Surrounding the moderator is the reflector, often composed of lead or graphite. This serves to redirect neutrons that have been scattered in the moderator medium but have not reached epithermal energy levels. Neutrons will next pass through a thermal neutron filter

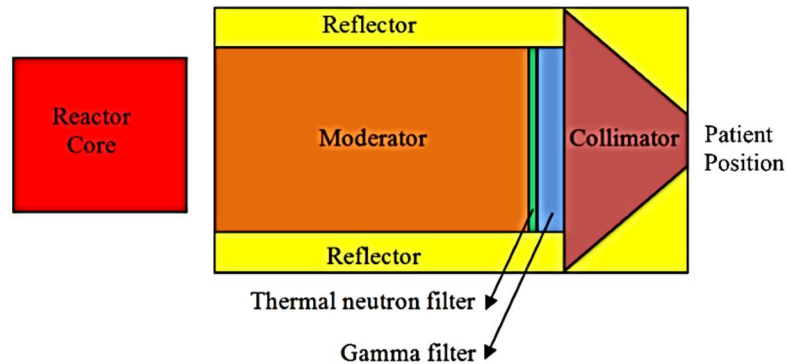


Figure 2. Neutron beam shaping assembly. Diagram of beam shaping assembly for neutron beam, adopted from (41).

(Cadmium or Gadolinium) and subsequently a gamma filter (Lead or Bismuth). Finally, a lead collimator may be used to produce the final beam dimensions.

While nuclear reactors were initially used to generate a thermal neutron beam, modifications were made to produce epithermal beams. The transition from thermal to epithermal neutron beams are more suitable to treat deep-seated tumors due to their improved penetration depth of 8-10 cm (7). For BNCT, an epithermal neutron beam (energy range 0.5 eV to 10 keV) should ideally have a minimum beam intensity of 10^9 epithermal neutrons $\text{cm}^{-2}\text{s}^{-1}$ (7). While increasing the intensity may be desirable to shorten treatment times, this will also increase beam contaminants such as fast neutrons (energy > 10 keV). Fast neutrons will produce high LET protons and can damage normal tissue in the treatment field.

Modern advancements using particle-accelerators can facilitate neutron beam production in a hospital setting. The company Neutron Therapeutics currently uses a 2.6 MeV electrostatic proton accelerator and a rotating, solid lithium target for generating neutrons. Coupled to the beam shaping assembly, this can be housed in a hospital setting.

1.4 Early BNCT Clinical Trials

The potential of BNCT for cancer therapy was recognized early by Locher in 1936, and the first patients with malignant glioma treated at the Brookhaven Graphite Research Reactor (United States) began in 1951 (38). From the years 1951-1961, 63 patients were treated in a series of clinical studies at either Brookhaven or Massachusetts Institute of Technology. At the time, 5 independent cohorts of patients received BNCT treatment and their median survival times (96 days, 97 days, 147 days, 3 months, and 5.7 months) were comparable to conventional radiation therapy at the time. Most concerning is that numerous patients had treatment complications, some fatal, which ultimately ceased further studies in the United States. Side effects included:

untreatable radiodermatoses of the scalp, postoperative infection of irradiation field, cerebral edema, and perivascular fibrosis.

The preliminary BNCT clinical studies failed due to several limitations. The biggest limitation was the lack of a tumor specific agent. The preliminary studies used borax and sodium pentaborate, neither of which have any tumor selectivity. This attributed to significant non-specific accumulation in normal tissue (blood, brain, and skin) and can explain the observed side effects (42). An equally important limitation was the availability of only a thermal neutron beam. Thermal neutrons have a low penetration depth, which biased more of the neutron dose being received by the skin, and a substantially lower dose actually penetrated to the tumor. With the advent of epithermal neutron beams, penetration depth was extended to approximately 9 cm for soft tissue (38).

After cessation of BNCT studies in the United States, the baton was passed to Japan. It was here that the introduction of two boronated compounds renewed interest in the BNCT field. The first, disodium mercaptoundecahydro-closo-dodecaborate $\text{Na}_2\text{B}_{12}\text{H}_{11}\text{SH}$ (BSH, sodium borocaptate) was investigated by Hiroshi Hatanka starting in 1968 (38). Additionally, in 1987, Mishima reported the used of p-boronophenylalanine (BPA) for the treatment of superficial melanoma. It was these pioneers that provided the most extensively studied BNCT agents to date.

1.5 Current BNCT Agents: BPA and BSH

BPA and BSH are the most extensively investigated agents in BNCT clinical trials, traditionally utilized in the treatment of melanoma and glioblastoma multiforme, respectively (**Figure 3**) (2, 4, 43). Since the ^{10}B isotope only has a natural abundance of 19.9%, BNCT agents must be enriched with ^{10}B during synthetic preparations to be maximally effective. The following sections highlight the preclinical and clinical progress made with BPA and BSH.

1.5.1 Boronophenylalanine (BPA)

The L-BPA enantiomer structurally resembles the amino acid L-phenylalanine, and is used clinically due to its higher accumulation in cancer cells compared to the D-enantiomer or racemic mixture (**Figure 3**) (44). Due to the poor solubility of BPA in water, BPA is often administered as a BPA-fructose adduct (45). However, the short shelf life of BPA-fructose after preparation makes clinical administration challenging (46). There is a well-established tradeoff between hydrophilicity of BPA agents and their cytotoxicity (with increasing water solubility there is a marked decrease in BPA derivative cytotoxicity in melanoma cells) (45). Although hydrophilic BPA will increase solubility and enable intravenous (*i.v.*) administration, this will decrease its blood-brain barrier (BBB) penetration (6).

The accumulation of BPA in cancer cells relies on the higher metabolic rate in these cells. BPA is also structurally analogous to tyrosine, which is a precursor for melanin synthesis (47); therefore, use of BPA in melanoma treatment relies on the principle that melanoma cells will have higher melanin synthesis (6). An additional mechanism proposes that BPA is taken up through the L-type amino acid transporter (47, 48). This system can transport neutral amino acid analogs containing aromatic side chains (49). Since human L-type amino acid transport 1 expression is upregulated in a wide range of cancers (including brain tumors), this allows agents like BPA to preferentially accumulate in cancerous tissues compared to surrounding normal tissues (36, 50). Additionally, BPA may preferentially accumulate in brain tumors compared to normal parenchyma due to a compromised BBB integrity within the tumor vasculature (12). Since BPA uptake is largely an active process, subpopulations of quiescent cancer cells may have lower BPA uptake, thereby decreasing BNCT efficacy (22).

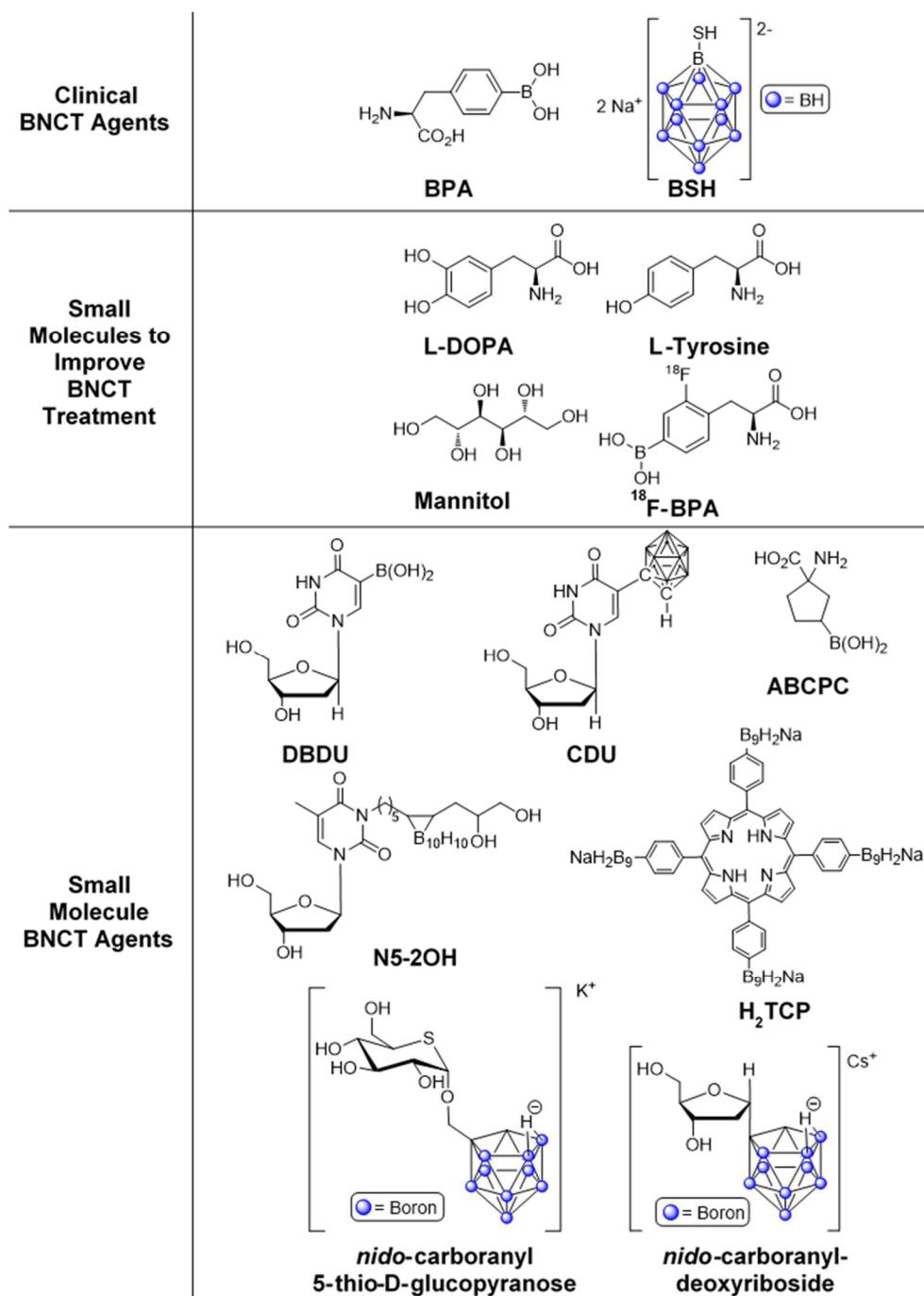


Figure 3. Small molecule agents for BNCT. L-boronophenylalanine (BPA) and sodium borocaptate (BSH) have been the most extensively studied agents clinically. L-3,4-dihydroxyphenylalanine (L-DOPA), L-tyrosine and mannitol have all been utilized to improve BPA and BSH tumor uptake. 4-borono-2-¹⁸F-fluoro-phenylalanine (¹⁸F-BPA) has been studied as a dual modality PET/BNCT agent. The following small molecules have all been proposed as novel BNCT agents: 5-dihydroboronyl-2'-deoxyuridine (DBDU), 5-(1-*o*-carboranyl)-2'-deoxyuridine (CDU), 1-amino-3-boronocyclopentanecarboxylic acid (ABCPC), 3-carboranyl thymidine derivative (N5-2OH), tetra-(4-*nido*-carboranylphenyl) porphyrin (H₂TCP), *nido*-carboranyl 5-thio-D-glucopyranose and *nido*-carboranyl deoxyriboside.

The biodistribution of BPA in GBM, melanoma, and head and neck cancer patients achieved T/B ratios ranging from 1.1 – 3.6 (11-14), T/N ratios of 1.1 – 2.9 (11, 14, 35), and tumor boron levels in the range of 1.8 – 34.8 ppm (11, 12, 14, 16, 35). This data illustrates that more selective and targeted agents are urgently needed for patients.

1.5.2 Sodium borocaptate (BSH)

BSH is an anionic carborane derivative and is administered as a sodium salt (**Figure 3**). Due to its anionic nature, BSH is thought to preferentially accumulate in brain tumors compared to normal parenchyma because of BBB disruption unique to the tumor (27, 51, 52), and in contrast to BPA, BSH accumulates passively and not by active transport (22). Early studies of BSH have noted that boron levels in normal brain are sometimes not even detectable (53). An additional notable difference is BSH contains 12 boron atoms per molecule while BPA contains only a single boron atom. Therefore, given an equal molar accumulation of BSH and BPA within a tumor, BSH will have delivered a 12-fold higher concentration of boron atoms compared to BPA, thereby facilitating the > 10 ppm ^{10}B levels required for effective BNCT. However, their administration is limited because of poor water solubility and cytotoxicity (54).

The biodistribution of BSH achieved T/B ratios ranging from 0.9 ± 0.4 to 1.2 ± 0.4 , T/N ratios in the range of 0.7 ± 0.1 to 3.6 ± 0.6 , and boron levels in the tumor ranged from 0.7 – 84.2 ppm (19, 27, 31). Again, this data illustrates that more selective agents are urgently needed.

1.5.3 Techniques to Improve BPA and BSH Uptake in Cancer Cells

Since there is a precedent of using BPA and BSH in clinical trials, techniques that increase their delivery to a tumor are a desirable concept. One common strategy is the pretreatment of cells with an amino acid analog such as L-3,4-dihydroxyphenylalanine (L-DOPA) (**Figure 3**). L-DOPA

is structurally similar to BPA, and both of these molecules may enter the cell through the L-type amino acid transport system (48). It is presumed that this transport system utilizes a substrate coupled antiport (exchange) mechanism (48). Therefore, pretreatment with a specific amino acid such as L-DOPA can improve the subsequent accumulation of BPA via this antiport mechanism (L-DOPA is exchanged for intracellular uptake of BPA). This mechanism has been validated with *in vitro* and *in vivo* studies using C6 glioma cells. Pretreatment of C6 glioma bearing rats with L-DOPA increased the BPA uptake in the tumor 2.7-fold higher than the BPA-only treated group, while accumulation in normal brain tissue did not vary significantly between the two groups (48).

In addition to L-DOPA, pretreatment of rat 9L gliosarcoma cells with L-tyrosine (**Figure 3**) resulted in a near 2-fold increase in BPA tumor uptake (47). While pretreatment with L-tyrosine increased uptake, simultaneous administration of BPA and L-tyrosine resulted in decreased BPA uptake. These results further support that an antiport mechanism can be utilized to improve BPA tumor accumulation.

Another technique used to improve boron accumulation in tumors is BBB disruption by a hyperosmotic agent such as mannitol (**Figure 3**). Intracarotid administration of BSH or BPA to F98 glioma-bearing rats, resulted in T/N ratios of 8.2 ± 1.3 and 5.9 ± 2.0 , respectively; but when combined with BBB disruption by mannitol, the BSH and BPA T/N ratios increased to 12.3 ± 4.7 and 7.5 ± 4.3 , respectively (55). Subsequent studies illustrated that co-administration of BPA or BSH with mannitol increased mean survival time of F98 glioma rats (56, 57). However, disruption of the BBB by mannitol has nonspecific effects and may be limited since this technique can also promote boron uptake in healthy brain tissue (58). Focused ultrasound techniques may be an alternative strategy to improve BPA uptake compared to traditional BBB disruption strategies (58).

In addition to improving tumor uptake of boronated compounds, an optimal response to BNCT

depends critically on performing the neutron irradiation at the time of maximal boron accumulation (or highest T/N ratio). One of the biggest limitations to BNCT is the ability to reliably determine when maximal boron accumulation has occurred in a patient (especially considering the variability that exists between patients). This challenge can potentially be overcome by positron emission tomography (PET) guided BNCT using a dual modality agent. The main advantage of a dual modality agent for BNCT is the ability to monitor the real-time boron accumulation within the patient's tumor. One example of a dual modality BNCT agent is 4-borono-2-¹⁸F-fluorophenylalanine (¹⁸F-BPA), a radiolabeled derivative of BPA (**Figure 3**). In head and neck cancers, ¹⁸F-BPA uptake significantly correlated with the uptake of ¹⁸F-fluorodeoxyglucose (59). Tumor/normal tissue ratios ranging from 1.5 to 7.8 have been reported with ¹⁸F-BPA administration for numerous tumor types (malignant gliomas, malignant melanomas and various head and neck cancers) (60). Furthermore, ¹⁸F-BPA has been shown to be preferentially taken up by L-type amino acid transporter 1 in human glioblastoma cells (49). Inhibition experiments demonstrated that BPA administration significantly decreased ¹⁸F-BPA uptake, indicating ¹⁸F-BPA may be a suitable imaging agent to estimate BPA uptake in glioma patients (49). A myriad of strategies for the radio halogenation of boron clusters has been reported previously (3). PET-guided BNCT has the potential to determine whether a patient will even benefit from BNCT, and this ultimately redefines the selection criterion of candidates for clinical trials (60).

1.6 Development of Novel BNCT Agents

With the modest T/N ratios achieved with BPA and BSH administration, the necessity for new boron delivery methods is obvious. The following sections aim to overview novel boron delivery systems and their relative advantages and limitations (summarized in **Table 1**).

Table 1. Summary of novel boron delivery systems for BNCT

Boron Delivery Vehicle	Proposed Mechanism of Accumulation	Advantages	Disadvantages
BPA	Cell membrane diffusion or uptake by L-type amino acid transporter [43].	Minimal cytotoxicity, clinical trial experience, membrane permeable.	Low percent boron composition, T/N ratio usually <4, short shelf life of fructose analog [42].
BSH	Compromised BBB due to rapid angiogenesis in brain tumor [48].	High percent boron composition, clinical trial experience, low uptake in normal brain tissue.	Net charge hinders cell membrane diffusion, cytotoxic, T/N ratio usually <4.
Nucleoside and Carbohydrate Analogs	Tumor accumulation via kinase mediated trapping [58].	Intra-nuclear accumulation (DNA incorporation) may lower dosing requirements for effective BNCT.	Human thymidine kinase-1 is cell cycle dependent; therefore treatment response may be cell cycle dependent.
Unnatural Amino Acids	L-type amino acid transporter upregulation in tumor increases uptake; accumulation occurs since cell cannot metabolize [38].	Nucleus penetration increases the probability of DNA damage (may lower dosing requirements). T/N ratios >4.	Only 1 boron atom per molecule.
Porphyrins	Accumulates via endosomal accumulation [67] or from leaky tumor vasculature [66].	Boron levels determined by spectrophotofluorimetric analysis [68]. Water soluble, minimally cytotoxic, dual-modality agent. High percent boron composition.	Intracellular boron levels did not achieve 20 ppm threshold for effective BNCT [67].
Antibody-Dendrimer Conjugates	Tumor epitope recognition [69].	Potential for high T/N selectivity based on tumor epitope expression.	Tumor and brain tissue uptake limited by BBB [72].
Cationic Polymers	EPR effect and/or targeting group (i.e., cationic moiety) [73].	Delivers a high boron payload. Polymer ratio can be fine tuned for ideal pharmacokinetic profile.	Large polymer size may lead to undesirable accumulation in other organs.
Cell-Membrane Penetrating Peptides	Facilitates transmembrane transport via macropinocytosis [74].	CPP improves uptake of agents with high percent boron composition but poor intracellular accumulation.	CPP may cause nonspecific uptake in other organs, which is undesirable during neutron irradiation.
Liposomes	Leaky tumor vasculature and EPR effect [37, 76, 77]; cationic liposomes recognize membrane negative charge [79].	Stable, minimally cytotoxic vehicle [78]. Uptake ratios superior than BPA alone; insoluble drugs may be encapsulated for delivery.	Liposome size >40 nm will likely not penetrate BBB [82]. Liposomes > 100 nm may be cleared by macrophages.
Nanoparticles	Enhanced permeability and retention effect of NPs [76, 77]. BPO ₄ NPs have increased selectivity from folic acid receptor upregulation [83].	Facile synthesis, stable NPs. Targeting moieties can be used. Versatile incorporation of boron agents.	Systemic NPs distribution increases off-target cell death during BNCT. Some NPs too large to cross BBB.

1.6.1 Nucleoside and Carbohydrate Analogs

Boronated deoxyribose derivatives have been investigated as a novel approach to improve boron uptake in tumor cells due to their higher metabolic activity (61). These agents are a primary substrate for human thymidine kinase-1 and achieve their tumor selectivity through subsequent phosphorylations which entraps them intracellularly (62). The first designed agents consisted of a boronic acid moiety or a carborane cage structure attached to the C-5 position of 2'-deoxyuridine (**Figure 3**) (62). A more recent generation of nucleoside derivatives are 3-carboranyl thymidine

analogs, in which the carborane group is attached with a linker to the N-3 position of thymidine (62). Barth *et al* have demonstrated superior drug uptake of the 3-carboranyl thymidine derivative N5-2OH compared to BPA with glioma *in vivo* biodistribution studies (**Figure 3**) (63). With convection-enhanced delivery (a catheter is used to deliver drug into the tumor) BPA achieved boron tumor levels of 68.3 ± 17.9 ppm, while N5-2OH achieved levels of 40.7 ± 11.3 ppm. However, N5-2OH accumulated more selectively (T/N = 8.5) compared to BPA (T/N = 3.6).

In addition to thymidine analogs, Hosmane *et al.* have synthesized and evaluated a series of carborane-appended 5-thio-D-glucopyranose (64) and deoxyribose derivatives (61) as promising BNCT agents (**Figure 3**). Previous generations of carbohydrate boron carriers commonly link the carborane moiety to the carbohydrate core using a glycosidic linkage; however, under physiologic conditions this linkage is susceptible to hydrolysis. To circumvent this stability concern, carborane-appended derivatives of 5-thio-D glucopyranose (a non-metabolized carbohydrate) and deoxyribose (containing a carbon-carbon linkage between the carborane and carbohydrate) have been evaluated (65). While both *nido*-carborane and *closo*-carborane carbohydrate derivatives were prepared with each scaffold, it was determined that *nido*-carborane derivatives were significantly less cytotoxic compared to their *closo*-carborane counterpart. Further studies with the *nido*-carborane derivatives of 5-thio-D-glucopyranose and deoxyribose illustrated preferential accumulation of these agent in hepatocarcinoma (SK-Hep1), prostate cancer (DU-145) and bladder carcinoma (T-24) models compared to BPA, BSH or BPA/BSH treatments (65). Additionally, treatment of a murine squamous cell carcinoma cell line (SCC-VII) with *nido*-compound illustrated a lower survival fraction compared to BPA after neutron irradiation. Further studies with carborane-appended carbohydrates may warrant clinical trials with these agents.

Carboranes linked to a DNA binding unit have also been explored as a novel boron delivery vehicle (54). DNA targeting is achieved by the interaction of a 5,6,7-trimethoxyindole moiety with DNA, analogous to its function in the anticancer agent duocarmycin A (54). Several hydroxymethylcarborane compounds were synthesized, and the two most promising derivatives had cytotoxicity values (ED_{50}) of 32 and 42.5 μM in human bronchial carcinoma cells (A549) and 7.5 and 10 μM in B-16 human melanoma cells. Treatment of B-16 cells with 10 μM of either hydroxymethylcarborane compound resulted in maximal intracellular boron levels of 2.3 and 3.7 ppm per 10^7 cells after just three hours. In contrast, a 1000 μM BPA solution required a 24 h incubation to achieve comparable levels (3.1 ppm per 10^7 cells) (54). Numerous other classes of boronated DNA-binding molecules have been explored (3).

Overall, 3-carboranyl thymidine analogs and carborane-appended carbohydrate derivatives have the potential advantage of intra-nuclear accumulation (DNA incorporation) that may lower dosing requirements for effective BNCT. Additionally, the Warburg effect indicates that most tumors will have increased uptake of carbohydrates compared to surrounding healthy tissue (65). However, one disadvantage of these agents is that their intracellular trapping is likely mediated through human thymidine kinase-1 phosphorylation; since human thymidine kinase-1 activity is cell cycle dependent, the treatment response may also be cell cycle dependent (6, 62).

1.6.2 Unnatural Amino Acids

It has been observed that boron derivatives of cyclic amino acids preferentially accumulate in GBM and metastatic melanoma tumors compared to BPA (66). While decreasing the ring size (6-, 5-, and 4-membered) of cyclic amino acids has been associated with increased tumor selectivity, the overall mechanism for tumor selectivity of unnatural amino acids is still largely unknown (67). The most promising candidate, 1-amino-3-boronocyclopentanecarboxylic acid (ABCPC, **Figure**

3), has been shown to achieve a T/B ratio of 8, T/N ratio of 21, and achieved intracellular boron accumulation in cancer cells of 28 ± 7 ppm in a B-16 melanoma mouse model (37, 66). Additionally, ABCPC is capable of penetrating the nucleus and delivering twice as much boron to T98G human glioblastoma cells compared to BPA (66). Similarly, treatment of F98 glioma bearing rats with ABCPC achieved a T/N ratio of 5 between infiltrating tumor cells and contiguous normal brain, and this level of selectivity is significant since previous studies with BPA report infiltrating tumor/normal brain tissue ratios of 1.5-2.0:1 (37).

The advantage of the unnatural amino acids is that their ability to penetrate the nucleus may lower dosing requirements for effective BNCT and provide a high T/N ratio; however, the disadvantage is that it delivers only a single boron atom per molecule.

1.6.3 Porphyrins

In addition to their application in photodynamic therapy as a photosensitizer, porphyrins have been conjugated to boron-rich moieties for BNCT applications (68). One such porphyrin, tetra-(4-nido-carboranylphenyl) porphyrin (H_2TCP), contains 36 boron atoms per molecule (**Figure 3**)(69). H_2TCP accumulates in tumors via leaky vasculature (70) and has an endosomal pattern of distribution (71). Using a B16F1 melanoma mouse model, H_2TCP treatment has been evaluated against BPA-fructose (72). Intra-tumoral injection of H_2TCP achieved a T/N ratio of approximately 6 with an associated tumor boron level of ~ 60 ppm. In comparison, *i.v.* administration of H_2TCP resulted in a T/N ratio slightly above 1 with tumor boron levels of 6 ppm. For either route of H_2TCP administration (intra-tumoral or *i.v.*), subsequent neutron irradiation resulted in a 5-6 day delay in tumor growth, but the most significant growth delay was observed in the BPA-fructose treatment arm.

Porphyrins offer the advantages of high water solubility, minimal cytotoxicity, a high percent boron composition, and their concentration levels in biological systems can be determined by relatively simple spectrophotofluorimetric analysis (72). However, one disadvantage is that porphyrins administered via an *i.v.* route may not be able to achieve intracellular boron levels >20 ppm for effective BNCT. In addition to BNCT, H₂TCP has demonstrated efficacy in photodynamic therapy and thus this agent should be investigated further as a potential BNCT/photodynamic therapy combination treatment regimen.

1.6.4 Antibody-Dendrimer Conjugates

Monoclonal antibodies (mAbs) specific for epidermal growth factor receptor (EGFR) have been investigated for the treatment of GBM due to the upregulation of EGFR in human GBM cancer cells. Two EGFR mAbs were utilized for a BNCT study: Cetuximab binds to the extracellular domain of human EGFR, thereby competitively inhibiting epidermal growth factor from binding, whereas mAbs L8A4 specifically recognizes the oncogenic variant EGFRvIII (and not wildtype EGFR) (73). For BNCT, each of these mAbs were conjugated to a boronated dendrimer, which was formed by conjugating methylisocyanato polyhedral borane anion Na(CH₃)₃NB₁₀H₈NCO to the terminal amino groups of a polyamidoamine dendrimer (**Figure 4**) (74). The boronated antibodies Cetuximab and L8A4 were administered via convection-enhanced delivery to F98 rat gliomas (a 1:1 composition of EGFR wildtype and EGFRvIII expressing glioma cells were used to reflect patient tumor heterogeneity). Co-administration of both Cetuximab and L8A4 achieved a T/N ratio of 9.9 and boron levels of 24.4 µg/g in tumor tissue (73, 75). Equally important, boron levels were undetectable in the blood (<0.5 µg/g). Rats with a composite tumor (F98_{EGFR} + F98_{EGFRvIII}) that received both mAbs and subsequent neutron irradiation had a median

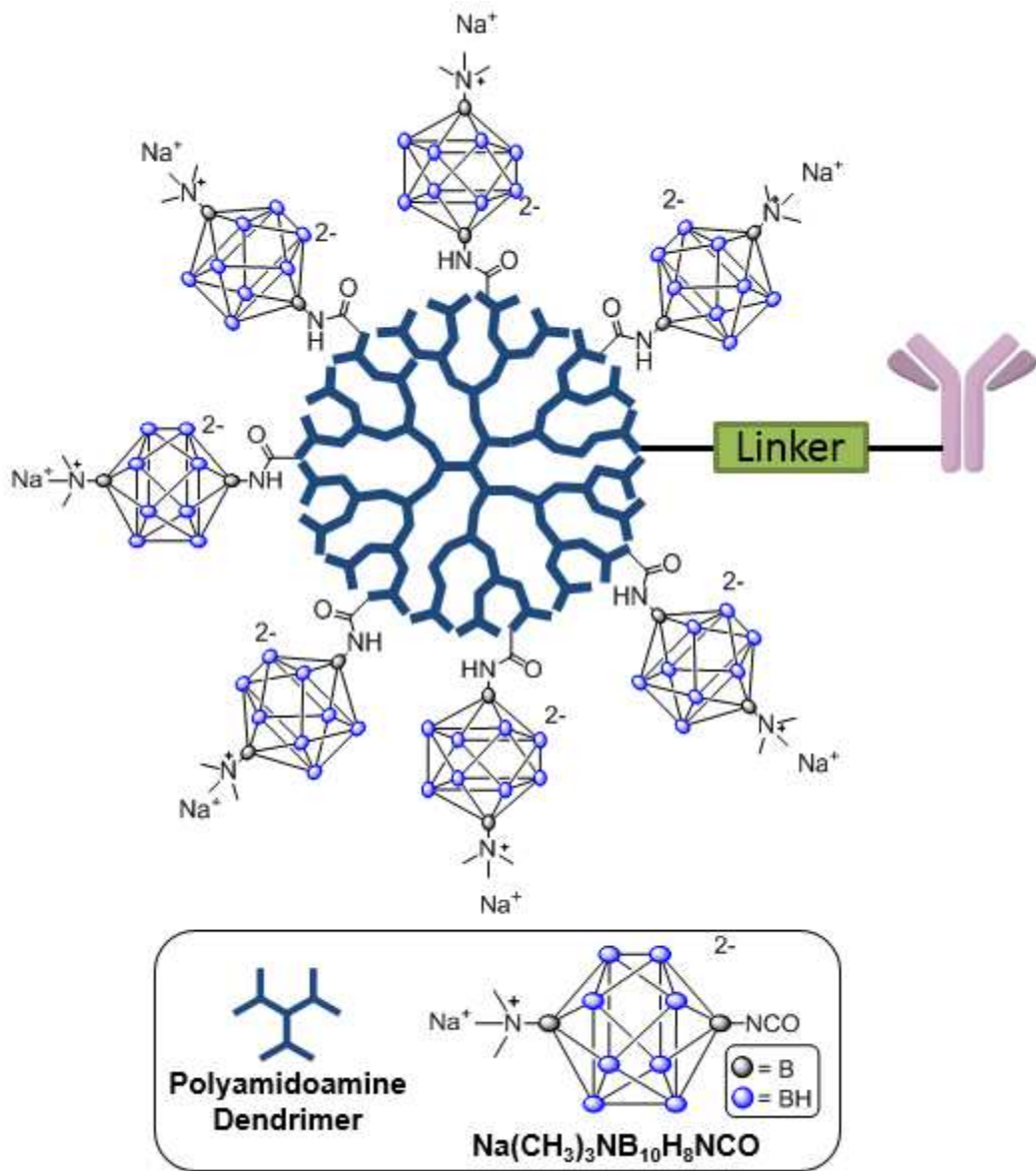


Figure 4. Example of monoclonal antibody targeting in BNCT. Monoclonal antibody (Cetuximab or L8A4) conjugated to a boronated polyamidoamine dendrimer.

survival time of 55 days; in contrast, rats that received only Cetuximab or L8A4 had median survival times of 38 and 36 days, respectively. This illustrates the importance of combination therapy with both antibodies for a heterogeneous glioma expressing both EGFR and EGFRvIII.

The advantages of boron-mAb conjugates are their high T/N selectivity and T/B ratios. However, one limitation is that systemic administration of mAbs will result in poor brain tumor uptake due to their limited ability to cross the BBB (76).

1.6.5 Cationic Polymers

Boronated cationic polymers have been used to target colon cancer polyps in a rat model. The polymers were administered locally by direct perfusion of the polymer solution into the colon lumen (77). The boronated copolymer (**Figure 5**) was constructed from 3 simple monomeric subunits: acrylamide forms the backbone of the polymer and was used to improve the aqueous solubility, N-acryloyl-diaminoethane served as the cationic moiety and allowed the polymer to accumulate in the negative cell surface space of the polyp, while aminophenylboronic acid was the boron source.

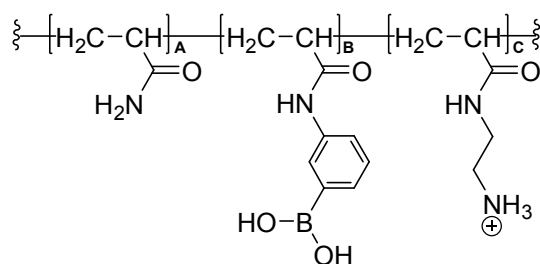


Figure 5. Boronated copolymer for use as a BNCT agent. The cationic copolymer contains a ratio of acrylamide (backbone), aminophenylboronic acid (boronated monomer), and N-acryloyl-diaminoethane (cationic monomer).

The copolymer achieved polyp to surrounding tissue boron ratios of 6.57 ± 2.05 , corresponding to boron levels of 88.5 ± 15.1 ppm in polyp tissue. In contrast, administration of free aminophenylboronic acid had a poor T/N selectivity of 1.23 ± 0.82 . An equally important finding was that boron levels detected in the blood, lymph nodes, kidney, liver and spleen were significantly lower after copolymer administration compared to free aminophenylboronic acid, due to the low non-specific uptake of polymer in these tissues. Such a boron delivery system easily

satisfies the tumor selectivity and intracellular boron level requirements for successful BNCT therapy.

Polymers have multiple advantages that make them a suitable boron delivery system for BNCT. First, copolymers can deliver a high boron load to the tumor, while having lower non-specific systemic distribution when administered directly to the intestinal tract. Second, the pharmacokinetics of a copolymer can be finely tuned by adjusting the ratio of the monomers that make up the copolymer. Additionally, copolymers may be linked to various targeting moieties to help improve their T/N ratio selectivity. The main disadvantage of polymers is that with systemic administration polymers may accumulate in filtering organs and have low penetration across the BBB in the case of treating glioma.

1.6.6 Cell-Membrane Penetrating Peptides

Although agents like BSH are desirable for BNCT due to their high percent boron composition, BSH does not readily cross the cell membrane (78). To overcome the poor intracellular accumulation of BSH, a cell-membrane penetrating peptide (CPP) was tethered to a peptide dendrimer containing BSH molecules (BSH-dendrimer-CPP, **Figure 6**) (78). *In vitro* studies using U87 glioma cells showed that treatment with BSH alone yielded intracellular boron levels of 15.9 ng $^{10}\text{B}/10^6$ cells. In contrast, treatment with the BSH-dendrimer-CPP reached boron levels of 5623.7 ng $^{10}\text{B}/10^6$ cells, a drastic increase in intracellular accumulation of BSH. This improved cellular uptake is in part attributed to the positively charged arginine rich portion of the CPP (11 arginine residues long) which is thought to promote intracellular accumulation of anionic BSH. Additionally, *in vivo* studies using U87 glioma cells injected into the striatum of nude mice followed by BSH-dendrimer-CPP *i.v.* injection in the tail vein showed preferential accumulation

of BSH only in the tumor center and edge; BSH-dendrimer-CPP was not detected in the normal brain area on high magnification by confocal microscopy (78).

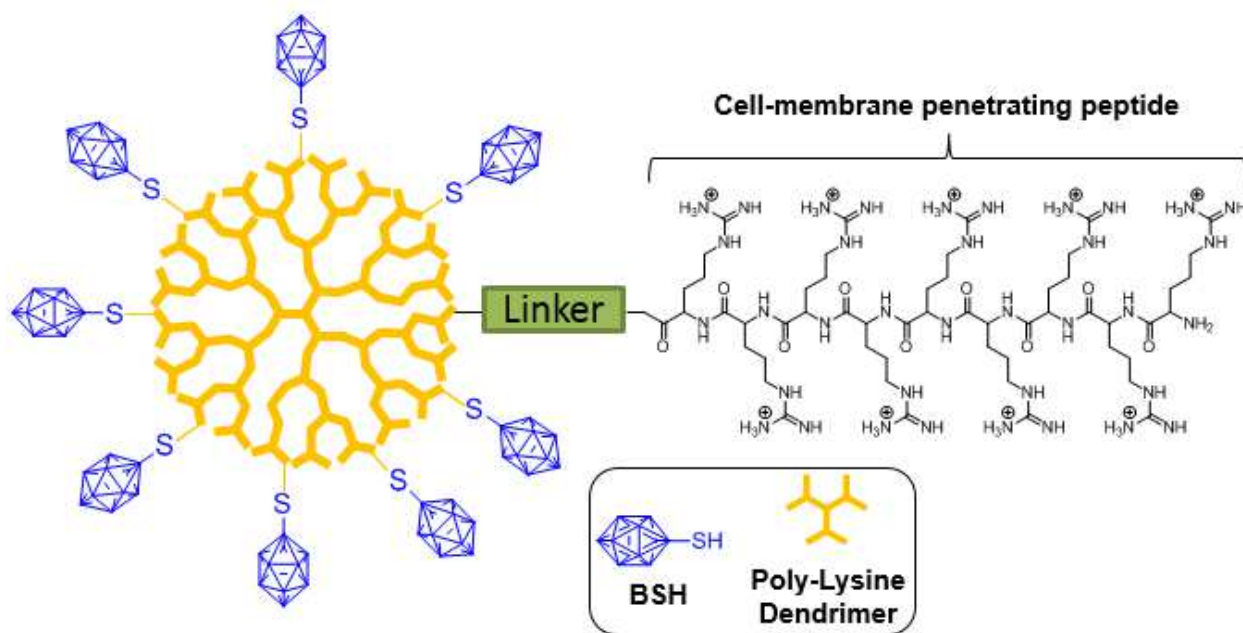


Figure 6. Cell-membrane penetrating peptide for BNCT. Schematic representation of BSH containing dendrimer with a cell-membrane penetrating peptide.

The advantage of a CPP is that it improves the uptake of agents with a high percent boron composition that typically have poor intracellular accumulation; however, a CPP may cause nonspecific uptake in other organs, which is undesirable during neutron irradiation.

1.6.7 Liposomes

Liposomes have been investigated as potential delivery vehicles for BNCT. Liposomes are closed phospholipid bilayers that can encapsulate a drug of interest (**Figure 7**) (79). Even without cell targeting, liposomes can improve drug delivery and reduce cytotoxicity of select agents (i.e. Doxorubicin) (79). Like nanoparticles, the liposome surface can also be modified to include targeting moieties. Liposomes are believed to accumulate within tumors because of local vasculature leakage known as the enhanced permeability and retention (EPR) effect (36, 79). A

majority of solid tumors have a defective blood vessel architecture coupled to an extensive production of vascular permeability factors (80, 81). This combination contributes to the EPR effect and facilitates the transport of macromolecules into the tumor. Specifically, macromolecules greater than 40 kDa can selectively leak out from tumor vessels and thereby are retained in the tumor tissue (80). Intra-tumoral liposomal accumulation relies significantly on the EPR effect. Phosphatidylcholine and dimyristoylphosphatidylcholine liposomes have recently been investigated for delivering the bis-*nido*-carborane dequalinium salt ($B_{18}C_{34}N_4H_{64}$) (82). This carborane is a delocalized lipophilic cation, and it is reported to selectively accumulate in the mitochondria of a tumor cell. These liposomes exhibited suitable stability (zeta potentials of -10 mV) and encapsulation of the bis-*nido*-carborane in a liposome significantly reduced its cytotoxicity compared to its free administration in U87 glioma cells.

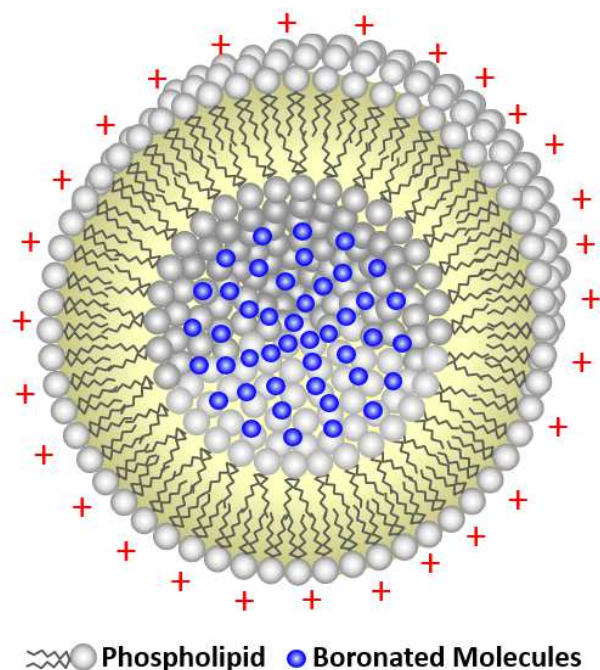


Figure 7. Illustration of boron-loaded liposome. Positively charged liposomes loaded with boron containing molecules.

Liposomal efficacy of delivering the carborane agents *o*-closocarboranyl β -lactoside (LCOB) and 1-methyl-*o*-closocarboranyl-2-hexylthioporphyrzine (H₂PzCOB) with varying liposomal compositions using cationic, anionic, and zwitterionic lipid formulations has also been investigated (83). Boron accumulation in DHD/K12/TRb rat colon carcinoma and B16-F10 murine melanoma cells was assessed by alpha spectrometry compared to BPA. While BPA treatment alone of DHD and B16-F10 cells showed uptake ratios of 0.07 and 0.2 respectively, cationic liposomes loaded with LCOB had uptake ratios of 4 and 20, respectively. Furthermore, cationic liposomes containing H₂PzCOB had an uptake ratio near 10 in DHD cells, indicating improved uptake compared to cationic LCOB liposomes in this cell line. Cationic liposomes had superior uptake compared to their anionic and zwitterionic counterparts, presumably due to their preferable interaction with a negatively charged mammalian membrane.

While liposome encapsulation can improve the delivery of BNCT agents, only a limited amount of boron can be contained within the liposome interior. To increase the potential boron payload to tumors, Hawthorne *et al* have designed a liposome system containing boron not only in the aqueous core but also in the bilayer membrane (84). The ammonio derivative Na₃[1-(2'-B₁₀H₉)-2-NH₃B₁₀H₈] is encapsulated into the aqueous core, while the liposome bilayer contains the lipophilic agent K[*nido*-7-CH₃(CH₂)₁₅-7,8-C₂B₉H₁₁]. After *i.v.* administration (2 injections 24 hours apart) of these liposomes into BALB/c mice containing EMT6 tumors (mouse mammary adenocarcinoma), a T/B ratio of 5.68 with a tumor boron concentration of 43 ppm was obtained 96 hours post-injection. These liposomes have also shown promising potential in a hamster cheek pouch oral cancer model (85).

Liposomal encapsulation of BNCT agents offers several potential advantages. Liposomes can improve the uptake and selectivity of delivering boron to tumors; additionally, drugs with poor

water solubility can be more suitable for administration within a liposome formulation. However, liposomes may have limited clinical potential for brain tumors because of size constraints. Only liposomes with diameters less than approximately 40 nm are able to penetrate the BBB adequately; liposomes larger than 100 nm may be taken up by macrophages and may be trapped in filtering organs (86).

1.6.8 Nanoparticles

Recent studies have investigated using nanoparticles (NPs) as a boron delivery system. Boron agents can be readily incorporated into nanoparticles via surface adsorption, encapsulation or direct covalent linkage (87). Analogous to liposomes, NPs rely significantly on the EPR effect for tumor accumulation. NPs may accumulate and be utilized to treat GBM and other brain tumors due to the compromised integrity of the BBB (88).

Boron phosphate NPs linked to folic acid have been proposed as a novel strategy for boron delivery (**Figure 8**). Non-functionalized boron phosphate NPs induced erythrocyte hemolysis and

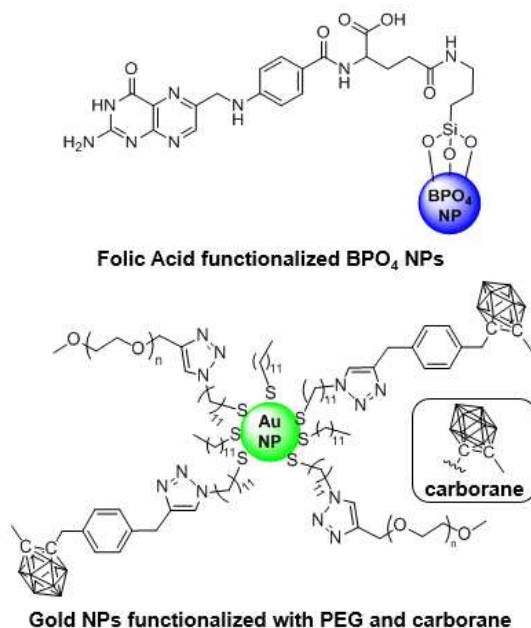


Figure 8. Nanoparticles for BNCT applications. Boron phosphate nanoparticles functionalized with folic acid and gold nanoparticles functionalized with PEG and carborane.

platelet aggregation, while these same NPs functionalized with folic acid did not exemplify significant hemolysis or platelet aggregation, suggesting these NPs can be a suitable boron delivery system (87). Additionally, the cytotoxicity of boron phosphate NPs containing folic acid was compared to BPA in both DHD rat colon adenocarcinoma and UMR rat osteosarcoma. It was determined that these NPs had comparable cytotoxicity to BPA and thus should be strongly considered as a new carrier for BNCT (87).

Carboranes linked to polyethylene glycol coated gold NPs may benefit from polyethylene glycol's enhanced permeability and retention effects (89, 90). Gold NPs were assembled starting with azido-terminated gold NPs followed by "click" chemistry with the corresponding PEG-alkyne (2000 MW) and carborane-alkyne (**Figure 8**) (89). The aforementioned NPs have hydrodynamic diameters ranging between 10-16 nm, thereby satisfying therapeutic size requirements; typically NPs less than 10 nm in diameter are freely filtered by the glomerulus, whereas NPs > 100 nm are removed by macrophages (89, 90). The aforementioned NPs strategies have promise as potential BNCT agents.

Similar to liposomes, the advantage of NPs loaded with boron is improved intracellular uptake and selectivity to tumors; however, NPs may have limited clinical potential for brain tumors because they are unable to penetrate the BBB adequately, and they may be trapped in filtering organs.

One of the main barriers facing drug delivery with particulate delivery vehicles such as liposomes and NPs is uptake by the reticuloendothelial system (RES). Uptake of particles by the RES is in part mediated by the liver, spleen and lungs (91). Increasing particle hydrophobicity or size is often correlated with increased uptake by the RES. Macrophage mediated clearance of particles can be minimized by creating particles with a hydrophilic surface and a diameter less than

100 nm (92). Coating particles with hydrophilic polymers and regulating particle size are some strategies used to overcome uptake by the RES.

1.7 Summary of Current BNCT Agents

BNCT agents have made considerable advances since the initial BNCT studies utilizing boric acid as the boron carrier. Although BPA and BSH are approved agents for BNCT clinical trials, their modest T/N ratios encourage the development of more selective agents. Improving the T/N ratio not only indicates a more selective agent, but this critical factor should minimize off target tissue damage and translate into prolonged patient survival. Boron-containing liposomes, polymers, monoclonal antibodies and nanoparticles are just a few of the presented strategies that can be used to improve BNCT efficacy. Patient populations must be carefully selected for BNCT trials, and it is vital that the pharmacokinetics of the boron agent are well known on a patient-to-patient basis. To insure maximal therapeutic response, neutron irradiation should occur during the peak T/N ratio. To assist this goal, agents that are readily detectable in patients with noninvasive methods (i.e. imaging modalities) may play a prominent role in future BNCT studies. With the current precedent of using co-administration of BPA and BSH in clinical trials, one must consider this principle and apply it to our next generation agents. Most importantly, BNCT may achieve the best clinical results in combination with surgical resection and/or chemotherapy. BNCT remains a viable treatment modality that warrants further investigation to help provide answers for those affected by cancers with no answer.

Chapter 2: Development of a Hypoxia Targeted Agent for BNCT

2.1 Introduction

Boron neutron capture therapy (BNCT) is an emerging treatment modality with the potential to minimize side effects and improve GBM patient survival (4). BNCT utilizes the neutron capture reaction of boron-10 (^{10}B) and its subsequent nuclear fission reaction to produce cellular death (93). After a ^{10}B atom absorbs a neutron, the resulting unstable ^{11}B isotope undergoes a nuclear fission reaction releasing an alpha particle, lithium-7 ion and gamma radiation (6). The path lengths of these newly generated linear energy transfer particles are typically 5-9 microns, thereby localizing the cytotoxic effect (6). Additionally, the cytotoxic effect is further localized since the nuclear fission reaction will only occur in boron-containing cells that fall within the neutron irradiation field.

Unlike radiation therapy, BNCT uses a non-ionizing neutron beam for irradiation. Therefore, if boron selectively accumulates in the tumor and minimally in the surrounding tissue, the off-target radiation effects common to traditional radiation therapy will be mitigated in BNCT. To date, L-boronophenylalanine (BPA) and sodium borocaptate (BSH) are the most commonly investigated BNCT agents in clinical studies. The challenge in developing an efficacious BNCT agent is to achieve adequate tumor/normal tissue (T/N) and tumor/blood concentration ratios (ideally greater than 3:1). Not only must an agent have a preferential tumor accumulation, it must also have limited systemic cytotoxicity.

2.1.1 Background on BNCT Treatment of Glioblastoma Multiforme

As of 2014, cancer is the second leading cause of death in the United States, contributing to 595,930 deaths (94). Historically with BNCT, glioblastoma multiforme (GBM) was the most common studied patient population. With an incidence rate of 3 per 100,000 people, GBM is the most common primary brain tumor in adults and represents approximately 50% of all gliomas (95) (96). A glioma is any tumor derived from glial cells, which are supportive cells of the nervous system. Gliomas may be classified as an astrocytoma (astrocyte derived), ependymoma (ependymal derived) or oligodendrogliomas (oligodendrocyte derived)(97). GBM is a grade IV astrocytoma, and has a rapid disease progression. The median overall survival for GBM is 12-18 months, and less than 10% of patients are alive 5 years post-diagnosis (95).

The current standard of care for GBM is macroscopic tumor resection, followed by radiation therapy with concomitant and adjuvant temozolomide (15, 98). The efficacy of temozolomide + radiotherapy was compared to radiotherapy only in a phase III trial conducted by the European Organization for Research and Treatment of Cancer (EORTC) and National Cancer Institute of Canada Clinical Trials Group (NCIC). The combination of radiotherapy + temozolomide resulted in an improved 2-year overall survival of 27.2% compared to 10.9% for radiotherapy alone (15, 98). After 5 years, overall survival for the combined group was 9.8%, and was 1.9% for radiotherapy only (36). Despite this hallmark study, there is still much room for improving patient survival. Even with therapy, patients experience a high recurrence rate of approximately 90% (99). The efficacy of XRT is limited by damage to surrounding normal brain tissues when irradiating the brain tumor externally. Additionally, the dosing and efficacy of chemotherapy is limited by systemic toxicity to organs and tissues.

High grade glioma patients enrolled in recent BNCT clinical trials have confirmed that BNCT is tolerated well and has comparable (or fewer) side effects than conventional XRT (14, 37). However, the median survival times of these trials was comparable to the standard of care (XRT and temozolomide). BPA and BSH typically have T/N ratios < 3 clinically which limits their therapeutic efficacy (93). These results emphasize the need to develop novel compounds with higher tumor specificity and improved T/N ratios.

Cancer is an ever evolving complex disease, comprised of environmental and genetic risk factors. There are 6 key biological hallmarks of cancer, as summarized by Hanahan and Weinberg (100). These are: resisting cell death, sustaining proliferative signaling, evading growth suppressors, activating invasion and metastasis, enabling replicative immortality and inducing angiogenesis. In addition to these factors, the importance of the tumor microenvironment, particularly hypoxia, is coming to light as a key factor contributing to tumor treatment resistance and relapse.

GBM tumors are highly proliferative (101, 102) with an extremely poor clinical prognosis even with aggressive therapy (36, 98). Like many solid tumors, the GBM primary tumor has a rapidly growing blood supply. GBM has a heterogeneous tumor microenvironment that has been shown to have areas with different oxygenation levels which reflect unique metabolic patterns (103). Highly oxygenated regions (close proximity to blood vessels) are characterized with fast tumor proliferation and oxidative metabolism (61), while hypoxic regions (with low oxygenation) are characterized by low proliferation and reductive metabolism (104). Hypoxic conditions in GBM tumors have been shown to decrease cell proliferation (105), induce metastasis (106), promote angiogenesis (107), and confer resistance to chemotherapy (108) and XRT (109). Resistance has been attributed to the development of a subpopulation of cancer stem-like cells (110) that

contribute to relapse in GBM (111, 112). A better understanding of tumor hypoxia may create new treatment opportunities.

2.1.2 Role of Tumor Hypoxia in Radiation and Chemotherapy Resistance

The main component of Earth's atmosphere is Nitrogen (78%), with oxygen being the second most abundant component (21%). Due to vascular and metabolic differences between organs, healthy tissues have a normal range of oxygen tensions (pO_2). A tissue is considered normoxic if the physiologic pO_2 is between 4.6-9.5%. While brain only has a pO_2 of 4.6%, the kidney cortex has a pO_2 of 9.5%. By comparison, low oxygen tensions resulting from an abnormal tumor vasculature results in hypoxic cells, with oxygen tension of 1-2% (113). While a tumor will consist of both hypoxic and normoxic cells, it is the hypoxic tumor microenvironment that has significant clinical implications to treatment resistance.

The hypoxic tumor microenvironment contributes to both chemotherapy and radiation therapy resistance. The simplest explanation of chemotherapy resistance can be described by considering diffusion. Due to an abnormal vascular network, oxygen diffusion is decreased to hypoxic niches throughout the tumor. Like oxygen, chemotherapeutics therefore will have diminished diffusion to certain hypoxic regions. Therefore, if the effective concentration of chemotherapy is never achieved, the cell will survive treatment. While the bulk (normoxic) tumor may initially respond favorably to therapy, the residual disease stemming from the hypoxic tumor microenvironment may ultimately contribute to relapse and disease progression.

For many cancer patients, chemotherapy is just a single component of their therapy. Many patients with a solid tumor will also receive radiation therapy. Radiation therapy (XRT) utilizes ionizing radiation to induce single and double strand breaks in DNA. If sufficient DNA damage occurs, the cell will undergo apoptosis. Interestingly, oxygen enhances the efficacy of radiation,

which is known as the oxygen enhancement effect. Oxygen is a potent radiosensitizer, and its presence will generate additional DNA damaging free radicals. Therefore, hypoxic cells with a low oxygen content are intrinsically radiation resistance - a higher radiation dose is required to effectively kill a hypoxic tissue compared to its normoxic counterpart, which is commonly described as an oxygen enhancement ratio (Radiation dose in hypoxia/Radiation dose in normoxia)(114).

While both the limited diffusion of chemotherapy, in addition to a decreased oxygen enhancement effect from radiation can promote tumor survival, there are numerous genetic changes that play an equally important role in tumor hypoxia (**Figure 9**) (104). The cellular response to hypoxia is mediated by a family of transcription factors known as hypoxia-inducible factors (HIF). In response to HIF signaling in hypoxia, both glycolytic and vascular endothelial growth factor pathways are upregulated thereby promoting tumor survival. Additionally, hypoxic cells may have increased expression of drug efflux proteins such as P-glycoprotein (PgP), also known as multidrug resistance protein 1. Hypoxic cells have an increased mutation rate, and some drugs (such as bleomycin) require oxygen for their mechanism of action. Furthermore, hypoxic

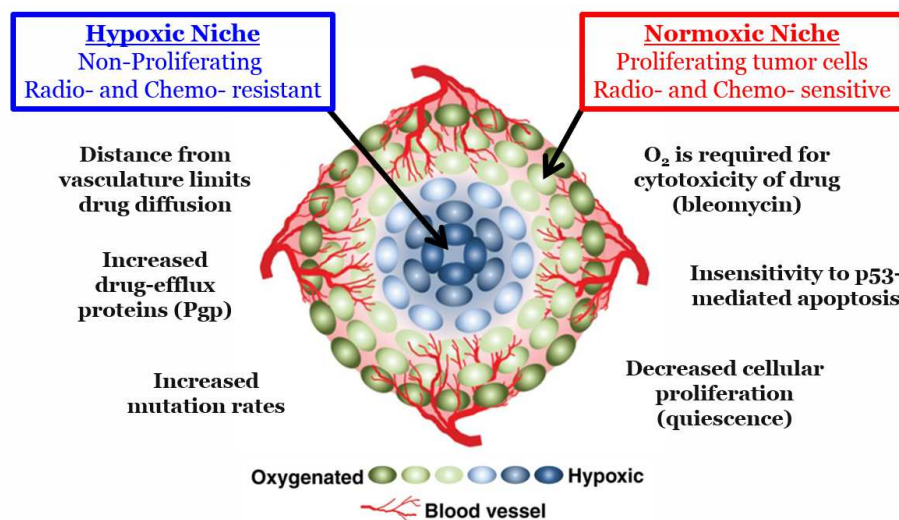


Figure 9. Hypoxia-mediated mechanisms of therapeutic resistance. In response to a hypoxic cellular environment, numerous biochemical changes contribute to chemotherapy and radiation resistance.

cells may have decrease cellular proliferation (quiescence). All of these factors, in addition to the continually mutating cancer genome contribute to therapeutic resistance.

The induction of a hypoxic tumor microenvironment can primarily be explained by two alternative hypotheses. Tumor hypoxia may be the result of either insufficient vascular supply to the tumor (outgrowing its supply) or arise from structural abnormalities in tumor vasculature networks compared to normal vessels. As a tumor continues to grow, it is accompanied by neoangiogenesis - the rapid proliferation of new blood vessels. For some solid tumors, the tumor growth will exceed this rate of angiogenesis, resulting in a tumor that has essentially outgrown its blood supply and has an insufficient vascularization density (114). If metabolic demands for oxygen exceed the available delivery from nearby vasculature, a hypoxic tumor microenvironment will develop. With increasing distance from a tumor blood vessel, both the delivery of oxygen and chemotherapeutics can be impaired (115). This creates a hypoxic tumor microenvironment that is resistant to treatment and may contribute to relapse in patients.

An alternative hypothesis of tumor hypoxia states that structural changes, and not the actual vasculature distribution, are responsible for induction of tumor hypoxia. Therefore, it is not that the tumor has “outgrown” its vascular supply, but rather the tumor vasculature that is present does not function normally (116). Tumor blood vessels are immature, tortuous and hyperpermeable. While normal tissue has a clear blood vessel hierarchy (arteriole → capillary → venule), this structural hierarchy is lost in a tumor and instead is a randomized distribution of vessels. Not only is the vessel distribution and hierarchy abnormal, but these vessels do not work as efficiently in the tumor. Tumor vessels are hyperpermeable since they are not consistently lined by smooth muscle. This increased leakiness directly results in higher interstitial fluid pressure, which creates a barrier for diffusion of both oxygen and chemotherapeutics. The increased interstitial fluid

pressure is especially relevant in the context of glioblastoma, in which the tumor is confined within the skull. Additionally, vessels that may have normal endothelium often have impaired flow due to their tortuous path and inconsistent diameter.

With its clear clinical impact, the need to study tumor hypoxia in the laboratory setting was evident. A typical cell culture incubator has an atmospheric composition of oxygen (21%), CO₂ (5%) and nitrogen (74%) with controlled humidity at 37°C (**Figure 10**). To treat cells under general hypoxia (1-2% O₂), a hypoxia chamber is utilized that displaces oxygen by use of additional nitrogen gas. Therefore hypoxic *in vitro* conditions will consist of oxygen (1%), CO₂ (5%) and nitrogen (94%) with controlled humidity at 37°C. Aside from cell culture within a hypoxic chamber, tumor hypoxia may be induced chemically with cobalt (II) chloride.

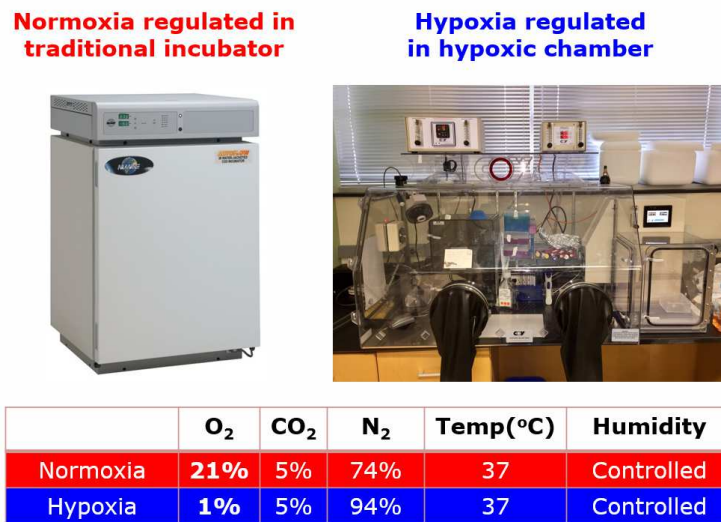


Figure 10. Comparison of normoxia and hypoxic incubators. Atmospheric composition of normoxic and hypoxic incubators used for *in vitro* studies.

In order to verify hypoxia mediated chemotherapy and radiation resistance in house, D54 glioma cells were studied *in vitro*. D54 cells incubated in either normoxia (21% O₂) or hypoxia (1% O₂) were treated with temozolomide (0-500 μM) for 96 hours. Cell viability was then assessed using MTT assay. While temozolomide concentrations are effective in normoxia, there is a

profound increase in cell survival in the hypoxia treatment group (**Figure 11 left**). This is likely attributed to the decreased cellular proliferation observed in hypoxia which eliminates the mechanism of action of temozolomide. Similarly, D54 cells exposed to increasing doses of ionizing radiation showed a marked resistance in hypoxia compared to normoxia (**Figure 11 right**).

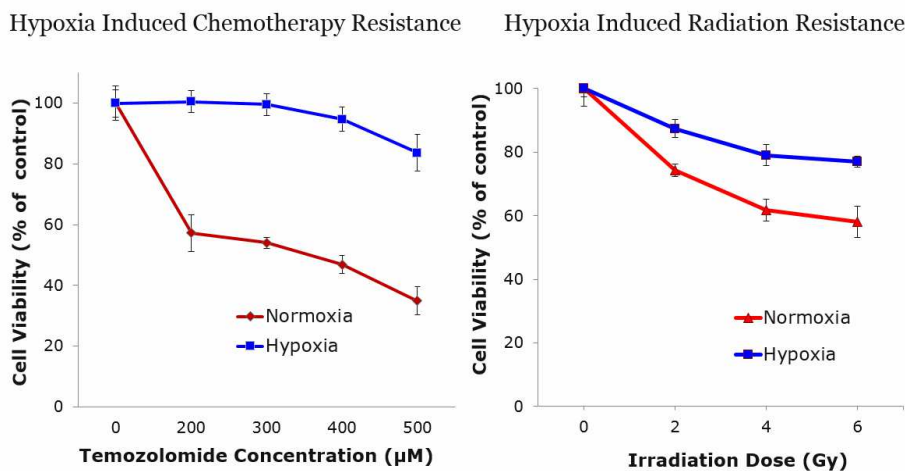


Figure 11. Chemotherapy and radiation resistance in hypoxia. Hypoxia-mediated resistance of D54 glioma cells to temozolomide treatment (left) or radiation therapy (right).

2.1.3 Molecular Probes of Tumor Hypoxia

With the realization that tumor hypoxia can adversely affect treatment outcomes, the need for clinical probes of tumor hypoxia arose. Being able to monitor the extent of tumor hypoxia can help in predicting patient treatment response. Patients with more extensive hypoxia may be less likely to respond favorably to radiation therapy. Oxygen levels in tissue may be probed physically by a polarographic oxygen electrode, or assessed through biopsy and immunohistochemistry. While electrode measurements were formally the gold standard, this is an invasive technique, which has limited clinical potential and introduces potential sampling error by reoxygenating the tissue during the measurement. Therefore, efforts have focused on studying tumor hypoxia by genetic and molecular markers. Tumor hypoxia can be assessed by endogenous (already present naturally

in the body) or exogenous markers (small molecules administered that preferentially accumulate in hypoxic tissue).

At the genetic level, assessing the upregulation of endogenous markers HIF-1 α and carbonic anhydrase IX (CA IX) is reflective of tumor hypoxia (117). HIF-1 α is a major transcription factor that regulates genes for angiogenesis, glucose metabolism, metastasis and cell survival (113). In response to tumor hypoxia, energy production is shifted towards anaerobic glycolysis (this shift is even present in aerobic tumor cells). This is associated with increasing levels of lactic acid, the metabolic end-product of anaerobic glycolysis. To assist in maintaining the extracellular pH, the activity of CA IX is upregulated (118). The contributions of HIF-1 α and CA IX are critical for tumor survival and confer resistance to chemotherapy and radiation.

While endogenous markers are more suitable for laboratory studies, the need for exogenous markers of hypoxia were evident for either immunohistochemistry staining of biopsies or clinical imaging (PET scan). The most well studied exogenous marker of cellular hypoxia is pimonidazole (sold under tradename Hypoxyprobe-1). Pimonidazole is a 2-nitroimidazole derivative, and its unique metabolism and retention in hypoxic cells has long been recognized (**Figure 12**) (114, 119). Pimonidazole is freely diffusible across the cell membrane, and therefore it will diffuse into normoxic and hypoxic tissues. However, the fate of pimonidazole metabolism is dependent on the oxygen tension within the cell. If oxygen is abundant in a normoxic cell, the nitro functional group will remain in its most oxidized state (**Figure 12**, red arrow). Even if a NO₂[·] radical forms, it will readily be oxidized back to a NO₂ group if oxygen is present. Therefore, pimonidazole will eventually diffuse out of the cell and be cleared by hepatic and renal mechanisms. However, in the setting of tumor hypoxia (**Figure 12**, blue arrows), the nitro group can first form a free radical (NO₂[·]), which is subsequently reduced further to a hydroxylamine (NHOH group) or even amine

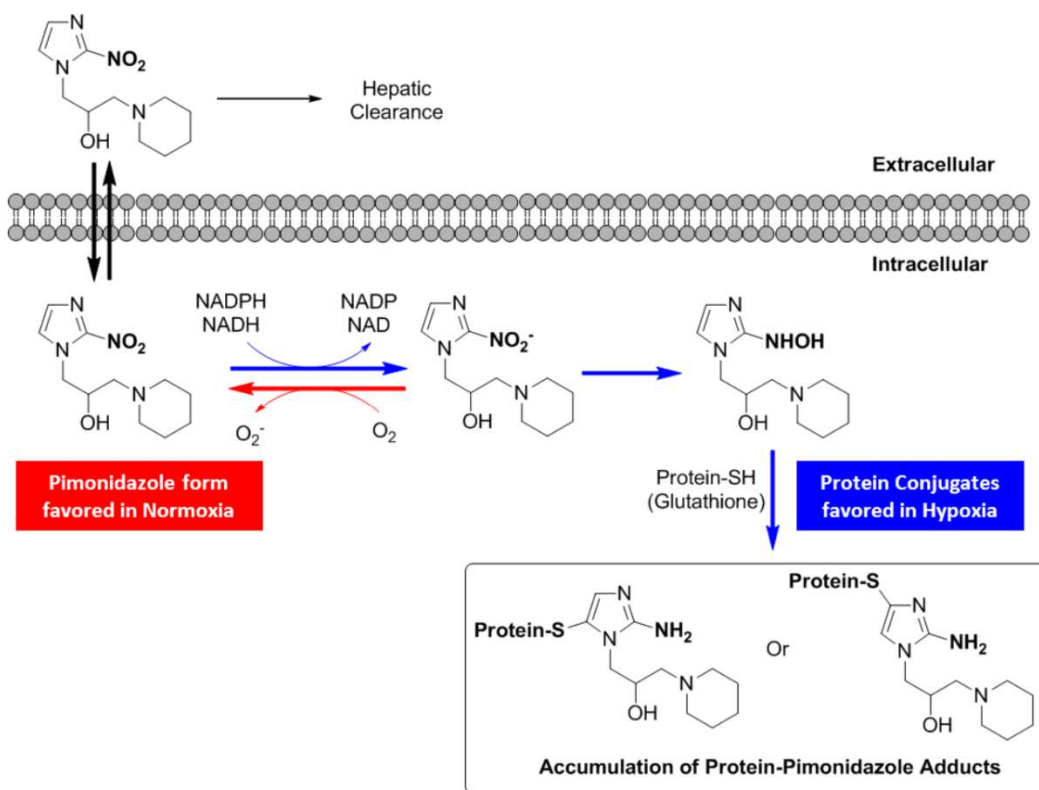


Figure 12. Mechanism of 2-nitroimidazole accumulation in hypoxic cells. Unique mechanism of pimonidazole metabolism in a normoxic (red arrow) or hypoxic cellular environment (blue arrows) leading to formation of protein conjugates.

(NH₂). This represents a dramatic shift in the electronics of the aromatic ring system. With the replacement of an extremely electron withdrawing group (NO₂) with an electron donating group (NH₂), thiol containing proteins in the cell (i.e. glutathione) can now react and trap the agent inside as a protein conjugate. Therefore, pimonidazole that enters a hypoxic cell will be fully reduced and trapped as a protein conjugate, where as in a normoxic cell pimonidazole will remain in its oxidized form and will be readily cleared.

Carlin *et al* have reported a nice example of pimonidazole uptake using a subcutaneous murine xenograft (120). As evident from the H&E stain, you can appreciate a hypoxic and necrotic center in the tumor without visual markers of hypoxia (**Figure 13 A**). When using a vascular perfusion marker Hoechst 33342, it can be appreciated that the periphery of the tumor has adequate

vascularization and is presumably normoxic, while the center of the tumor has less perfusion and is likely hypoxic (**Figure 13 B**). As shown with pimonidazole administration before sacrifice, followed by staining with pimonidazole monoclonal antibody, there is significant uptake of this hypoxic marker in the less perfused tumor center (**Figure 13 C**).

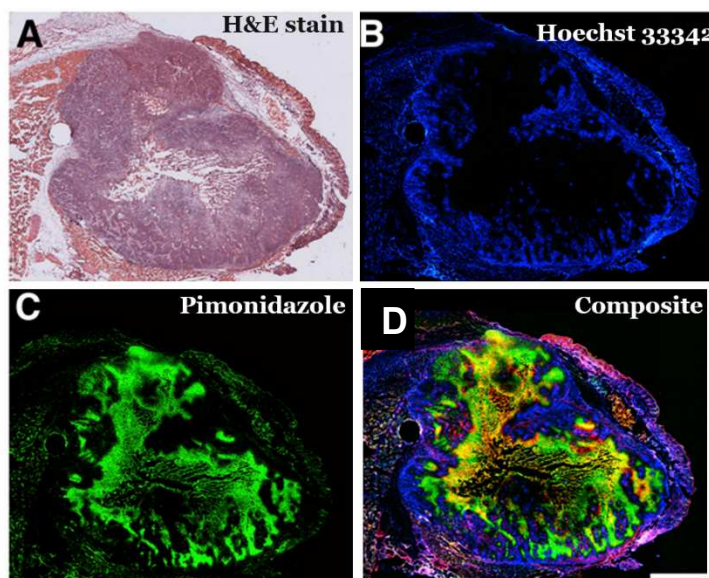


Figure 13. Immunohistochemical staining with pimonidazole. Subcutaneous mouse xenograft (SQ20b) sectioned and compared by **a.)** H&E stain, **b.)** Hoechst 33342 vascular perfusion marker, **c.)** binding of monoclonal antibody to pimonidazole and **d.)** composite image of **a-c**. Modified from Carlin S *et al* (120).

Based on the success of pimonidazole immunohistochemical staining, the potential to modify the 2-nitroimidazole scaffold for PET applications was realized. Around 2011, ^{18}F -fluoromisonidazole (^{18}F -FMISO) was considered the clinical gold standard agent for hypoxia PET probes (**Figure 14**). Sharing the 2-nitroimidazole aromatic system common to pimonidazole, its mechanism of accumulation is analogous. A distinct structural class of exogenous hypoxia PET agents is ^{64}Cu -diacetyl-bis(N(4)-methylthiosemicarbazone) (^{64}Cu -ATSM). Like pimonidazole and ^{18}F -FMISO, ^{64}Cu -ATSM is a lipophilic agent that can freely cross the cell membrane (**Figure 14**). Unlike ^{18}F -FMISO, the PET active isotope is chelated in ^{64}Cu -ATSM. When ^{64}Cu -ATSM enters a hypoxic cell, the Cu(II) -ATSM complex is reduced to an unstable Cu(I) -ATSM complex (in

normoxia, the complex remains in its more oxidized Cu(II) state)(114). Following this reduction, Cu(I) becomes dissociated and is trapped by intracellular copper chaperone proteins. Once again, we observe that reductive chemical processes are favored in the hypoxic environment, and can lead to the preferential retention of a PET isotope in a hypoxic cell compared to normoxic cells.

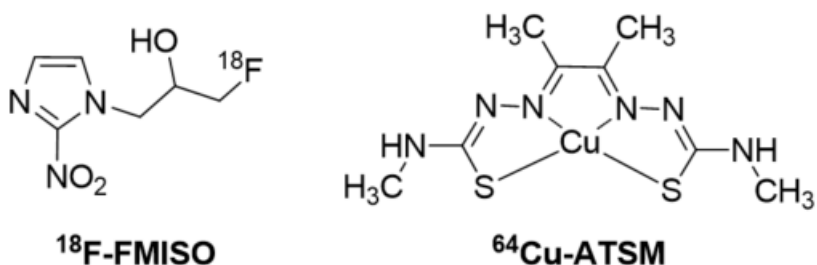


Figure 14. Clinical PET agents for monitoring tumor hypoxia. ¹⁸F-FMISO and ⁶⁴Cu-ATSM have distinct mechanisms for targeting a hypoxic tumor microenvironment and are used for PET imaging.

Cu-ATSM accumulates 2-9 times faster in hypoxic cells compared to normoxic cells (cell line dependent). In a small cohort of non-small cell lung cancer patients receiving radiation therapy, the tumor/muscle (T/M) uptake ratio of Cu-ATSM was evaluated in 14 patients by PET imaging. (121, 122). Patients that responded to chemotherapy (5 complete, 3 partial) had an average ⁶⁴Cu-ATSM uptake ratio 1.5 ± 0.4 . In comparison, 6 patients that did not respond to radiation had a mean ⁶⁴Cu-ATSM T/M ratio of 3.4 ± 0.8 . This indicates that the tumor/muscle ratio of Cu-ATSM uptake may predict therapeutic response. However, to date, there is still a discrepancy with whether ¹⁸F-FMISO or ⁶⁴Cu-ATSM is the more reliable predictor of tumor hypoxia (120). The future evolution of hypoxic PET tracers can be adapted for intensity-modulated radiation therapy. Co-registering hypoxia PET tracer images to CT scan images will guide radiation therapy. Areas of pronounced hypoxia need to receive a higher dose of radiation since there is a diminished oxygen enhancement effect (123).

In summary, the clinical significance of tumor hypoxia created the need for non-invasive imaging techniques to probe tissue oxygenation. We have observed that a hypoxic tumor microenvironment is chemotherapy and radiation resistant, and a more hypoxic tumor typically has a poorer clinical prognosis. Therefore, the ability to target this hypoxic and often therapy-resistant region would clearly be desirable for cancer treatment, and the development of agents that target hypoxic regions is warranted.

2.2 Hypothesis – Targeting Hypoxic Microenvironment

It has long been recognized that 2-nitroimidazole derivatives are capable of selectively accumulating in hypoxic cells (124, 125). In this dissertation, we hypothesized that a boronated 2-nitroimidazole derivative would preferentially accumulate in the tumor while sparing the surrounding (normoxic) healthy tissue, thereby improving the boron T/N ratio (**Figure 15**). Additionally, this is desirable since hypoxic cells tend to be more resistant to chemotherapy and radiation. Herein we present the chemical synthesis and biological evaluation of the boronated 2-

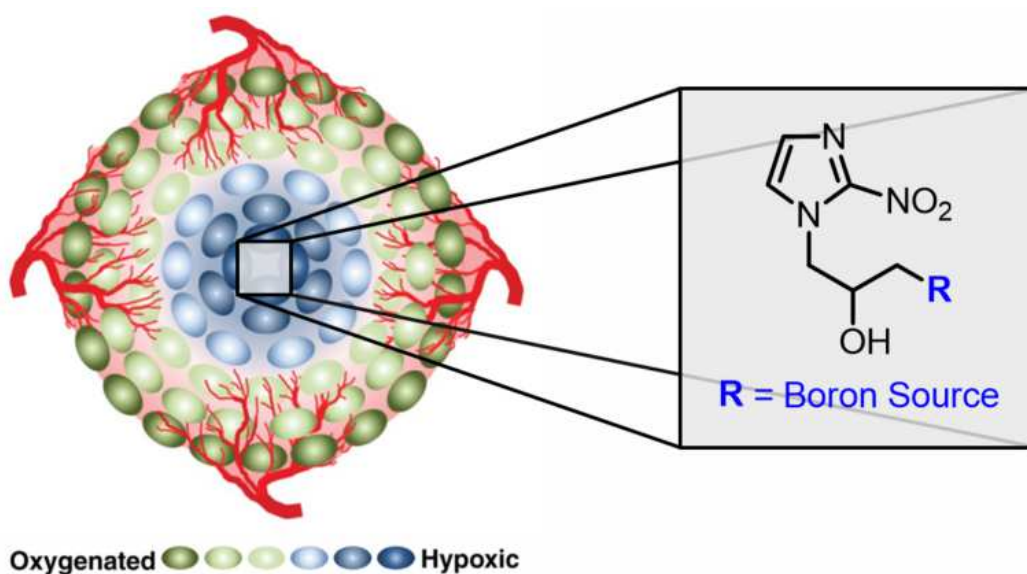


Figure 15. Targeting hypoxic tumor microenvironment. Hypothesis that the hypoxic tumor microenvironment can be targeted with boronated 2-nitroimidazole derivatives.

nitroimidazole derivative B-381. This derivative had low toxicity and a preferential accumulation in hypoxic glioma cells, making it a suitable candidate for future BNCT studies. In the future, the 2-nitroimidazole scaffold may even be suitable for modification with multi-boronated derivatives.

2.3 Materials and Methods

2.3.1 Reagents and Cell Culture

All synthetic reagents for the chemical synthesis were purchased from Sigma Aldrich (St. Louis, MO). Glioma (D54 and U87) and hippocampus (HT22) cell lines were a kind gift from Dr. Dinesh Thotala (Department of Radiation Oncology, Cancer Biology Division, Washington University in Saint Louis School of Medicine). All cell lines were cultured in Dulbecco's Modified Eagle's Medium (DMEM, Corning CellGro, Mediatech, Manassas, VA) supplemented with 20% fetal bovine serum (FBS, Gibco, Life Technologies, Grand Island, NY), 2 mmol/L of L-glutamine, 100 U/mL Penicillin and 100 µg/mL Streptomycin (CellGro, Mediatech, Manassas, VA). Before plating, cells were washed with phosphate-buffered saline (PBS, Corning CellGro, Mediatech, Manassas, VA), trypsinized with 0.05% Trypsin-EDTA 1x (Gibco, Life Technologies, Grand Island, NY), spun for 5 minutes (1000 RPM) and resuspended in fresh DMEM media. Peripheral blood mononuclear cells (PBMCs) were isolated from pheresis leukopaks from the Siteman Cancer Center (Washington University in Saint Louis). Red Blood Cell Lysis Buffer 1x (BioLegend, San Diego, CA) was added to whole blood, gently vortexed and incubated at room temperature for 15 minutes (protected from light). PBMCs were washed with PBS and resuspended in fresh DMEM media. For normoxic conditions, cells were cultured at 37°C (5% CO₂) in a NuAire water jacket incubator (Plymouth, MN). For hypoxic conditions, cells were cultured at 37°C with 0.5% O₂ concentration in a hypoxic chamber (Coy Laboratory Products, Grass Lake, MI).

2.3.2 Synthesis of Boronated 2-nitroimidazole Derivative B-381

Piperidine-4-boronic acid pinacol ester hydrochloride (73 mg, 0.296 mmol) was dissolved in saturated sodium bicarbonate solution (1 mL). Ethanol (50 mL) was added, mixed for several minutes, followed by addition of sodium sulfate (until no clumping was observed). This mixture was filtered and transferred to a 100 mL round bottom flask. Thereafter 1-(2,3-Epoxypropyl)-2-nitroimidazole (50 mg, 0.296 mmol) was added and the mixture refluxed for 5 h. After the starting material was consumed, the mixture was concentrated on a rotary evaporator. Methanol was added to the crude oil resulting in precipitation of the product B-381 (IUPAC name: 1-(2-nitro-1H-imidazol-1-yl)-3-(4-(4,4,5,5-tetramethyl-1,3,2-dioxaborolan-2-yl)piperidin-1-yl)propan-2-ol). The precipitate was isolated and the chemical structure was confirmed by liquid chromatography-mass spectrometry and proton nuclear magnetic resonance ($^1\text{H-NMR}$) spectroscopy. The molecular weight of the product was confirmed to be 381 g/mole, giving rise to the compound abbreviation B-381.

2.3.3 Cell Viability Assay

Cell viability was assessed by MTT (3-(4,5-dimethylthiazol-2-yl)-2,5-diphenyltetrazolium bromide) assay as described previously (126). Briefly, HT22, PBMCs, D54 and U87 cell lines were cultured in normoxia (21% O_2) or hypoxia (0.5% O_2) and treated for 24 h or 72 h with B-381 or BPA (0, 0.01, 0.1, 1, 10, 100 μM). After treatment, MTT solution was added for 3 h followed by the addition of 10% sodium dodecyl sulfate solution. The absorbance was read the following day at 570 nm using a plate reader.

2.3.4 HPLC Assay for Detection of B-381

B-381 was analyzed using high performance liquid chromatography (HPLC, Agilent 1100 series, Santa Clara, CA) with a reverse phase C-18 column (Agilent Zorbax Eclipse XDB C18), at a flow rate of 1 mL/min and operating pressure range of 70-85 Barr. An acetonitrile gradient containing 0.1% trifluoroacetic acid was used as the mobile phase: the gradient was increased from 0 to 10% acetonitrile (from time 0 to 7 minutes) and then decreased back to 0% acetonitrile (from time 7 to 14 minutes). A calibration curve was formed by plotting the area under curve (AUC) of the B-381 HPLC peak (at retention time = 5 min, $\lambda = 330$ nm) for the concentration range of B-381 (0 to 10 $\mu\text{g/mL}$). The linear correlation for the curve had a $R^2 = 1$, with a limit of detection approximately 0.1 $\mu\text{g/mL}$. B-381 has a wavelength of maximum absorbance of $\lambda_{\text{max}} = 330$ nm (Supplementary Figure 1).

2.3.5 Cellular uptake of B-381 *in vitro*

PBMCs, D54, U87 or HT22 cells (1×10^6 cells/well) were cultured overnight under normoxia. The following day, cells were incubated in normoxic or hypoxic conditions for 4 h in serum free media, then B-381 was added with a final concentration of 10 $\mu\text{g/mL}$ for 48 h. Additionally, B-381 solution was added to wells with no cells to serve as a no-cellular uptake control. It was observed that the AUC remained constant for this control over the experimental timeline. Media samples were collected from each well at 0 and 48 h, and analyzed by the aforementioned HPLC assay for B-381 concentration. Percent uptake of B-381 was calculated as % Uptake = $[(\text{AUC}_{\text{Control}} - \text{AUC}_{\text{Sample}}) / \text{AUC}_{\text{Control}}] * 100$.

2.3.6 Cellular uptake of BPA *in vitro*

PBMCs, D54, U87 or HT22 cells (1×10^6 cells/well) were cultured overnight under normoxia. The following day, cells were incubated in normoxic or hypoxic conditions for 4 h in serum free media, then BPA was added with a final concentration of 10 $\mu\text{g/mL}$ for 48 h. Also, BPA solution was added to wells with no cells to serve as a no-cellular uptake control. Media samples were collected from each well at 0 and 48 h, and then were digested with concentrated nitric acid for two days. Samples were diluted with deionized water to a final acid concentration of 5% (v/v) and were filtered through a 0.22 micron polyethersulfone syringe filter (DiKMA Technologies, Lake Forest, CA) and analyzed using Inductively Coupled Plasma Optical Emission Spectrometry (ICP-OES, Optima 7300 V series, Perkin Elmer, Waltham, MA). Samples were analyzed for boron content ($\lambda = 249.677$ nm) against a calibration curve of boron standards of 0, 5.2, 15.625, 31.25, 62.5, 125 and 250 parts per billion (ppb) prepared from a 10 parts per million boron standard solution (Inorganic Ventures, Christiansburg, VA). BPA percent uptake was calculated as % Uptake = $[(\text{Boron}_{\text{Control}} - \text{Boron}_{\text{Sample}}) / \text{Boron}_{\text{Control}}] * 100$.

2.3.7 Tumor Retention of BPA and B-381 *in vivo*

Approval for all animal studies was obtained from the Ethical Committee for Animal Experiments at Washington University in St. Louis Medical School. Athymic Nude-Foxn1^{nu} mice (N=10, females, 6 week old) were obtained from Envigo (Indianapolis, IN). Mice were anesthetized with ketamine/xylazine and bilaterally injected with 3.5×10^6 D54 glioma cells under the skin of each hindlimb (two injections per mouse). Two weeks post-injection both tumors were palpable under the skin. The mice were split into control (N=1) or treatment (N=9) groups. Each mouse in the treatment group was anesthetized and received two intra-tumoral injections: the left tumor received BPA (23.3 mg/kg mouse, equivalent to 0.02 mmol boron/mouse) while the right

tumor received B-381 (42.9 mg/kg mouse, equivalent to 0.02 mmol boron/mouse). Mice were sacrificed at 8 (N=3), 24 (N=3) and 48 (N=3) h post-injection, and tumors were excised, weighed and digested in concentrated nitric acid. Samples were diluted with deionized water to a final acid concentration of 5% (v/v) and analyzed by ICP-OES for boron content which was normalized to tumor weight (reported as ng of boron/g of tumor (ppb)).

2.3.8 B-381 *in vivo* Biodistribution

Five (N=5) athymic Nude-Foxn1^{nu} mice were subcutaneously injected with 3.5×10^6 D54 glioma cells in their back. When the subcutaneous tumors were approximately 0.5 cm³, four mice each received a 200 μ L intravenous (*i.v.*) tail vein injection of B-381 (dose 100 mg/kg in 10% w/v captisol solution). The fifth mouse did not receive an injection and was used as control. After 24 h, the mice were anesthetized, blood samples were collected, and the tumors were resected. Blood and tumor samples were weighed and digested in nitric acid. After diluting to a final acid concentration of 5% (v/v) with deionized water, samples were analyzed for boron concentration by ICP-OES and normalized to blood or tumor mass.

2.3.9 B-381 Plasma half-life

Six C57BL/6 mice (N=6) were injected intravenously with B-381 (50 mg/kg in 10% w/v captisol). Blood was collected from the mice under anesthesia using a submandibular bleeding technique (127) at 5 min, 1, 2, 4, 6 and 24 h ($n \geq 3$ for each time point). The blood samples were weighed, digested in nitric acid and analyzed by ICP-OES for boron concentration (normalized to mass of each blood sample).

2.4 Results

2.4.1 Synthesis and characterization of boronated nitroimidazole derivative B-381

In an effort to design a BNCT agent capable of targeting the hypoxic tumor microenvironment, a facile 1-step synthesis of a boronated 2-nitroimidazole derivative was devised. In short, commercially available piperidine-4-boronic acid pinacol ester and 1-(2,3-epoxypropyl)-2-

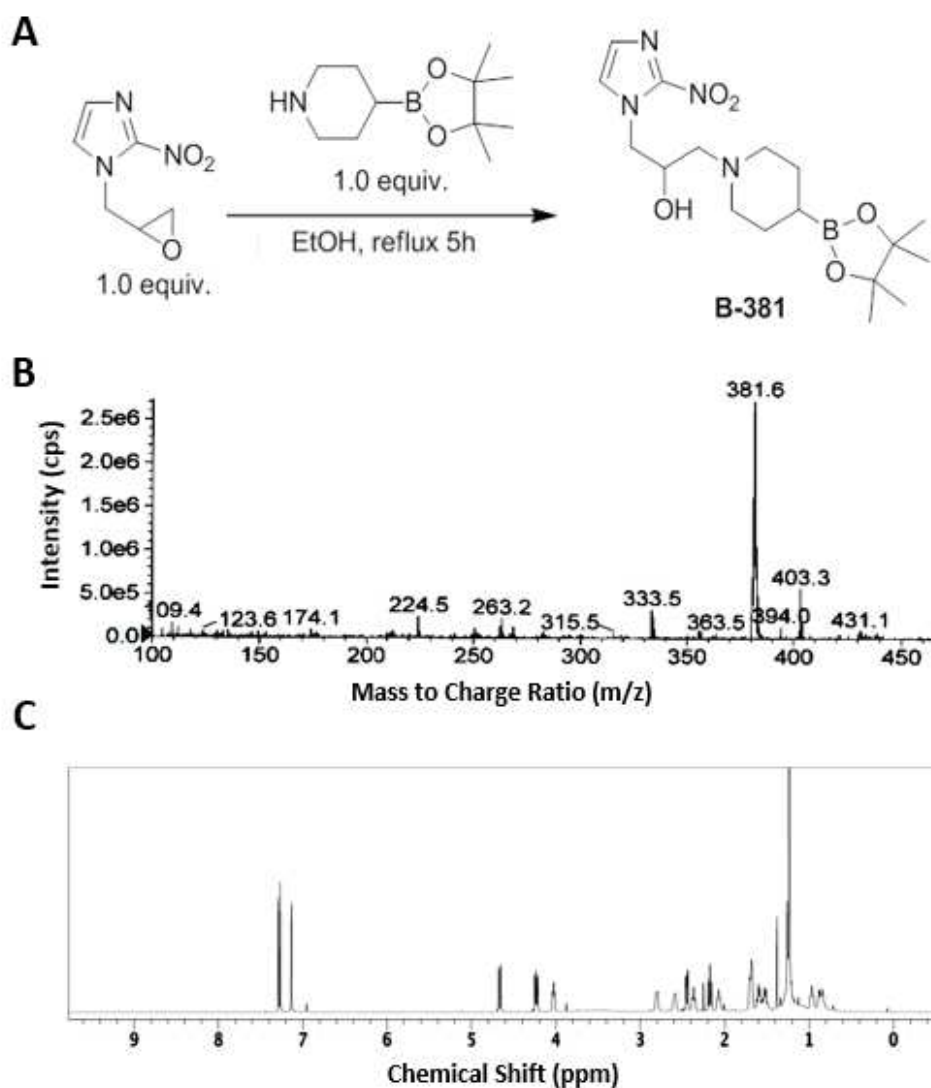


Figure 16. Synthesis and characterization of boronated 2-nitroimidazole B-381. Chemical synthesis (A), mass spectrum (B) and ^1H nuclear magnetic resonance spectrum in deuterated chloroform (C) of B-381 (IUPAC name: 1-(2-nitro-1H-imidazol-1-yl)-3-(4-(4,4,5,5-tetramethyl-1,3,2-dioxaborolan-2-yl)piperidin-1-yl)propan-2-ol).

nitroimidazole were refluxed in anhydrous ethanol to generate the boronated 2-nitroimidazole derivative termed B-381 (**Figure 16 A**). The resulting product had a corresponding mass to charge (m/z) ratio of 381.6 (**Figure 16 B**), and the structure was further validated by $^1\text{H-NMR}$ spectroscopy (**Figure 16 C**, **Supplementary Figure 2**) and $^{13}\text{C-NMR}$ (**Supplementary Figure 3**). It is important to note that neutralization of the piperidine HCl salt with sodium bicarbonate is necessary to prevent undesired epoxide ring opening by the chloride ion. The chloride ion will out compete the secondary amine on the piperidine ring and will attack the primary carbon of the epoxide. Chloride will prevent the formation of B-381 and instead the predominate product will be a chloride opened epoxide with a $m/z = 206$ (**Supplementary Figure 4**).

2.4.2 The effect of B-381 and BPA on viability of normoxic and hypoxic cells *in vitro*

We next evaluated the effect of B-381 compared to the extensively studied BNCT agent BPA on cell viability. In normoxia (21% O_2) B-381 illustrated minimal cytotoxicity in all cell lines evaluated (D54, U87, HT22 and PBMCs) up to concentrations of 100 μM (**Figure 17 A**). The cytotoxicity profile of B-381 was nearly identical under hypoxia (0.5% O_2) (**Figure 17 B**). By comparison, BPA showed minimal cytotoxicity at concentrations up to 100 μM in all cell lines evaluated in both normoxic (**Figure 17 C**) and hypoxic (**Figure 17 D**) conditions. Additionally, the long-term cytotoxicity of B-381 was evaluated in normoxia and hypoxia for the D54 cell line. Even after a 72 h treatment of B-381 with concentrations of 100 μM , no cytotoxicity was observed (**Supplementary Figure 5**). Furthermore, even concentrations of 1.5 mM does not reach IC_{50} values for B-381 (**Supplementary Figure 5**).

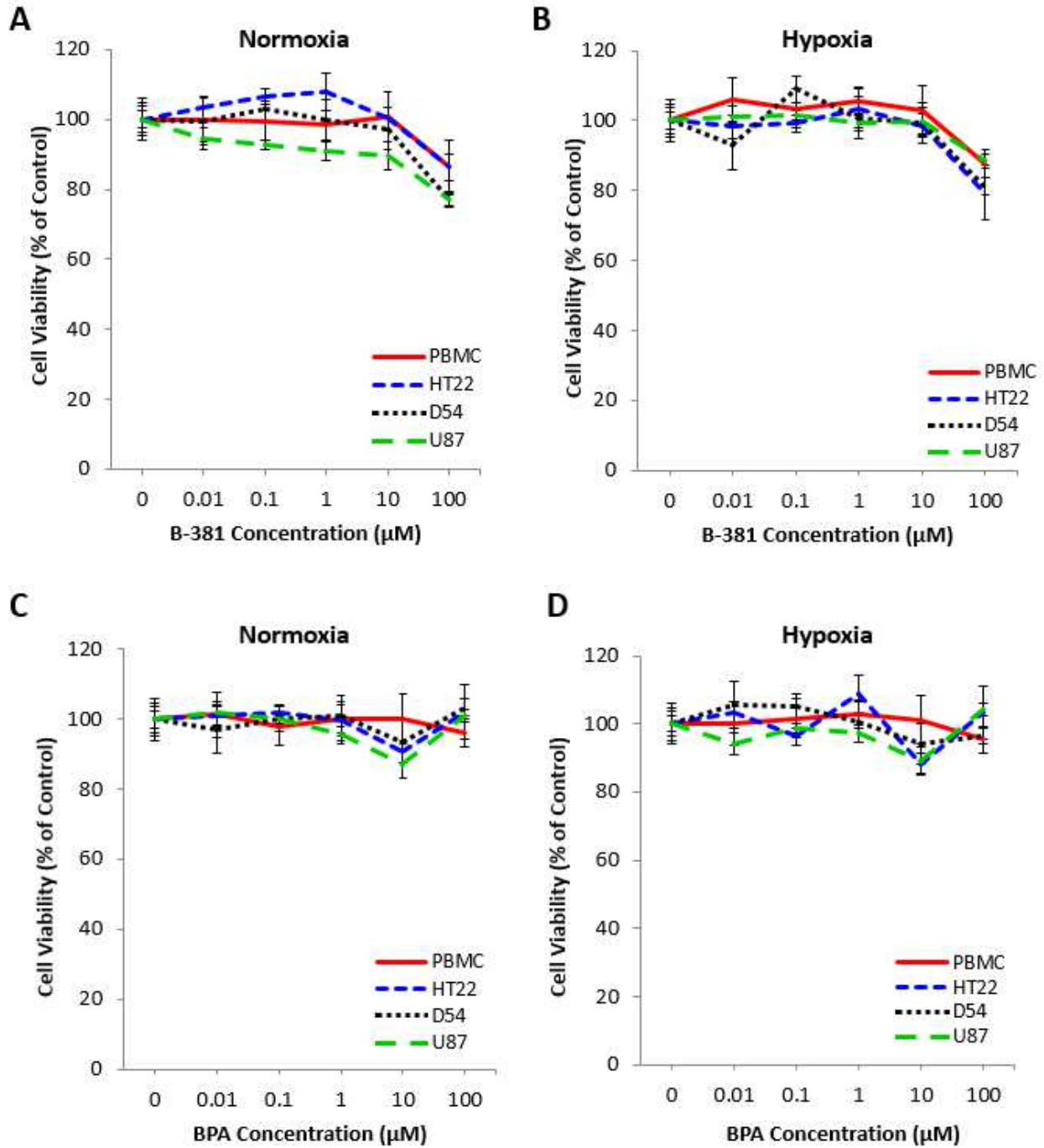


Figure 17. The effect of B-381 and BPA on viability of normoxic and hypoxic cells *in vitro*. The effect of a 24 h treatment with B-381 (A and B) and BPA (C and D) on the viability of PBMCs from healthy subjects, hippocampal cell line HT22, and glioma cell lines D54 and U87 when cultured in normoxia (A and C) and in hypoxia (B and D). Viability was analyzed using MTT assay normalized to untreated control.

2.4.3 Cellular uptake of B-381 and BPA in normoxic and hypoxic cells *in vitro*

A reverse phase HPLC assay was developed to assess the *in vitro* cellular uptake of B-381. B-381 had a retention time of 5 minutes (**Figure 18 A**) and exhibited a linear dynamic range between 0-10 $\mu\text{g/mL}$ with a $R^2 = 1$ (**Figure 18 B**). Cells were treated for 48 h with 10 $\mu\text{g/mL}$ of B-381 under normoxia (PBMCs, HT22, D54 and U87) or hypoxia (D54 and U87). Percent uptake was calculated by comparing the AUC values for B-381 in media aliquots at 0 and 48 h time points. Additionally, the AUC for B-381 was stable for 48 hours when incubated in only cell culture media (to insure the change in AUC was not a result of drug degradation)(**Supplementary Figure 6**).

B-381 had a low cellular uptake of $< 5\%$ after 48 h in all cell lines treated under normoxic conditions (PBMCs, HT22, D54 and U87). By contrast, D54 and U87 glioma cell lines treated under hypoxia had significantly higher B-381 uptake of 21% and 25%, respectively (**Figure 18 C**). Subsequently the *in vitro* cellular uptake of BPA was evaluated using ICP-OES. Boron standards between 0-250 ppb had a linear dynamic range with a $R^2 = 0.9992$ (**Figure 18 D**). Using 10 $\mu\text{g/mL}$ of BPA under normoxia (PBMCs, HT22, D54 and U87) or hypoxia (D54 and U87), BPA had a low percent uptake of approximately $< 5\%$ in all conditions evaluated (**Figure 18 E**). These results indicate that B-381 preferentially accumulates in hypoxic glioma cells compared to BPA.

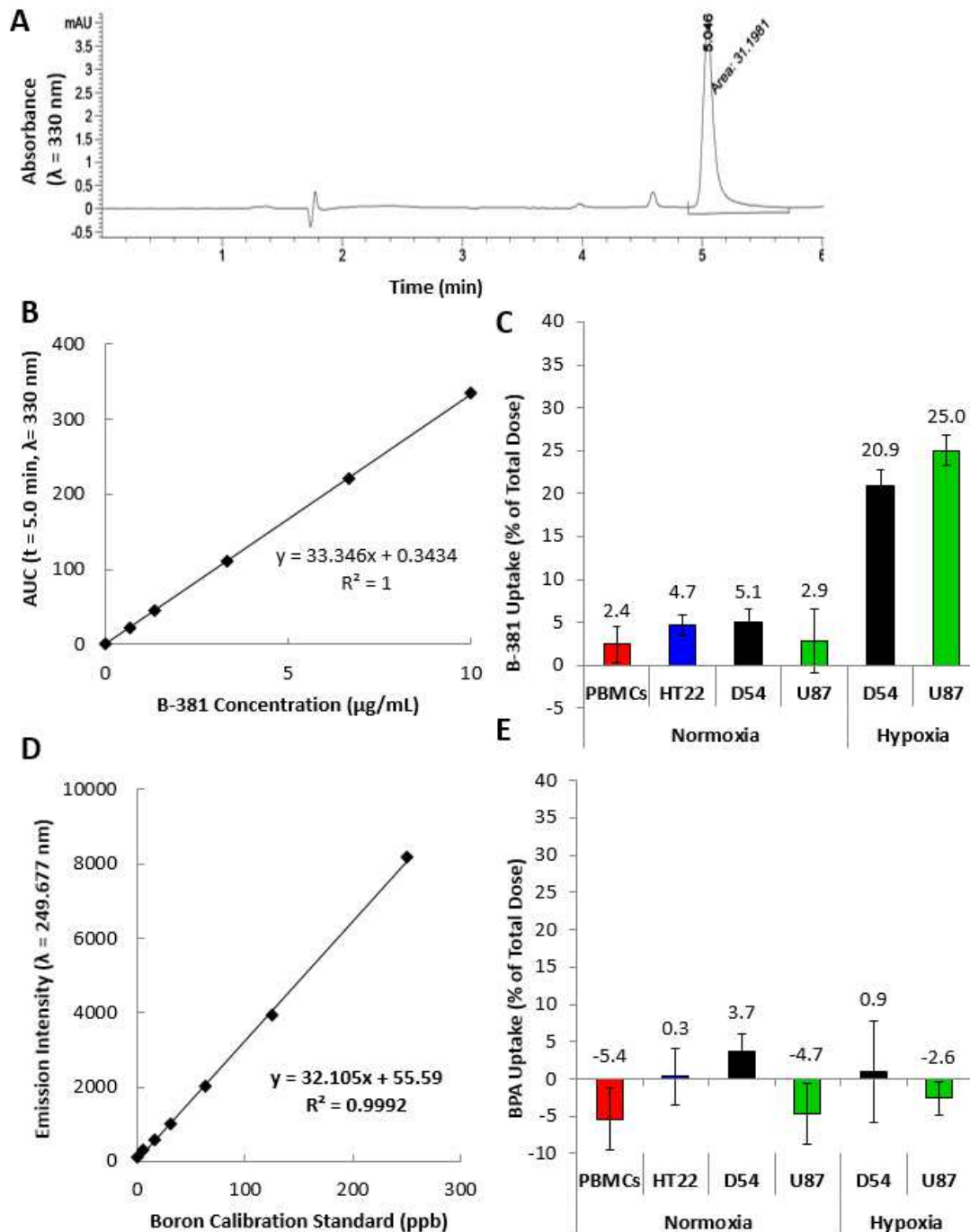


Figure 18. Cellular uptake of B-381 and BPA in normoxic and hypoxic cells *in vitro*. Representative HPLC chromatogram for B-381 on a C-18 column with a 0-10% acetonitrile gradient (containing 0.1% trifluoroacetic acid) in water over 7 minutes with a retention time = 5 min ($\lambda = 330 \text{ nm}$) (A). Calibration curve of B-381 for HPLC cellular uptake study (B). Cellular uptake of B-381 in normoxic PBMCs from normal subjects, normoxic hippocampal cell line HT22, and in normoxic and hypoxic glioma cell lines D54 and U87 (C). Calibration curve of BPA for detection of boron using ICP-OES (D). Cellular uptake studies of BPA in normoxic PBMCs from normal subjects, normoxic hippocampal cell line HT22, and in normoxic and hypoxic glioma cell lines D54 and U87 (E).

2.4.4 *In vitro* mechanistic study of B-381 accumulation in hypoxic cells

In order to further confirm that B-381 has preferential uptake in hypoxic glioma cells, an *in vitro* cell sorting experiment was performed. Preliminary experiments in house validated a robust increase in pimonidazole uptake in D54 cells incubated in hypoxia (1% O₂) compared to normoxic controls (**Supplementary Figure 7**). We investigated whether the anti-pimonidazole antibody could recognize B-381, but there did not appear to be cross-reactivity of the antibody. Therefore, a cell sorting experiment was planned that would sort hypoxic and normoxic cells based on their pimonidazole labeling, and then boron content would be determined to assess B-381 uptake.

To accomplish this, D54 glioma cells were cultured in normoxia (21% O₂) or hypoxia (1% O₂) and treated with B-381 followed by addition of pimonidazole. Following treatment, cells were trypsinized, fixed with 70% ethanol and treated with anti-pimonidazole monoclonal antibody. Thereafter the normoxic and hypoxic cell populations were mixed, to simulate the heterogeneous tumor microenvironment present from an *in vivo* sample. Using the Siteman cell sorting facility, the lowest 5% (dim) and highest 5% (bright) FITC positive populations were collected (**Figure 19 a**). The dim population is representative of normoxic cells, because they demonstrate low uptake of the hypoxia marker pimonidazole. In contrast, the bright population represents the most hypoxic cells, since the 2-nitroimidazole derivative has formed intracellular protein conjugates. After cell sorting, 500,000 normoxic (dim) and 500,000 hypoxic (bright) cells were collected. It was clear after sorting that the populations were truly enriched, with a 40-fold higher MFI in the bright population compared to the dim population (**Figure 19 b**).

The normoxic and hypoxic enriched cell populations were then microwave digested in 5% nitric acid and analyzed for boron content by ICP-OES. The hypoxic enriched population (high anti-Pimonidazole FITC signal intensity) had a boron content of 19.9 ppb, while the normoxic

enriched population had a signal of 1.5 ppb (**Figure 19 c**). Therefore B-381 has a 13.2-fold higher uptake in hypoxic cells compared to normoxic cells. Since B-381 and pimonidazole share the 2-nitroimidazole structural motif, this data supports that B-381 accumulates analogous to pimonidazole in hypoxic cells due to the formation of protein conjugates.

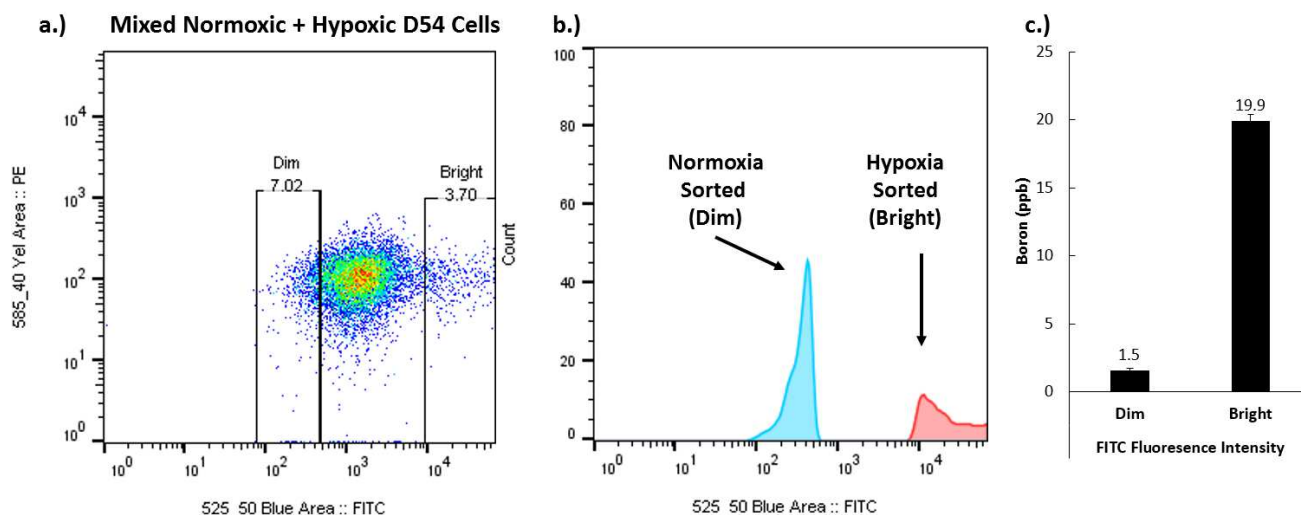


Figure 19. *In vitro* cell sorting of normoxic and hypoxic glioma cells. a.) Cell sorting gating for normoxic (dim) and hypoxic (bright) D54 cells based on anti-Pimonidazole FITC signal b.) Post cell-sorting illustrated a 40-fold higher MFI for hypoxic (bright) cells compared to normoxic (dim) cells c.) Boron content in dim (anti-Pimonidazole FITC low) and bright (anti-Pimonidazole FITC high) enriched cell populations determined by ICP-OES.

2.4.5 Tumor retention, biodistribution and pharmacokinetics of B-381 *in vivo*

To eliminate the biodistribution and metabolic components associated with B-381 administration, an intra-tumoral injection of B-381 was compared to BPA to verify the tumor retention of B-381 due to its presumed formation of protein conjugates in a hypoxic microenvironment. A D54 glioma xenograft mouse model was utilized to compare the *in vivo* tumor accumulation of B-381 and BPA. Mice containing bilateral hindlimb D54 glioma tumors were injected intra-tumorally with equimolar concentrations of BPA or B-381. Following injection, mice were sacrificed at 8, 24 or 48 h. Tumors were excised, digested and boron

concentration was determined with ICP-OES. The tumor concentration of BPA and B-381 was nearly identical 8 h post-injection ($1,595 \pm 274$ ppb and $1,130 \pm 152$ ppb, respectively, **Figure 20 A**). However, at 24 and 48 h post-injection, the concentration of BPA was almost undetectable. In contrast to BPA, the tumor demonstrated a long-term retention of B-381, with 9.5-fold and 6.4-fold higher boron levels at 24 and 48 h, respectively.

Following the observed preferential hypoxic tumor accumulation of B-381 *in vivo* (**Figure 20**

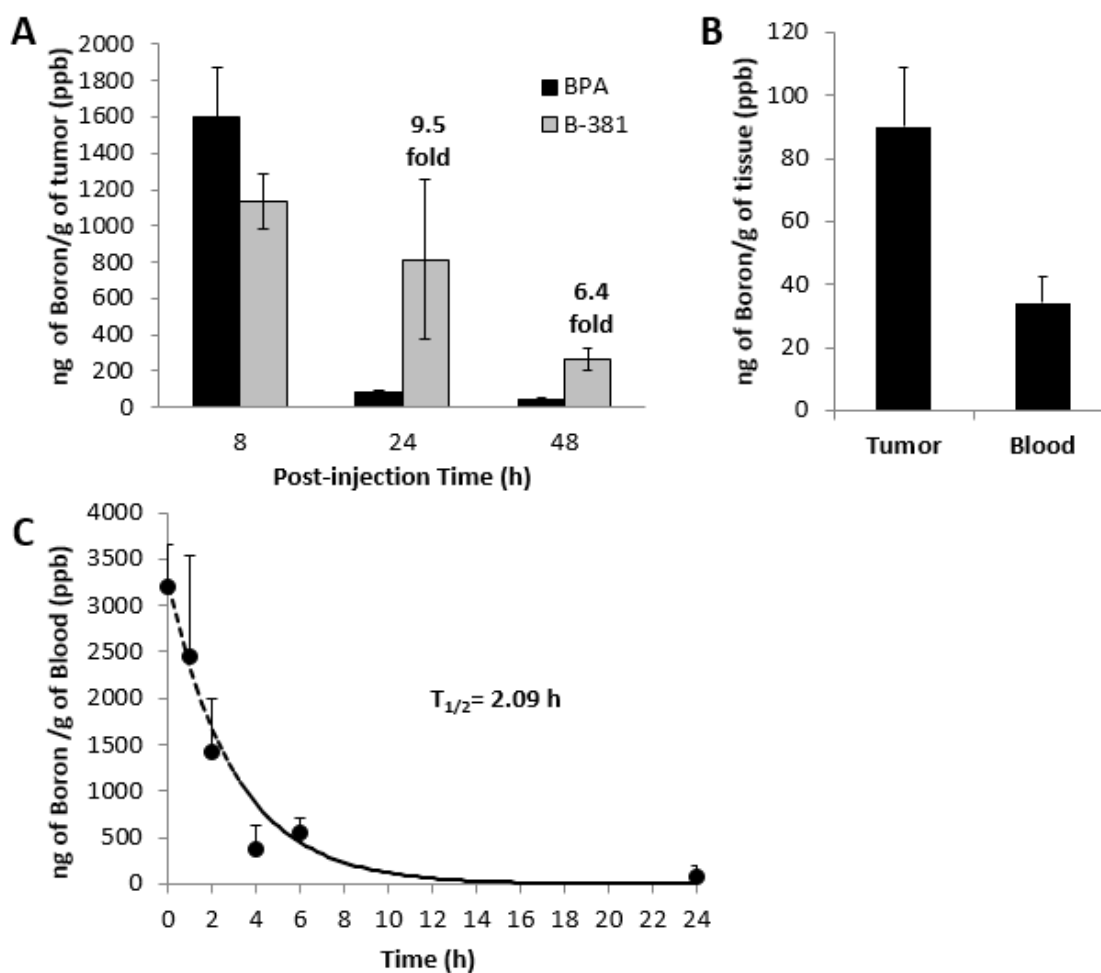


Figure 20. Tumor retention, biodistribution and pharmacokinetics of B-381 *in vivo*. (A) Tumor boron concentration analyzed by ICP-OES after intra-tumoral injection of left tumor with BPA (23.3 mg/kg mouse, equivalent to 0.02 mmol boron/mouse) and intra-tumoral injection of right tumor with B-381 (42.9 mg/kg mouse, equivalent to 0.02 mmol boron/mouse). (B) Biodistribution of boron 24 h after intravenous injection of 100 mg/kg B-381 into D54 glioma bearing mice, sacrificed 24 h post-injection and boron content determined by ICP-OES. (C) Pharmacokinetic analysis of boron blood levels after intravenous injection of 50 mg/kg of B-381 using naïve mice analyzed by ICP-OES.

A), the biodistribution of B-381 was investigated. Five (N=5) athymic nude mice containing subcutaneous D54 glioma tumors were treated with B-381. Four mice received an *i.v.* injection of B-381, while the fifth mouse did not receive an injection and was used as a control. After 24 h, the boron content in tumor and blood was determined by ICP-OES. B-381 had preferential tumor accumulation, in which average tumor boron levels were 89.9 ± 18.9 ppb, while blood levels were 34.2 ± 8.0 ppb (**Figure 20 B**). This correlated to a tumor/blood ratio of 2.6.

An *in vivo* pharmacokinetic study was performed to determine the plasma half-life ($T_{1/2}$) for B-381. In brief, C57BL/6 mice received an *i.v.* injection of B-381. Blood was collected at 5 min, 1 h, 2 h, 4 h, 6 h and 24 h post-injection, and boron levels were determined by ICP-OES (**Figure 20**). Immediately following *i.v.* injection, a maximal boron level of $3,205 \pm 458$ ppb was detected (time = 5 min). Based on first order elimination kinetics, it was determined that B-381 was quickly eliminated from the blood with a $T_{1/2} = 2.09$ h.

2.5 Discussion

BNCT is a promising therapeutic approach based on the nuclear fission reaction of boron that is triggered by neutron irradiation. The resulting intracellular production of high-energy alpha particles can target tumor cells for destruction while having less off-target associated cytotoxicity compared to XRT and chemotherapy (4, 93). However, the potential of BNCT to have a targeted tumoricidal effect is limited by the ability of a boronated agent to accumulate specifically in the tumor (ideally $T/N > 3$). Clinical trial agents BPA and BSH in glioma have suffered from poor tumor selectivity, with T/N ratios of 1.1 – 2.9 for BPA (11, 14, 35) and 0.7 - 3.6 for BSH (19, 27, 31). Therefore, in order to improve the therapeutic potential of BNCT, there is an urgent need to develop novel boronated tumor selective compounds.

To improve tumor selectivity in the setting of glioma, we envisioned that the hypoxic tumor microenvironment could be exploited as a targeting strategy. Hypoxic tumor cells contribute to chemotherapy (108) and XRT (109) resistance. Various factors such as increased expression of drug efflux pumps, decreased cell proliferation and oxygen-dependent cytotoxicity all play important factors in hypoxia-mediated drug resistance (104). It was previously shown that these hypoxic areas have more reductive rather than the normal-cell oxidative metabolism (104), and we hypothesized that this property could be used to specifically target these tumor regions.

It has long been recognized that 2-nitromidazole derivatives can selectively accumulate in hypoxic cells. The most recognized 2-nitroimidazole derivative is pimonidazole, which is a gold-standard immunohistochemical marker of hypoxia (128). In hypoxia, the nitro functional group undergoes a series of reductions and is converted to an amine (119). This makes the nitroimidazole ring susceptible to forming intracellular protein conjugates with thiol-containing proteins such as glutathione, which in turn causes accumulation of the nitroimidazole derivative in hypoxic cells. In an oxygen rich (normoxic) environment, the nitro functional group remains in its oxidized form, thereby preventing the formation of the aforementioned protein conjugates. This differential metabolism in normoxic versus hypoxic cells has been utilized to develop a PET imaging agent for hypoxic tumor regions. ¹⁸F-Fluoromisonidazole is a clinically used fluorinated-2-nitroimidazole PET agent for monitoring tumor hypoxia in glioma patients (129). Therefore, we hypothesized that synthesizing a boronated 2-nitromidazole derivative should be able to deliver boron preferentially to hypoxic glioma cells.

Herein we report the synthesis of B-381, which is a novel boronated derivative of 2-nitroimidazole (**Figure 16 A**). B-381 is readily synthesized utilizing a one-step reaction with commercially available precursors and is easily purified as a precipitate in methanol. After

precipitation, B-381 has a clear mass spectrum (**Figure 16 B**) with a single major peak observed on the HPLC chromatogram (**Figure 16 A**). Consistent with the structure of B-381, we observed a characteristic singlet peak in the $^1\text{H-NMR}$ spectrum (integrating to 12 protons) that is a result of 4 methyl groups found in the pinacol ester group. Additionally, the aromatic region contained 2 nitroimidazole ring protons, while the remaining NMR peaks in the aliphatic region accounted for the final 14 protons (**Figure 16 C, Supplementary Figure 2, Supplementary Figure 3**).

In order to be a suitable drug candidate for BNCT, the boronated agent must have low systemic cytotoxicity (93). Dose-limiting toxicities could prevent sufficient tumor boron levels being reached which are required for BNCT to achieve a therapeutic effect. The cytotoxicity profile of B-381 in both normoxia and hypoxia is analogous to routinely studied BPA, and concentrations up to 100 μM can be studied with minimal cytotoxicity (**Figure 17**). Additionally, B-381 exhibited a superior cytotoxic profile compared to BSH, which has an IC_{50} value of 2.5 μM (130).

While BPA and BSH are the most extensively studied BNCT agents, their suboptimal T/N ratios observed in patients (usually $\text{T/N} < 3$) limits the efficacy of BNCT (93). An ideal BNCT agent would have minimal systemic cytotoxicity, and most importantly, selective tumor accumulation with a T/N ratio of 3:1 or greater (1-4, 6, 8-10). *In vitro* cellular uptake studies demonstrate that B-381 selectively accumulated in a hypoxic tumor environment. Specifically, B-381 accumulated 4.1-fold higher in hypoxic D54 and 8.6-fold higher in hypoxic U87 cells compared to their normoxic controls (**Figure 18 C**). Additionally, compared to HT22, cellular uptake of B-381 in hypoxic D54 and U87 translated into T/N ratios of 4.4 and 5.3, respectively. On the other hand, the clinically used compound BPA showed very low uptake of boron in the cells, and showed poor tumor selectivity (**Figure 18 E**). The level of B-381 tumor selectivity satisfies requirements for effective BNCT and should be adequate to minimize off-target side

effects to normal brain cells. Furthermore, the tumor selectivity of B-381 is higher than clinical T/N ratios achieved with BPA and BSH, which commonly have a T/N ratio between 0.7 – 3.6 (11, 14, 19, 27, 31, 35).

Intra-tumoral injection of B-381 *in vivo* showed that it was selectively retained in the tumor significantly longer than BPA. While tumor boron levels were almost undetectable in the tumor at 24 and 48 h post-injection of BPA, B-381 had significantly longer tumor retention with values at 24 h similar to boron levels at 8 h (**Figure 20 A**). These results may be a direct result of B-381 forming intracellular protein conjugates in the hypoxic tumor microenvironment, which would be consistent with the *in vitro* results and with the known mechanism of 2-nitroimidazole compound accumulation. The long-term retention of B-381 can offer a clinical advantage compared to BPA, providing a longer therapeutic window for neutron irradiation.

In addition to the selective tumor retention, the tumor/blood ratio is an important factor to demonstrate selective uptake in the tumor and prevent damage to normal blood vessels during BNCT. To determine the tumor/blood ratio of B-381, mice received an *i.v.* injection of B-381 and boron levels were detected in the tumor and blood 24 h post-injection. We found that B-381 accumulated in the tumor against the concentration gradient, in which the tumor boron level was about 3-fold higher than the blood. These findings again indicate that B-381 is a good candidate for use in BNCT. However, we observed relatively low levels of tumor boron accumulation following *i.v.* injection of B-381, which can be attributed to fast elimination of the drug from the plasma. Therefore, we performed a pharmacokinetic analysis of B-381 following *i.v.* injection which found that it was quickly eliminated from the plasma ($T_{1/2} = 2.09$ h). Thus, it is not surprising that the tumor boron content was lower following the *i.v.* injection. This is a classic drug delivery problem, where a drug is effective in the tumor environment but suffers from poor

pharmacokinetics. Therefore, to maximize its anti-tumor efficacy, B-381 can benefit from a drug delivery system that reduces pharmacokinetic elimination and improves tumor delivery. This will be explored further in Chapter 3.

2.6 Conclusions

In conclusion, we have reported the synthesis and preliminary biological evaluation of B-381 as a novel agent for BNCT. B-381 had minimal cytotoxicity, preferentially accumulated in hypoxic cells, and demonstrated longer tumor retention in an *in vivo* glioma model compared to BPA. It achieved significant tumor/normal tissue ratios as well as tumor/blood ratios which satisfy the requirements for selective and successful BNCT. However, due to the shorter half-life of B-381, the free administration of B-381 could benefit from frequent dosing intervals or continuous infusion in future studies. B-381 presents a new class of BNCT agents in which their selectivity to tumors is based on tumor metabolism and biology. Future studies are warranted to synthesize similar compounds with better pharmacokinetics, or for the development of drug delivery systems to improve boron delivery to the tumor environment.

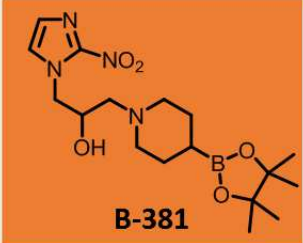


2.7 Future Directions - Synthesis of multi-boronated derivatives B-346 and B-403

Improving *in vivo* tumor boron delivery can be accomplished using two strategies. The first strategy includes optimizing delivery of B-381 with a drug delivery system. B-381 will be incorporated into a thermal sensitive liposome, and hyperthermia will be used to trigger local release in the tumor. This will be the focus of Chapter 3.

The second strategy is to investigate multi-boronated 2-nitroimidazole derivatives. Multi-boronated 2-nitroimidazole derivatives will have the potential to deliver a higher boron payload

per molecule. Two additional multi-boronated derivatives have been synthesized for future studies in the laboratory (Table 2).

Table 2. Synthesized mono- and multi-boronated 2-nitroimidazole derivatives for BNCT studies.

Boronated 2-nitroimidazole derivatives for BNCT			
Boron Atoms per Molecule	1 boron atom	10 boron atoms	10 boron atoms
Synthetic Steps	1 step	1 step	3 steps

The first multi-boronated derivative B-346 would increase the boron payload to 10 boron atoms per molecule, compared to just a single boron atom in B-381. A simple one-step synthesis was devised. Commercially available m-carborane-1-thiol will undergo a nucleophilic substitution reaction with 1-(2,3-Epoxypropyl)-2-nitroimidazole (Figure 21). After reacting in ethanol at room

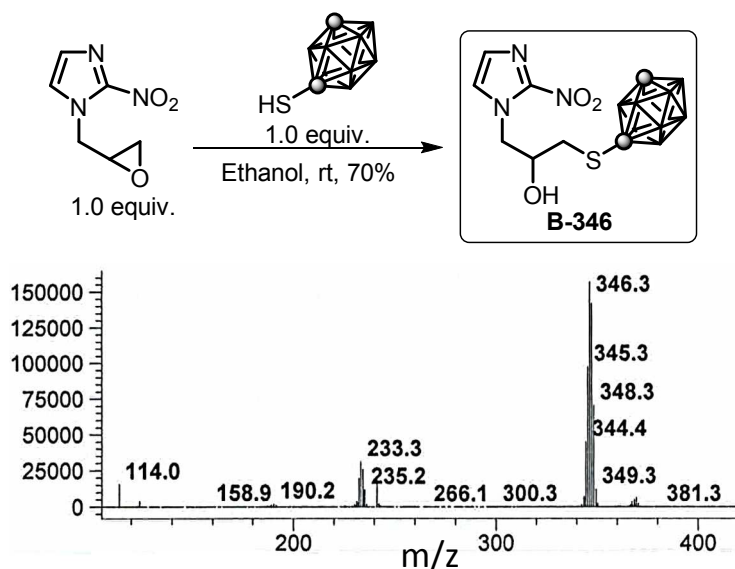


Figure 21. Synthesis of B-346. Synthesis (top) and LC-MS (bottom) of multi-boronated derivative B-346. For clarity, gray spheres in the carborane cage are carbon, while remaining atoms are boron.

temperature, the desired product B-346 precipitated overnight and is readily isolated by filtration. A unique isotope signature is present in the mass spectrum due to the abundance of boron-10 and boron-11 isotopes (**Figure 21**). $^1\text{H-NMR}$ is consistent with the B-346 structure, which contains 1 pair of aromatic protons (consistent with the 2-nitroimidazole ring) and a broad multiplet resulting from the carborane cage protons (**Supplementary Figure 8**).

A second multi-boronated agent B-403 was envisioned. This derivative introduced an amine linker connecting the carborane moiety to the nitroimidazole scaffold. The proposed synthesis of B-403 consisted of 3 steps (**Figure 22**). The presence of the amine functional group could facilitate drug loading in the future by improving water solubility.

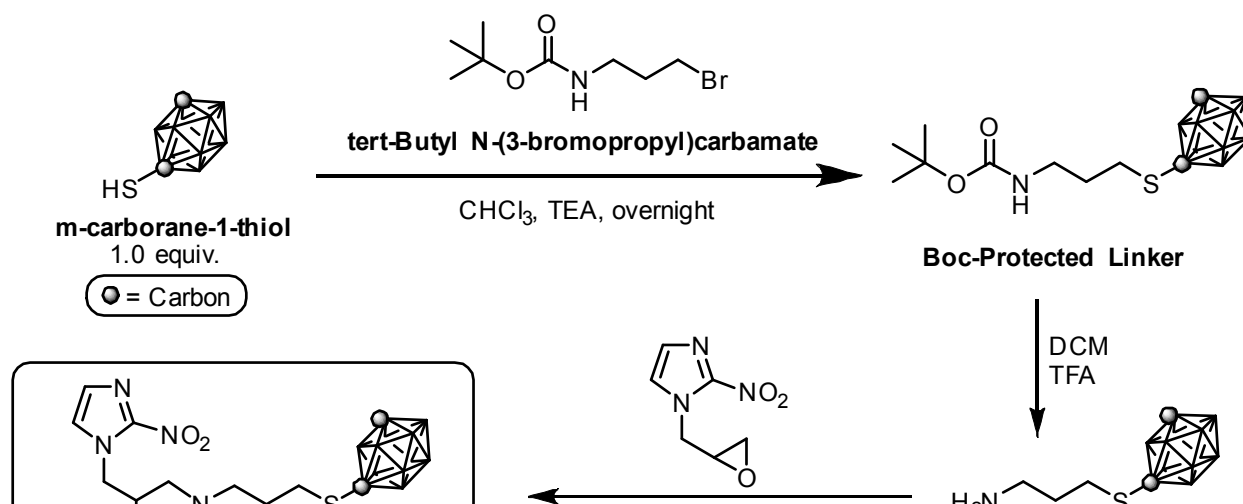


Figure 22. Synthetic route for B-403. Overview of multi-boronated derivative B-403 synthetic route. For clarity, gray spheres in the carborane cage are carbon, while remaining atoms are boron.

The synthetic route to B-403 is slightly more challenging since the starting materials are not UV active at 254 nm and cannot readily be monitored by thin layer chromatography. Therefore, reactions were monitored using LC-MS (Gradient of 5/95 acetonitrile:water (0.05% TFA) to 95/5 over 5 minutes with a 1 minute hold at the end on a C18 column). The first step of the synthesis is

a nucleophilic substitution reaction with *m*-carborane-1-thiol and *tert*-Butyl *N*-(3-bromopropyl)carbamate to form a Boc-protected linker (**Figure 23 a**). The resulting Boc-protected linker is produced in near quantitative yield. Triethylamine (TEA) and overnight conditions are needed for the complete consumption of *tert*-Butyl *N*-(3-bromopropyl)carbamate starting material. After reacting several hours, the presence of unreacted *tert*-Butyl *N*-(3-bromopropyl)carbamate

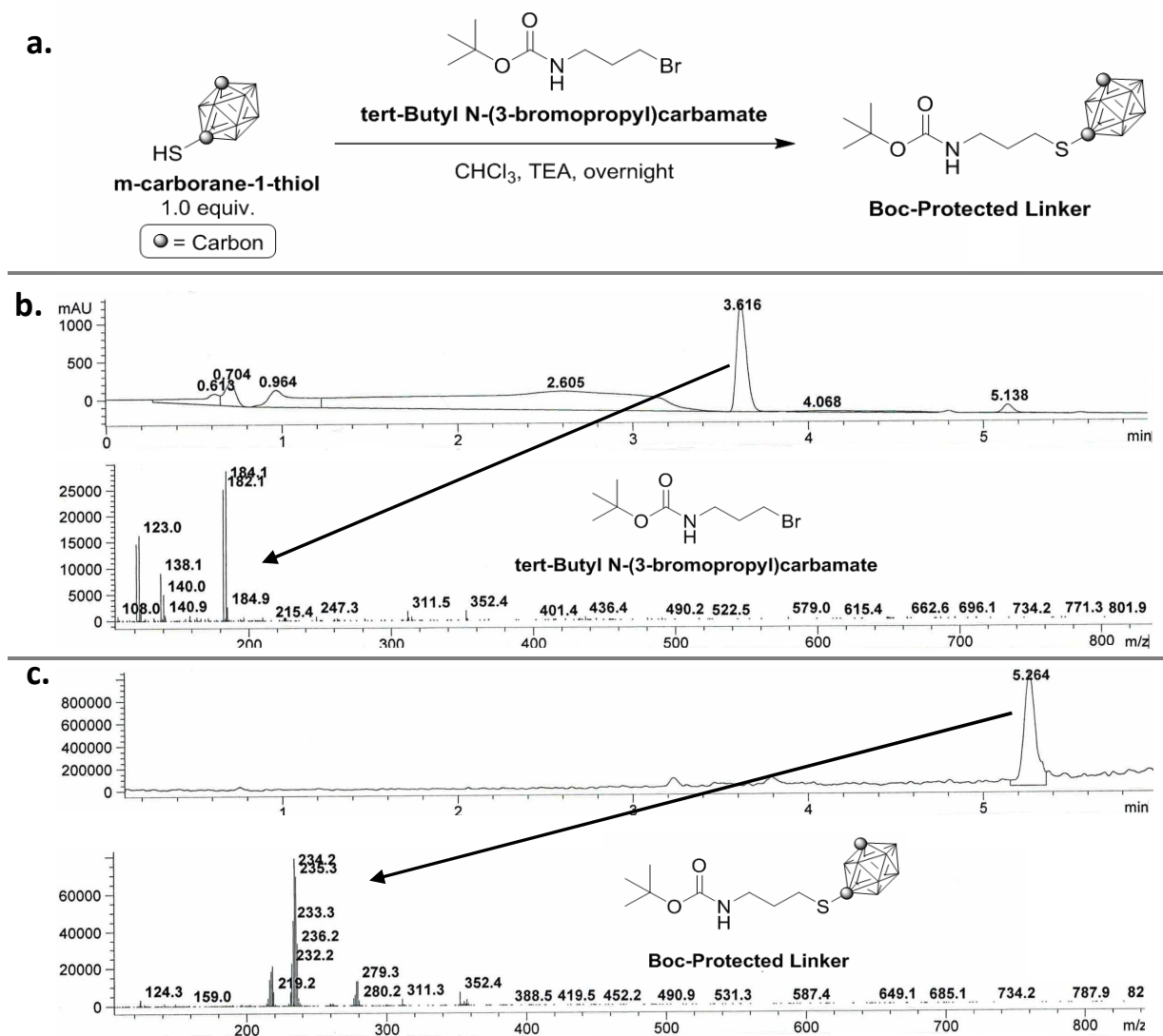


Figure 23. Synthesis of Boc-protected linker for B-403 synthesis: **a.)** Reaction conditions for synthesis of Boc-protected linker. **b.)** Several hours after starting reaction there is unconsumed starting material by LC-MS. *Tert*-Butyl *N*-(3-bromopropyl)carbamate has a retention time of 3.6 minutes and characteristic bromine isotope pattern. **c.)** The product has a retention time of 5.2 minutes and a complex bromine isotope pattern resulting from 10 boron atoms (note parent compound *m/z* 334.5 not observed due to fragmentation and loss of *t*-butyl (-57) and CO₂ (-44)).

starting material can readily be identified by its characteristic bromine isotope pattern (**Figure 23 b**). When the reaction is complete, the major peak on the HPLC chromatogram has a retention time of 5.2 minutes with a complex bromine isotope pattern produced by 10 boron atoms (**Figure 23 c**). Notably, the desired product $m/z = 334$ is not observed on the LC-MS. This is a result of the easily fragmented Boc protecting group, which upon ionization will fragment and lose t-butyl (-57 mass units) and CO_2 (-44 mass units). Therefore m/z peaks of 277 and 233 are present due to the loss of CO_2 and t-butyl from the parent compound.

After synthesis of the Boc-protected amine linker, the Boc group was removed by using excess trifluoroacetic acid (60 equivalents) in dichloromethane (**Figure 24 a**) in quantitative yield.

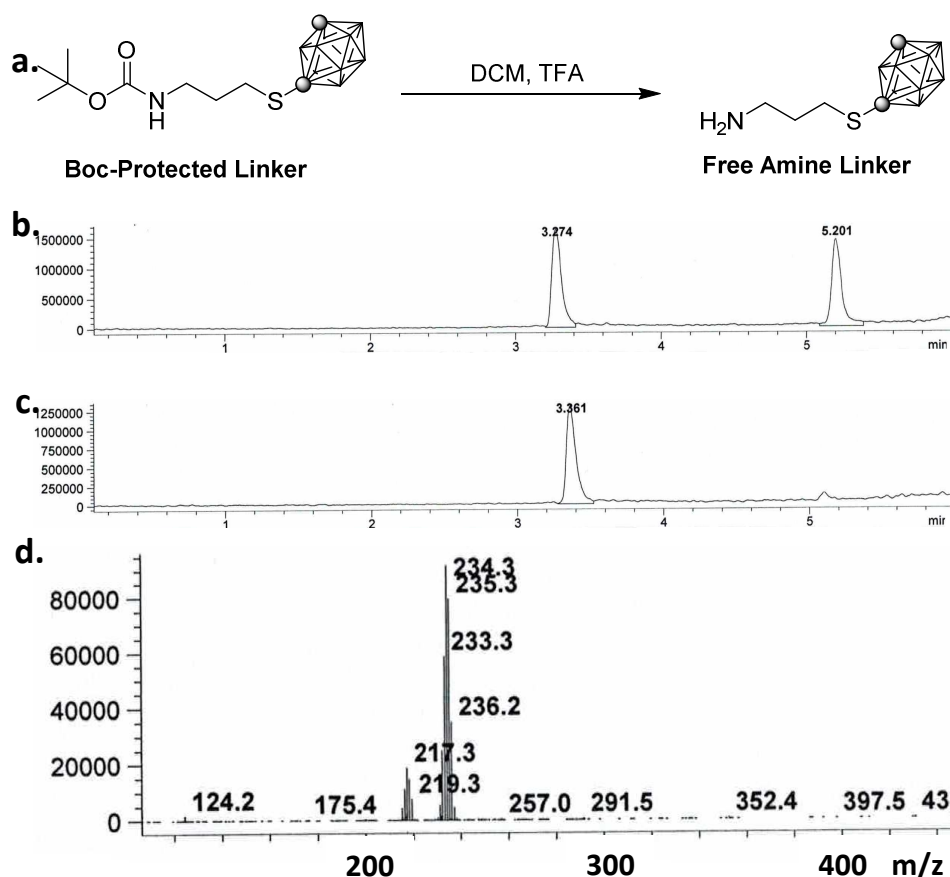


Figure 24. Synthesis of free-amine linker for B-403 synthesis. a.) Boc-deprotection of amine linker is 2nd step of B-403 synthesis. **b.)** LC-MS of incomplete deprotection. **c.)** LC-MS of completed deprotection. **d.)** Both starting material (Boc-protected linker) and product (free amine linker) have predominant peak of $m/z = 233$, but the peak $m/z = 277$ is only present from fragmentation of the Boc group.

While the Boc-protected starting material has a retention time of 5.2 minutes, the free amine product has a new retention time of 3.3 minutes (**Figure 24 b, c**). However, both of these compounds will have the predominate peak $m/z = 233.3$ present. Upon closer examination, the free amine linker mass spectrum does not have a peak at $m/z = 277$ (**Figure 24 d**). The presence of this peak is only generated due to fragmentation of the *t*-butyl group which is only present in the starting material. It is also logical that the free amine (more polar) will travel faster through a reverse phase column.

The final step of the B-403 synthesis utilized the free amine linker to open the epoxide functional group of the 2-nitroimidazole (**Figure 25 a**). The reaction was allowed to reflux in a minimal amount of chloroform overnight. The desired product B-403 should actively absorb at 254 nm due to presence of an aromatic system. The HPLC chromatogram of the crude reaction mixture revealed an asymmetric tail to the peak found at 3.3 minutes (**Figure 25 b**). The presence of both $m/z = 233$ and $m/z = 403$ at this retention time indicated that residual starting material (free amine) and product traveled similarly through the column (**Figure 25 c**). The reaction mixture was purified using normal phase column chromatography (10% methanol in dichloromethane), and the resulting LC-MS indicated pure B-403 (**Figure 25 d**). The structure was also confirmed by $^1\text{H-NMR}$ spectroscopy (**Supplementary Figure 9**).

Future studies with multi-boronated derivatives B-346 and B-403 have the potential to greatly increase tumor boron content. This is achievable because each molecule delivers 10 boron atoms, compared to just a single boron atom for B-381 or BPA. Future *in vitro* and *in vivo* studies can assess delivery of these agents as either a free drug or encapsulated into a thermal sensitive liposome.

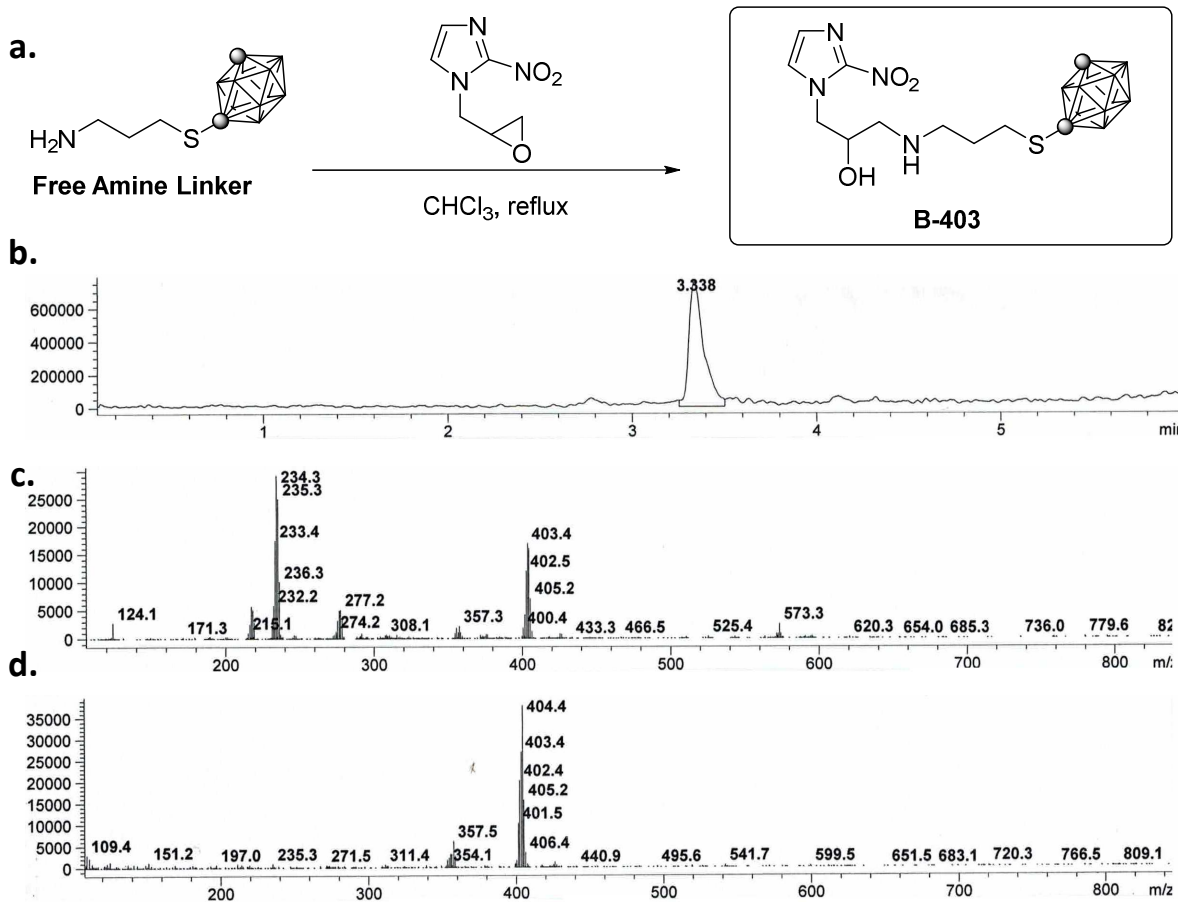


Figure 25. Final synthetic step for B-403 synthesis. a.) Final reaction of B-403 synthesis. **b.)** HPLC chromatogram of B-403 reaction mixture before column chromatography. Note that starting material and product have an identical retention time of 3.3 minutes indicated by the asymmetric tail on mass spectrometry chromatogram **c.)** Before column purification, the crude reaction mixture contained a mixture of free amine starting material ($m/z = 233.5$) and desired product ($m/z = 403$). **d.)** After column purification only the desired product $m/z = 403$ was present.

Chapter 3: Investigation of Thermal Sensitive Liposomes for improving delivery of boronated agents

3.1 Introduction

Chapter 2 highlighted that initial *in vivo* studies with intra-tumoral injection of B-381 demonstrated a long-term retention (9.5-fold higher at 24 hours) compared to an equimolar dose of BPA (**Figure 20 A**). When D54 glioma cells were sorted into normoxic (low pimonidazole uptake) and hypoxic (high pimonidazole uptake) populations, B-381 had a 13.2-fold higher drug concentration in hypoxic cells compared to normoxia. However, *in vivo* studies with *i.v.* administration of B-381 resulted in lower tumor boron concentration (~100 ppb, **Figure 20 B**). A follow up pharmacokinetic study verified that B-381 is cleared from the plasma rather quickly with a 2 hour half-life (**Figure 20 C**). To improve delivery of B-381, thermal sensitive liposome (TSL) formulations were investigated for two reasons: 1.) to enhance the plasma half-life of B-381 and 2.) to improve tumor boron content via localized drug release triggered by hyperthermia.

3.1.1 History of Thermal Sensitive Liposomes

Liposomes are closed phospholipid bilayers that have long been recognized for their ability to improve drug delivery while minimizing off target cytotoxicity. Recently thermal sensitive liposomes have been designed to have a stable drug payload at physiologic temperature (37°C) but engineered to have high permeability under mild hyperthermia (42-43°C). Administration of a thermal sensitive liposome will enhance drug delivery to a hyperthermic region due to increased blood flow, improved vascular permeability and localized drug release at the tumor site (131). Additionally, hyperthermia will improve tissue diffusion which is traditionally restricted from high interstitial fluid pressure (this is even more pronounced when a tumor is confined to the cranium like glioblastoma).

The use of TSLs is an emerging field, with doxorubicin loaded TSLs being one of the more thoroughly studied systems (135, 136). ThermoDox (Celsion) is a TSL formulation of doxorubicin currently in Phase III clinical trials for non-resectable hepatocellular carcinoma. Patients with a single, 3-7 cm lesion treated with radiofrequency ablation (temperatures > 42°C) + ThermoDox showed a 2.1 year higher overall survival compared to patients only receiving radiofrequency ablation (Figure 26).

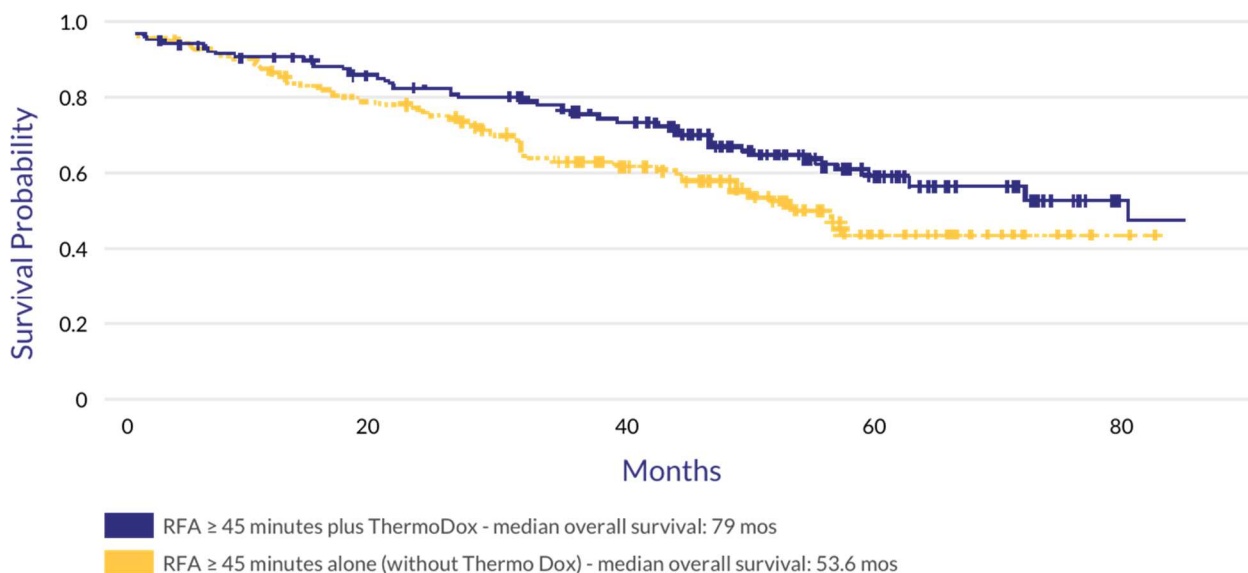


Figure 26. Benefit of ThermoDox added to radiofrequency ablation (RFA). Subgroup analysis of ThermoDox Phase II clinical trial demonstrated increase in overall survival. Figure from <http://celsion.com/thermodox/>.

3.1.2 Mechanism of TSL Drug Release

Thermal sensitive liposomes are designed to have highest permeability in a mild hyperthermic range (41-43°C). Previously reported doxorubicin TSL formulations consisted of a 80:15:5 molar ratio of DPPC/DSPC/DSPE-PEG₂₀₀₀ (135). The TSL permeability and subsequent release of hydrophilic drugs is highest under mild hyperthermia (41-43°C) because the major component of the liposome formulation, DPPC, has a melting phase transition temperature (T_m) of 41.4 °C (137). This represents the phase transition of the phospholipid going from a solid gel-like state to a more

disordered liquid-crystalline state (135, 136). The molar ratio of phospholipids and their respective T_m values will affect the membrane permeability at a given temperature. In this previously reported doxorubicin formulation, DSPC ($T_m = 54.9\text{ }^\circ\text{C}$) is added to minimize baseline release at physiological temperature (37°C), and DSPE-PEG₂₀₀₀ increases blood circulation time by decreasing uptake by the reticuloendothelial system (137).

When TSLs are incubated at temperatures below the T_m , the membrane has low permeability, and hydrophilic drugs in the aqueous core will not be significantly released. This is because at the lower temperature, the phospholipids are in a more ordered state and it is difficult for a hydrophilic drug to pass through a hydrophobic bilayer (**Figure 27**, left panel). The maximum permeability of the TSL occurs when the temperature = T_m (**Figure 27**, center panel). At T_m , there is a significant

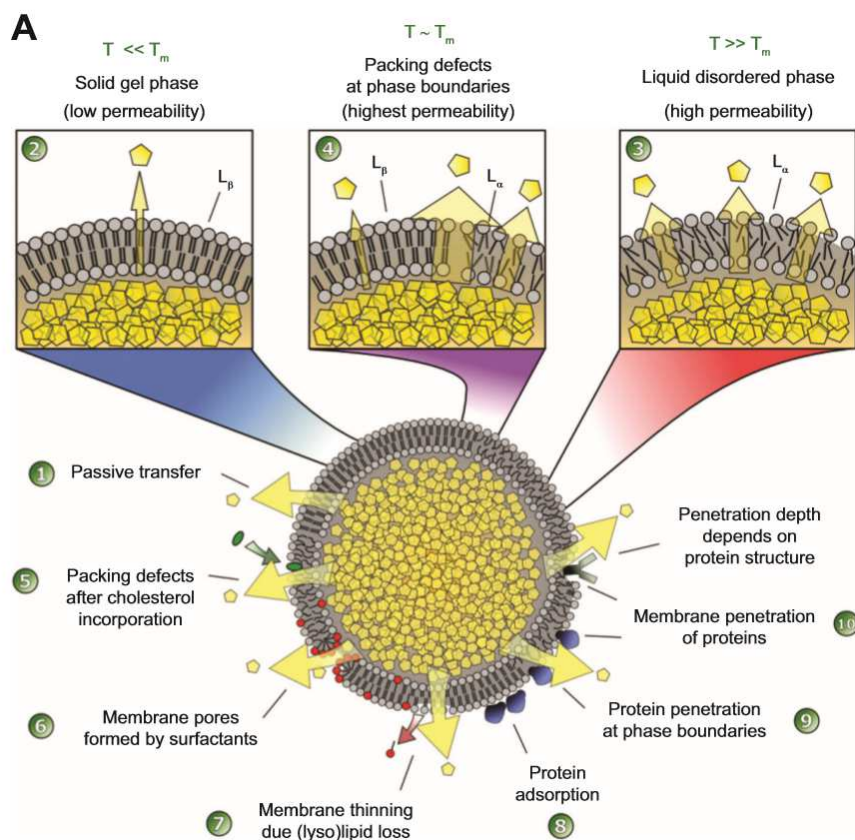


Figure 27. Temperature dependence of thermal sensitive liposome permeability. Thermal sensitive liposomes have the highest permeability at a temperature equal to the phase transition temperature T_m of the major phospholipid component of the formulation. Figure adopted from (135, 136).

phase transition from the gel-like state to the liquid-crystalline state. This creates packing defects in the liposome membrane, which creates pores for maximal drug release (135, 136). Although counterintuitive, increasing the temperature above T_m does not increase permeability further (**Figure 27**, right panel). At higher temperatures, the packing defect at phase boundaries (gel-like versus liquid-crystalline) is diminished.

3.1.3 Passive and Active Drug Loading of TSLs

Drugs may be incorporated into either the liposome phospholipid bilayer or the aqueous core. Drugs that are lipophilic are suitable for incorporation into the lipid bilayer which is mediated by van der Waals forces (the presence of substituents such as long alkyl chains can further enhance bilayer incorporation). Drugs that are loaded into the aqueous core may be loaded via passive or active processes (136). Passive drug loading is diffusion driven, whereas active drug loading allows accumulation of a drug against its concentration gradient (**Figure 28**). A nice illustration provided by Kneidl *et al* outlines the active loading of doxorubicin compared to the passive loading of gemcitabine into liposomes. Using an established pH gradient across the liposome bilayer (aqueous core pH = 4, bulk solution pH = 7), the amine functional group of doxorubicin will be neutral at pH = 7 but will become protonated at pH = 4. The protonation of doxorubicin has a two-fold effect (**Figure 28**). First, the protonated, charged drug will no longer be able to freely diffuse across the liposome bilayer, so it is essentially trapped inside. Second, the protonated form of doxorubicin is removed from the equilibrium equation (Le Chatelier's principle) which allows additional diffusion of another free amine form of doxorubicin into the liposome. This is the key component that allows doxorubicin to accumulate against its concentration gradient. In comparison, passive loading of a drug such as gemcitabine is diffusion limited (**Figure 28**). Since

gemcitabine freely diffuses across the liposome bilayer, the concentration will equilibrate and depend on the bulk solution concentration.

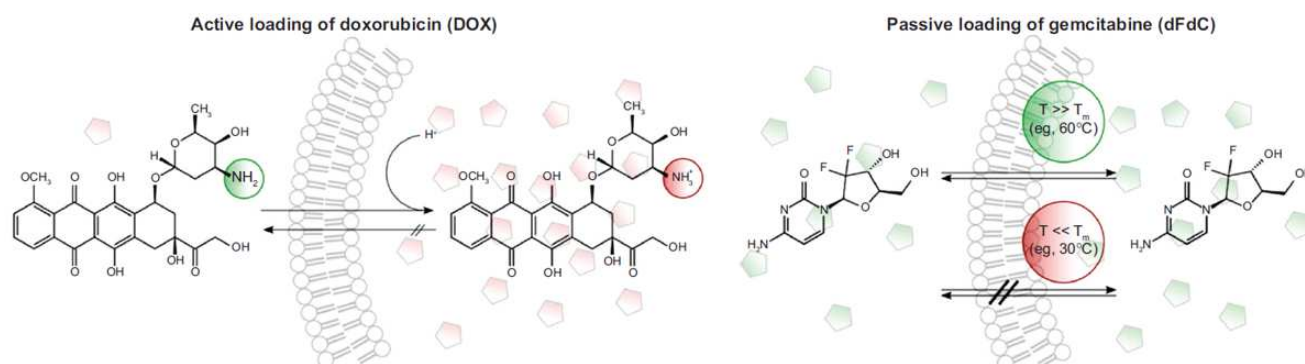


Figure 28. Active and passive drug loading of liposomes. Liposomal drug loading can be an active or passive process. Active loading of doxorubicin against its concentration gradient (left) and passive loading of gemcitabine which is diffusion limited (right)(136).

3.2 Hypothesis - First Application of TSLs in BNCT

The most extensively evaluated agent in BNCT clinical trials is 4-borono-L-phenylalanine (BPA), commonly administered intravenously as a BPA fructose adduct (BPA-f). This boronated phenylalanine derivative has minimal systemic cytotoxicity but has limited ability to accumulate preferentially in a tumor (usually a tumor/normal tissue ratio < 3) (138). The hurdle of optimal tumor drug delivery has long been recognized in the BNCT field and numerous strategies to improve delivery such as nanoparticles, liposomes, and monoclonal antibodies have shown promise (138). Chapter 2 presented the synthesis and evaluation of B-381, which is able to target the hypoxic (and often therapy resistant) glioma tumor microenvironment (139). In a hypoxic microenvironment ($pO_2 < 10$ mm Hg) 2-nitroimidazole derivatives form intracellular protein conjugates leading to preferential accumulation (124, 125).

Despite the development of liposomal formulations for BNCT (137), to date, the efficacy of thermal sensitive liposomes (TSLs) have not been evaluated in the BNCT field. Based on successful drug candidates like ThermoDox, in addition to the well-known benefit of liposomal drug formulations, we hypothesized that a thermosensitive liposome containing BPA-f will have

superior drug delivery compared to free drug. Transient induction of mild hyperthermia (42 °C) at the tumor site will promote local liposomal drug release from a thermal sensitive liposome. Furthermore, we hypothesized that delivery of previously reported B-381 would have superior long-term tumor retention compared to BPA-f due to the unique intracellular protein conjugation common to 2-nitroimidazole derivatives.

3.3 Materials and Methods

3.3.1 Reagents

All chemical reagents were purchased from Sigma Aldrich (St. Louis, MO) unless explicitly stated otherwise. 2-nitroimidazole derivative B-381 was synthesized in house (139). Phospholipids 1,2-dipalmitoyl-sn-glycero-3-phosphocholine (DPPC), 1,2-distearoyl-sn-glycero-3-phosphocholine (DSPC), and 1,2-distearoyl-sn-glycero-3-phosphoethanolamine-N-[amino(polyethylene glycol)-2000] (ammonium salt) (DSPE-PEG₂₀₀₀) were purchased from Avanti Polar Lipids (Alabaster, AL). BPA fructose adduct (BPA-f) was prepared fresh according to a previously published protocol before liposome loading (140).

3.3.2 Liposome Synthesis and Characterization

General Liposome Synthesis: Liposomes were prepared using thin-film hydration followed by microextrusion at 60°C (Avanti Mini Extruder)(**Supplementary Figure 10**). To prepare lipid films, the desired phospholipid formulation (60 total mg) was dissolved in 5 mL chloroform and concentrated on a rotatory evaporator at 40°C at 280 revolutions per minute. It is imperative that the lipid film is kept under vacuum for a minimum of 20 minutes before removing (residual chloroform vapors will dissolve lipid film). The dry lipid film is then rehydrated for 1 hour at 280 rpm (60°C) with the desired pre-warmed buffer (see below). Following rehydration, each liposome

mixture is microextruded at 60°C using 200 nm and 100 nm polycarbonate membranes sequentially. Liposome suspensions were ultracentrifuged at 39,000 rpm for 2 hours (4°C) and resuspended in 150 mM NaCl and 20 mM HEPES solution (pH = 7 adjusted with NaOH). Average particle size, polydispersity index and zeta potential were determined by dynamic light scattering measurements (Malvern Zetasizer Nano ZS). Encapsulation efficiency was determined by doxorubicin fluorescence intensity or ICP-OES boron analysis.

Doxorubicin Loaded TSL (Dox-TSL): A cholesterol-free (0 mole %) doxorubicin TSL (Dox-TSL) was prepared according to previously reported molar ratio of 80:15:5 DPPC/DSPC/DSPE-PEG₂₀₀₀ respectively (135). Additionally, a novel doxorubicin loaded non-thermal sensitive liposome (Dox-Non-TSL) was synthesized with a 0:95:5 DPPC/DSPC/DSPE-PEG₂₀₀₀ molar ratio to serve as a temperature-independent liposome control. Doxorubicin was actively loaded using a pH gradient method. For doxorubicin TSLs, the lipid film was rehydrated for 1 hour at 280 rpm (60°C) with 5 mL of 300 mM sodium citrate (adjusted to pH = 4 with HCl). After synthesizing Dox-TSL containing sodium citrate buffer (pH=4), the TSLs are ultracentrifuged and resuspended in 1 mL of HEPES buffer (pH = 7) containing doxorubicin (1 mg/mL) and incubated for 1 hour at 39°C. Doxorubicin encapsulation efficiency was determined from doxorubicin fluorescence intensity in supernatant compared to a volume normalized resuspension of Dox-TSL.

B-381 Loaded TSL (B-381-TSL): B-381 loaded TSLs containing 0, 10, 20 and 30 mole % cholesterol (B-381-TSL) with DPPC/DSPC/DSPE-PEG₂₀₀₀/cholesterol molar ratios of 80:15:5:0, 71:14:5:10, 64:12:4:20, 56:10:4:30, respectively, were also evaluated. B-381 drug loading with passive and active techniques was investigated. Passive drug loading was attempted using two methods. This first method dissolved B-381 (1 or 5 mg) along with the phospholipids in

chloroform during lipid film preparation, which was then rehydrated with PBS. The second and more successful method resuspended the lipid film with a 300 mM sodium citrate (pH=4) solution containing 40 mg/mL of B-381. Active drug loading of B-381 was also investigated using the previous doxorubicin pH gradient loading method. For this, the lipid film was rehydrated for 1 hour at 60°C with sodium citrate buffer (pH = 4), microextruded, ultracentrifuged and then resuspended in HEPES buffer (pH = 7) containing 3 mg/mL of B-381. After incubating for 1 hour at 39°C, the liposomes were ultracentrifuged and resuspended in drug-free HEPES. To determine B-381-TSL encapsulation efficiency, ICP-OES was used to determine volume normalized boron content in the resuspended liposomes compared to the removed supernatant boron level from the various methods.

BPA-f Loaded TSL (BPA-f-TSL): BPA-f loaded TSL (BPA-f-TSL) containing 0 or 10 mole % cholesterol with DPPC/DSPC/DSPE-PEG₂₀₀₀/cholesterol molar ratios of 80:15:5:0 and 71:14:5:10 were synthesized. A non-thermal sensitive liposome loaded with BPA-f (BPA-f-Non-TSL) was synthesized with a 0:85:5:10 DPPC/DSPC/DSPE-PEG₂₀₀₀/cholesterol molar ratio to serve as a negative control. For BPA-f TSL, only a passive drug loading technique was investigated. Using 1 mL of a freshly prepared BPA-f solution (30 mg/mL in pH = 7 water) (140), the lipid film was resuspended for 1 hour at 60°C. After microextrusion and ultracentrifugation, the liposome was resuspended in drug-free HEPES (pH=7). Encapsulation efficiency was also determined using ICP-OES boron analysis.

3.3.3 Determining Doxorubicin TSL Content

A calibration curve of doxorubicin standards was prepared. Doxorubicin fluorescence intensity was determined using a plate reader (Excitation: 482 nm; Emission: 594 nm). Fluorescence

intensity of resuspended Dox-TSL was compared to a volume normalized fluorescence intensity of the residual supernatant from the drug loading method.

3.3.4 Determining Boron Content in TSLs or Tissue

For water bath and HIFU release experiments, boronated drug release from thermal and non-thermal liposome formulations was analyzed using Inductively Coupled Plasma Optical Emission Spectrometry (ICP-OES, Optima 7300 V series, Perkin Elmer, Waltham, MA). Dialysate sample aliquots were diluted with 18 megaohm water and contained 5% nitric acid (v/v). Samples were analyzed for boron content ($\lambda = 249.677$ nm) against a calibration curve of boron standards in 5% nitric acid between 0 and 250 parts per billion (ppb) prepared from a 10 parts per million boron standard solution (Inorganic Ventures, Christiansburg, VA). For *in vivo* experiments, tumor and organs were resected, weighed, and digested using a MARS 6 Microwave Digestion System (CEM Corporation, Matthews, NC). All samples were then brought to a normalized final volume of 4 mL containing 5% nitric acid (v/v). Control organs were utilized to establish baseline signal for each organ type, and final reported boron levels were normalized to organ mass.

3.3.5 Water bath release experiments

In general, 500 μ L aliquots of liposome stock solution were transferred inside of a 14 kDa Dialysis Membrane (6.4 mm x 10 mm, Ward's Science, ON, Canada). The dialysis bag was placed in 50 mL of PBS buffer at either 37°C or 42°C and 100 μ L aliquots were collected at various time points (**Supplementary Figure 11**). The dialysate aliquots were resuspended to a final volume of 3 mL in 5% nitric acid and analyzed for boron content by ICP-OES. The dialysis bag contents were mixed into the bulk volume at the end of the experiment and used as a 100% control to determine % release.

3.3.6 HIFU release experiments

A small cylindrical plexiglass chamber was designed in house capable of holding 500 μL of liposome solution without attenuating ultrasound waves (**Supplementary Figure 12 A**). The top and bottom cylindrical opening was sealed with Tegaderm allowing transmission of HIFU waves through the sample chamber while retaining sample volume. The sample chamber was completely filled without air bubbles, and was submerged in a degassed water bath. The HIFU focus was aligned directly in the center of the chamber, and real-time thermocouple measurements of sample chamber verified mild hyperthermia (42-43° C) was maintained during a 10, 30 or 60 minute treatment period (**Supplementary Figure 12 B**). Following treatment, the 500 μL liposome aliquot was removed, centrifuged at 39,000 rpm, and the resulting liposome pellet and supernatant were volume normalized and boron content was determined by ICP-OES for determining percent drug release

3.3.7 In Vivo Tumor Implantation

Approval for all animal studies was obtained from the Ethical Committee for Animal Experiments at Washington University in St. Louis Medical School. D54 Glioma cell line was a kind gift from Dr. Dinesh Thotala (Department of Radiation Oncology, Cancer Biology Division, Washington University in Saint Louis School of Medicine). Prior to *in vivo* implantation, cells were cultured in Dulbecco's Modified Eagle's Medium (DMEM, Corning CellGro, Mediatech, Manassas, VA) supplemented with 20% fetal bovine serum (FBS, Gibco, Life Technologies, Grand Island, NY), 2 mmol/L of L-glutamine, 100 U/mL Penicillin and 100 $\mu\text{g}/\text{mL}$ Streptomycin (CellGro, Mediatech, Manassas, VA).

Prior to *in vivo* implantation, cells were washed with phosphate-buffered saline (PBS, Corning CellGro, Mediatech, Manassas, VA), trypsinized with 0.05% Trypsin-EDTA 1x (Gibco, Life

Technologies, Grand Island, NY), spun for 5 minutes (1000 RPM) and resuspended in fresh DMEM media and Matrigel (Corning) according to manufacturer protocol. Athymic Nude-Foxn1^{nu} mice (N=10, female, 6 weeks old) obtained from Envigo (Indianapolis, IN) were anesthetized with ketamine/xylazine and bilaterally injected with Matrigel solution under the skin of each hindlimb (two injections per mouse, 1.5×10^6 D54 cells per tumor). Mice were grown to an average tumor size of 300 mg and were clearly palpable to facilitate isolated heating of just 1 tumor per mouse.

3.3.8 *In Vivo* Comparison of BPA-f, BPA-f-TSL and BPA-f-Non-TSL with or without hyperthermia

The mice were split into control (N=1) or 3 treatment groups: BPA-f free drug (N=3), BPA-f-TSL (N=3) or BPA-f-Non-TSL (N=3). Mice were anesthetized and positioned under tygon tubing (Inner Diameter = 0.375 inches) connected to a water bath circulator maintained at 43°C with a high flow rate (**Supplementary Figure 13 A**). The tygon tubing contained a series of three 1 cm² openings sealed with a single layer of TegadermTM (3M) to facilitate heat transfer while preventing leaks (**Supplementary Figure 13 B**). This facilitated heating 3 mice simultaneously. Mice were positioned carefully to only heat their left tumor while the right tumor served as control (**Supplementary Figure 13 C**). The variability between mice was minimized since each mouse had a hyperthermia-treated (43°C) and control (37°C) tumor. A thermometer placed against the hyperthermia window remained stable at 42-43°C over the treatment period to validate stable heating and prevent reaching thermoablative temperatures > 45°C. Mice were exposed to a 5 minute pre-hyperthermia heating period prior to tail vein injections of either BPA-f free drug, BPA-f TSL, and BPA-f Non-TSL (normalized to have equimolar boron content). After 30 minutes of hyperthermia exposure, blood was collected and mice were immediately sacrificed for organ

collection. All excised tissues were weighed, digested with microwave digestion system, diluted with deionized water to a final acid concentration of 5% (v/v) for ICP-OES analysis.

3.3.9 *In Vivo* Retention of BPA-f and B-381 TSL Formulations

Twelve (N=12) athymic nude-Foxn1^{nu} mice containing bilateral D54 glioma flank tumors were split into 2 treatment groups receiving equimolar boron injections of either BPA-f TSL (N=6) or B-381 TSL (N=6). All mice were subjected to 5 minutes of hyperthermia, followed by tail vein injection of liposomes and 30 minutes of hyperthermia exposure. For each treatment group, 3 mice were sacrificed immediately after hyperthermia treatment (t = 30 minutes) while 3 mice were not sacrificed for 24 hours post-treatment. Blood and organs were collected, weighed and analyzed by ICP-OES for boron content.

3.4 Results & Discussion

3.4.1 Drug release from Dox-TSL

Before thoroughly studying BPA-f and B-381 TSLs, it was desirable to validate the temperature dependent release from the previously reported Dox-TSLs (135). The release of doxorubicin from Dox-TSL (80:15:5 DPPC/DSPC/DSPE-PEG₂₀₀₀ molar ratio) and Dox-non-TSL (0:95:5 DPPC/DSPC/DSPE-PEG₂₀₀₀ molar ratio) was compared in a dialysis experiment (**Figure 29**). With the omission of DPPC, the Dox-non-TSL formulation should not exhibit a thermal sensitive release since DSPC has a T_m of 54.9°C, well above mild hyperthermia temperatures (therefore permeability will be low, **Figure 27**).

The encapsulation efficiency of doxorubicin using the sodium citrate loading method was 67% for the TSL formulation. Dox-TSL and non-TSL liposome aliquots (500 µL) were transferred to

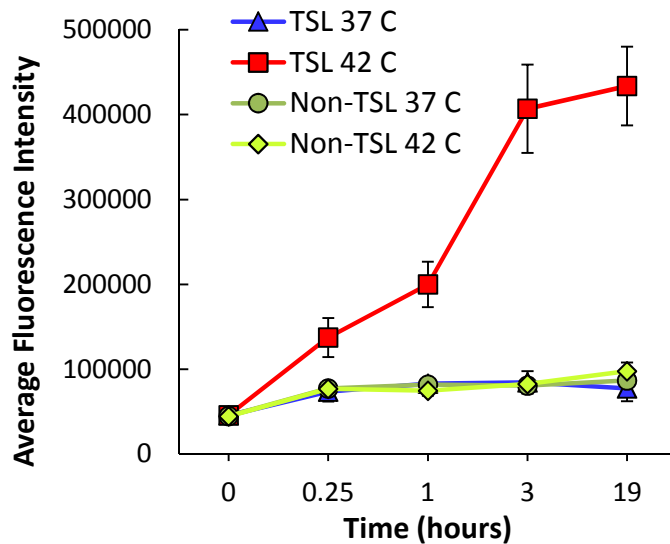


Figure 29. Temperature dependent release of doxorubicin from Dox-TSL and Dox-Non-TSL formulations. Liposome aliquots were incubated in a closed 14 kDa dialysis membrane at 37°C or 42°C.

14 kDa dialysis membranes and incubated at 37°C or 42°C. Doxorubicin release was determined by monitoring average fluorescence intensity in the dialysate at 0.25, 1, 3, and 19 h (**Figure 29**). Doxorubicin fluorescence intensity (λ_{EX} : 482 nm; λ_{EM} : 594 nm) was measured in the dialysate overtime. The Dox-TSL formulation had significant doxorubicin release at 42°C but had minimal release at 37°C. As expected, the non-TSL containing a higher DSPC content eliminated thermal sensitivity and had minimal release at 37°C and 42°C.

Additionally, the thermal effect of heating on liposome size (**Figure 30 a**) and polydispersity (**Figure 30 b**) was evaluated by exposing the Dox-TSL formulation to heating at 21, 37, 42, and 60°C. Liposome particle size and polydispersity remain stable even after heating at 60°C for 1 hour. This data supports that mild hyperthermia causes a transient increase in membrane permeability, but does not significantly cause liposome aggregation or degradation, which would be reflected by changes in average particle size and polydispersity.

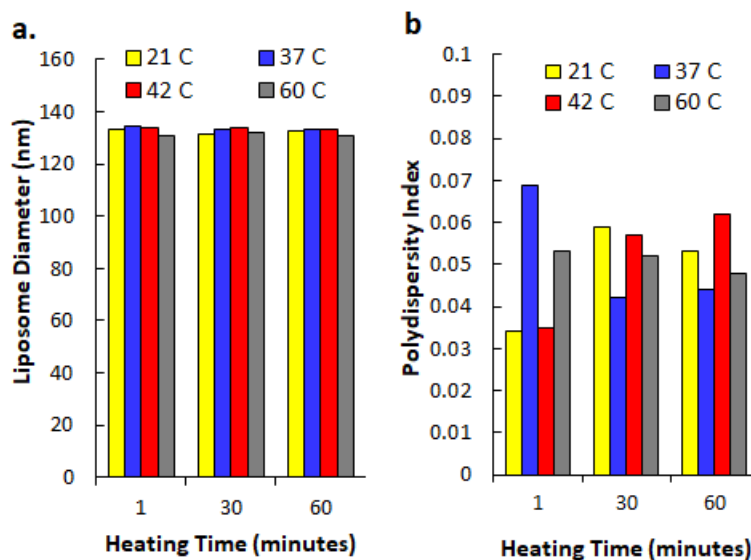


Figure 30. Thermal sensitive liposome size and polydispersity stable with heating. a.) Change in TSL average diameter as a function of heating time at 21, 37, 42 or 60 °C. b.) Change in TSL polydispersity index as a function of heating time at 21, 37, 42 or 60 °C.

3.4.2 Passive Loading of B-381 into TSL Lipid Bilayer

Following synthesis of the preliminary Dox-TSL, various drug loading strategies were investigated to incorporate B-381 into a TSL. To determine B-381 drug loading, the encapsulation efficiency was determined after the TSL synthesis. In general, the liposome mixture was ultracentrifuged, and the supernatant and liposome pellet were volume normalized. Both components were acidified with 5% HNO₃ and boron content was determined by ICP-OES.

Two passive loading methods of B-381 were investigated. First, B-381 was dissolved in chloroform along with the phospholipids during formation of the lipid film. The lipid film was then rehydrated with PBS and B-381 could be passively incorporated into the liposome bilayer. This strategy was not largely successful, and resulted in encapsulation efficiencies of 0.75% and 6.9% (for 1 and 5 mg of B-381 added to lipid film, respectively (**Figure 31**)). Additionally, attempting to dissolve B-381 into PBS subsequently used to rehydrate the lipid film resulted in equally poor encapsulation (0.6%). This is not surprising because of the poor water solubility of B-381. To improve the encapsulation efficiency, active drug loading methods were investigated.

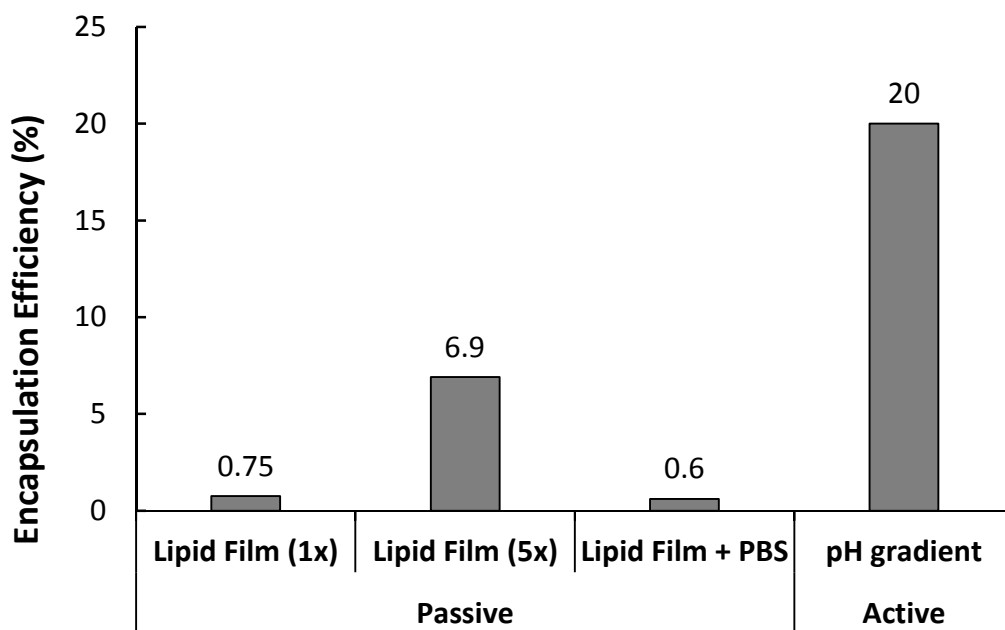


Figure 31. Initial drug loading of B-381 into thermal sensitive liposome. Summary of B-381 passive and active loading encapsulation efficiencies into thermal sensitive liposomes.

3.4.3 Active Loading of B-381 into TSL Aqueous Core with pH gradient

In order to improve B-381 loading efficiency, a pH gradient loading method was utilized (135). To create a liposomal pH gradient, the liposome was synthesized using a sodium citrate buffer adjusted to pH = 4. After centrifugation, the liposome was resuspended in a neutral HEPES buffer (pH = 7.4) which contained B-381. Following incubation at 39°C for 1 hour, an encapsulation efficiency of 20% was obtained, correlating to a boron liposome content of 71 ppb boron/mg of lipid (**Figure 31**). This liposome formulation (B-381-TSL-active) was investigated further with a preliminary *in vivo* pilot study.

In a preliminary pilot study, mice with bilateral subcutaneous D54 glioma tumors were investigated. After *i.v.* tail vein injection of B-381-TSL-active (100 μ L, 644 ng of boron), one tumor was immediately heated with HIFU for 30 minutes, while the contralateral tumor served as a control. Tumors were excised, microwave digested in nitric acid and analyzed by ICP-OES. For both the HIFU treated and control tumor, boron detection was barely above the limit of detection

for the instrument (**Figure 32**). Additionally, the 100 μ L liposome injection was also analyzed as a positive control, and only had a boron signal of 214.7 ppb (644 ng of boron/ 3 g water for analysis). Therefore, the boron payload of the liposome needs to be increased for adequate *in vivo* detection.

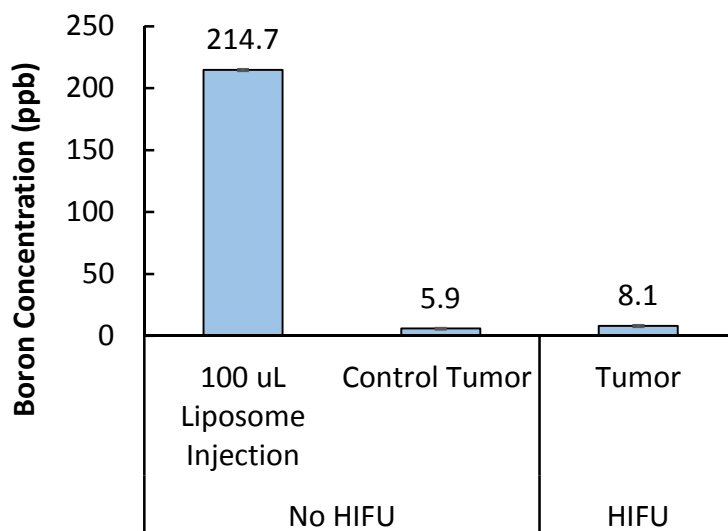


Figure 32. Pilot *in vivo* study with B-381 thermal sensitive liposome. Pilot *in vivo* study of B-381 TSL-active formulation using a bilateral D54 glioma xenograft model in which one tumor received 30 minutes of HIFU while the other tumor served as control.

Various changes to the B-381 loading process were attempted to increase the liposome boron content (from 71 ppb boron/mg of lipid). The liposome loading process was repeated using a 250 mM ammonium sulfate gradient, a super concentrated B-381 stock for drug loading (10 mg/mL) and different loading temperatures for 1 hour (39, 43, 50 and 60°C)(**Figure 33**). The most efficient encapsulation efficiency of 3% was achieved at 39°C, but the boron content in the TSL was only modestly improved to 86 ppb boron/mg of lipid. Furthermore, if the incubation time at 39°C was increased > 12 hours, the boron content only increased to 93 ppb boron/mg of lipid.

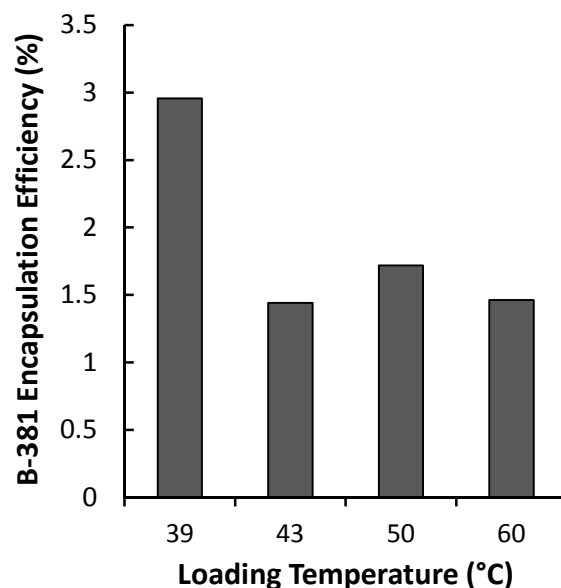


Figure 33. Drug loading efficiency of B-381 as a function of temperature. Alternative active drug loading method of B-381 into TSL using an ammonium sulfate gradient with 1 hour incubation at the following temperatures.

3.4.4 Passive Loading of B-381 into TSL Aqueous Core

Previously a pH gradient loading method achieved 20% B-381 encapsulation efficiency in the thermal sensitive liposome. However, increasing the boron content further for *in vivo* applications using the pH gradient method proved challenging because of its limited solubility in HEPES buffer (~10 mg/mL). Since B-381 had limited solubility in HEPES buffer (~10 mg/mL), the solubility of B-381 in sodium citrate buffer was investigated. B-381 is readily soluble in sodium citrate buffer at 40 mg/mL. Therefore, a super concentrated solution of B-381 was added directly to the lipid film during liposome synthesis, thereby passively entrapping the drug in the aqueous core. While the encapsulation efficiency is lower (~5%), the liposome boron content is approximately 10-fold higher using this passive loading method compared to the previous pH gradient loading method. Additionally, since the BPA fructose adduct (BPA-f) is one of the main clinically investigated BNCT agents, this agent was also investigated in a TSL formulation. Therefore, the primary

liposome formulations investigated in the remainder of this chapter were passively loaded with B-381 or BPA-f.

3.4.5 Characterization of Optimized TSLs

After the preliminary loading studies, it was determined that the highest boron content could be achieved by passively loading B-381 and BPA-f. To stabilize baseline release at physiologic temperature, our optimized B-381-TSL and BPA-f-TSL formulations included 10 mole % cholesterol, giving a final 71:14:5:10 molar ratio of DPPC/DSPC/DSPE-PEG₂₀₀₀/cholesterol (**Figure 34**). The necessity to include 10% cholesterol is outlined in the following section. Using lipid film rehydration with aqueous solutions of either BPA-f (30 mg/mL) or B-381 (40 mg/mL), these agents were passively entrapped in the aqueous core (**Figure 34**). Unbound drug was removed by centrifugation, and BPA-f-TSL, BPA-f-Non-TSL and B-381-TSL formulations were characterized by DLS (**Figure 34**). The liposome formulations have a narrow size range between 133.6 to 143.9 nm, with polydispersity indices between 0.034 and 0.052 indicating a homogenous population. Encapsulation efficiencies were < 5% which is anticipated for a passive loading method. Using ICP-OES, the final boron content in the liposome stocks ranged from 1317-1801 ppb, which was used to insure equimolar boron doses for *in vivo* studies. This is a marked improvement over the B-381-TSL that was loaded by the pH gradient method and only had a signal of 214.7 ppb (**Figure 32**).

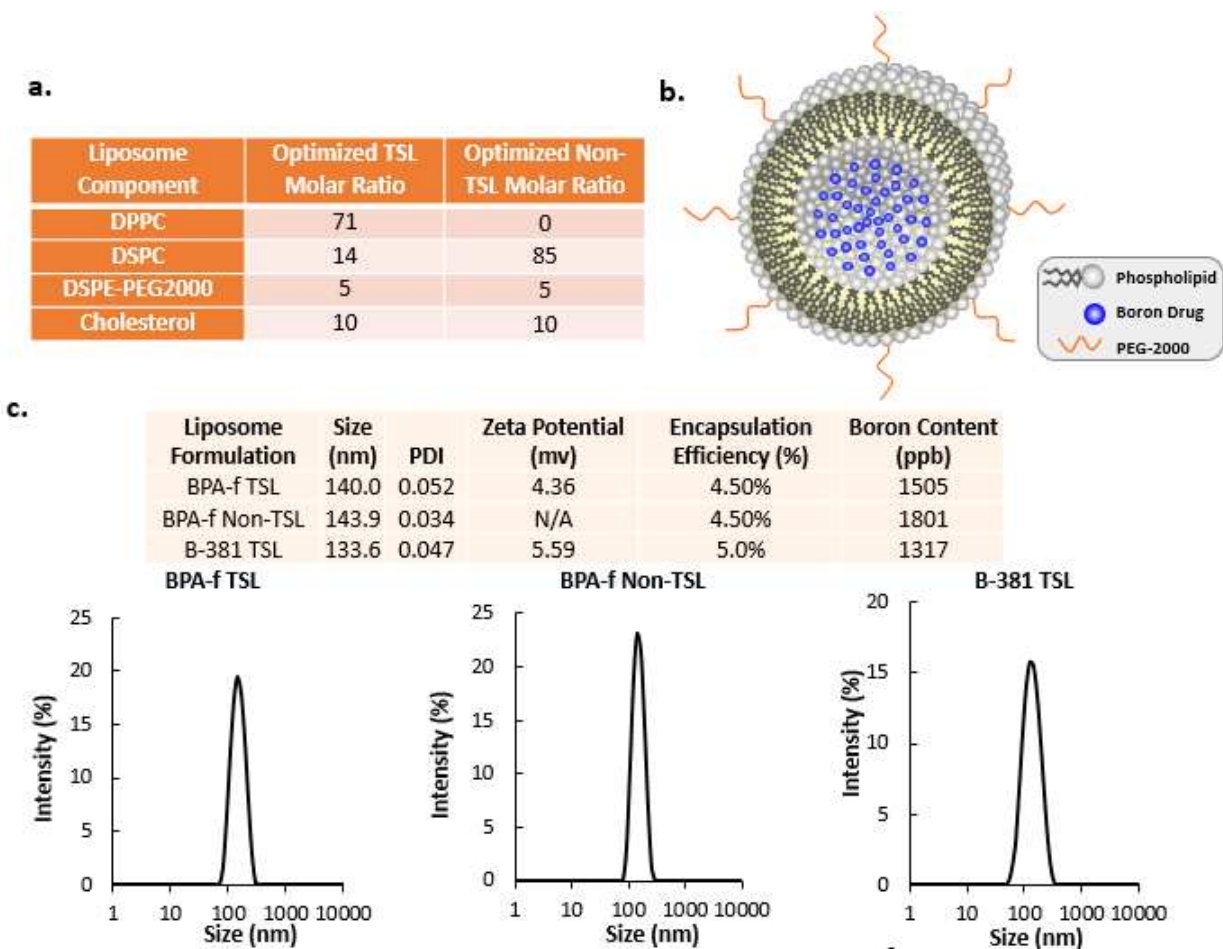


Figure 34. Liposome Synthesis and Characterization. **a.)** Optimized phospholipid molar ratios for thermal (TSL) and non-thermal sensitive liposome (non-TSL) formulations; **b.)** Illustration of a TSL containing boronated drug in aqueous core **c.)** Liposome size, polydispersity index (PDI), zeta potential, encapsulation efficiency and boron content of liposomes used for *in vivo* studies.

3.4.6 Temperature Dependent Release from Optimized TSLs

After characterizing the TSL and non-TSL formulations, the release of B-381 was evaluated with the cholesterol free B-381-TSL (**Figure 35 A**). After just 10 minutes of heating at 42°C, almost 100% the B-381 content is released, with no significant increase at 60 minutes. In contrast, 40% of the B-381 total dose is released after 10 minutes of heating at 37°C, with an increase to 50% at 60 minutes. Furthermore, it was observed that 10 or 60 minutes of HIFU exposure (regulating temperature between 42-43°C) was equally effective for drug release, which is practical

for clinical translation compared to heating with a water bath. Despite the preferential drug release observed at 42°C, it was undesirable to have 40% release at physiologic temperature.

To decrease the baseline B-381 release at physiologic temperature, the incorporation of cholesterol in the formulation was evaluated after 10 minutes of heating at 37 or 42 °C (**Figure 35**

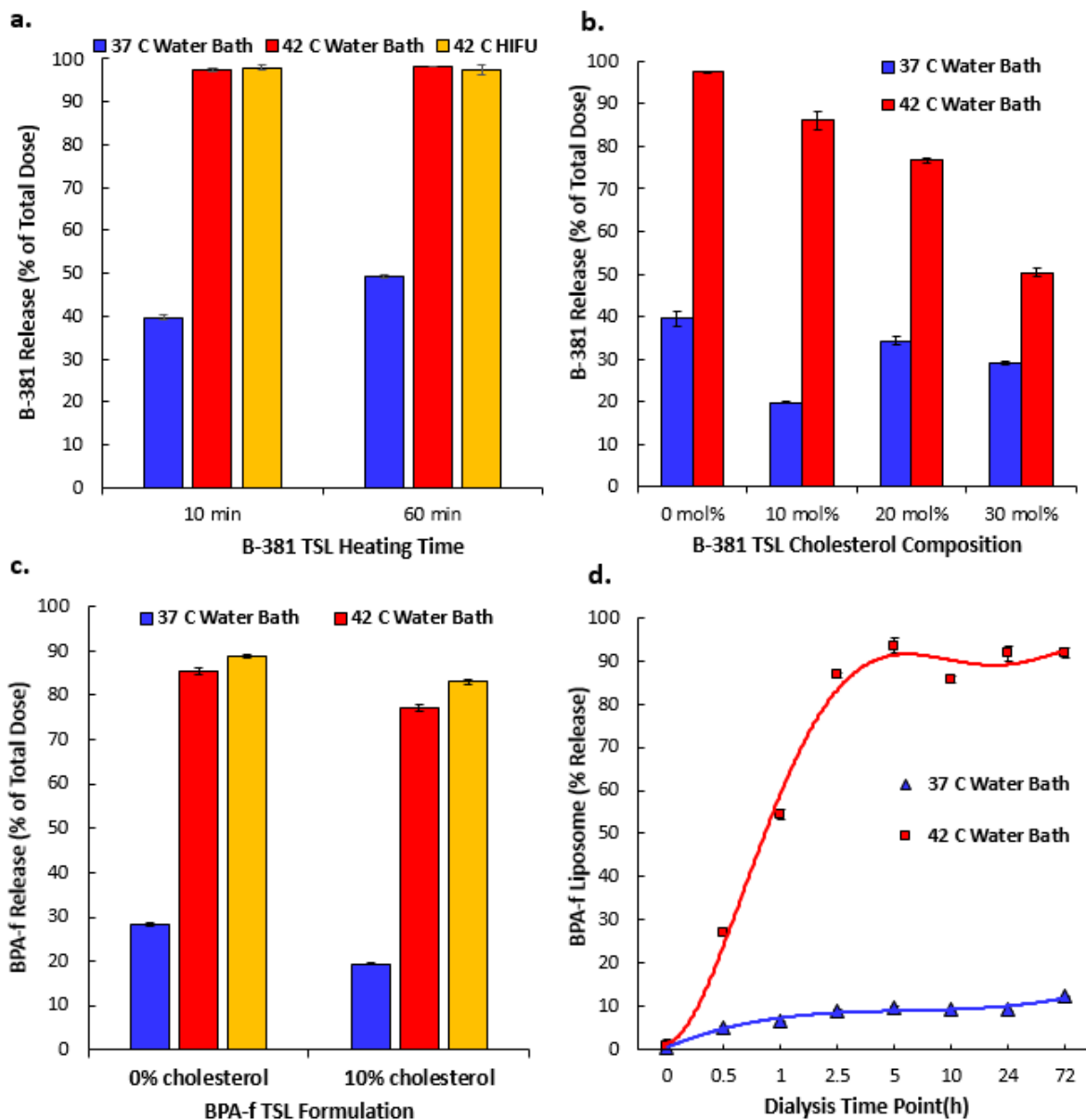


Figure 35. Water Bath and HIFU Triggered Drug Release from TSLs. a.) B-381 release from thermal sensitive liposome after water bath or HIFU exposure for 10 or 60 minutes. b.) Effect of varying cholesterol composition on B-381 release from thermal sensitive liposome after 10 minute water bath exposure at 37 or 42 °C. c.) Effect of cholesterol stabilization on BPA-Fructose thermal sensitive liposome after 30 minute water or HIFU exposure. d.) Dialysis release study of BPA-f formulation over time.

B). 10, 20 and 30 mole % cholesterol was compared to the cholesterol free formulation. The optimal formulation contained 10 mole % cholesterol, which reduced physiologic release to 20% at 37°C while remaining thermal sensitive at 42°C (releasing ~90% of B-381 payload). B-381 formulations that contained 20 and 30 mole % cholesterol demonstrated decreased thermal sensitivity. Therefore, the B-381-TSL containing 10 mole % cholesterol was chosen for *in vivo* studies.

The role of cholesterol was also evaluated in the BPA-f-TSL formulation (**Figure 35 C**). After 30 minutes of water bath incubation at 42°C, approximately 85% BPA-f was released from 0% cholesterol formulation while 77% release was observed for 10 mole % cholesterol. At 37 °C, the cholesterol free formulation had 28% release, while this was decreased to 19% for the 10 mole % cholesterol formulation. Therefore, the 10 mole % BPA-f formulation was chosen for *in vivo* studies. Additionally, 30 minutes of HIFU exposure with a temperature range of 42-43°C was equally effective at drug release in both formulations. Finally, drug release from the 10 mole % BPA-f-TSL formulation was evaluated over a 72 hour dialysis release experiment (**Figure 35 D**). After 2.5 hours, nearly 90% of the BPA-f content is released at 42°C. In contrast, only approximately 10% of BPA-f content is released after 72 hours at 37°C. This represents a near 9-fold higher drug release in mild hyperthermia compared to physiologic temperature. For *in vivo* applications, the drug release is much more rapid, as these experiments require longer time points since BPA-f is diffusing across the dialysis membrane.

3.4.7 *In Vivo* Analysis of B-381 and BPA-f TSLs

After finding 10 mole % cholesterol stabilizes drug release at 37°C but remains temperature sensitive at 42°C, the BPA-f-TSLs and B-381-TSLs were evaluated *in vivo*. Athymic nude mice contained bilateral D54 glioma tumors on their right and left flank (2 tumors/mouse)(**Figure 36**

A). Mice were positioned carefully so only the left tumor would be heated against a hyperthermia treatment window attached to a water circulator designed in house (**Supplementary Figure 13**). After 5 minutes of pre-hyperthermia treatment, mice were injected via tail vein with equimolar boron content of BPA-f free drug, BPA-f-TSL, and BPA-f-non-TSL (**Figure 36 B**). After a 30 minute exposure to hyperthermia (43°C), blood was collected and mice were sacrificed. For free drug administration, there was not a significant difference in BPA-f tumor uptake at 37 °C (341 ppb) compared to 42 °C (216 ppb). In contrast, BPA-f-TSL showed an 8.4-fold higher accumulation at 42 °C (692 ppb) compared to the 37 °C side (82.2 ppb). This indicates that drug is rapidly released on the hyperthermia treated tumor side, and there is not a significant accumulation due to EPR effect on the 37 °C side given the short experimental time point of 30 minutes.

In comparison to free administration of BPA-f, the TSL formulation has a 3.2-fold higher accumulation when comparing hyperthermia treated tumors. Finally, BPA-f-non-TSL administration resulted in no detectable signal at 37°C and a signal of only 104 ppb on the hyperthermia treated side. This is consistent with water bath experimental data (**Figure 29**) where the non-TSL liposome does not exhibit increased permeability at 43°C. Furthermore, the non-TSL formulation indicates that the improved drug delivery observed with BPA-f-TSL is indeed due to hyperthermia triggered release, and is not just simply a result of improved accumulation due to the EPR effect. In addition to tumor boron levels, biodistribution of all 3 drug vehicles was also evaluated (**Figure 36 C**). While free BPA-f is rapidly cleared from the circulation 30 minutes post-administration, both BPA-f-TSL and BPA-f-Non-TSL have prolonged circulation. This data further supports that the TSL formulation locally released BPA-f whereas the non-TSL did not

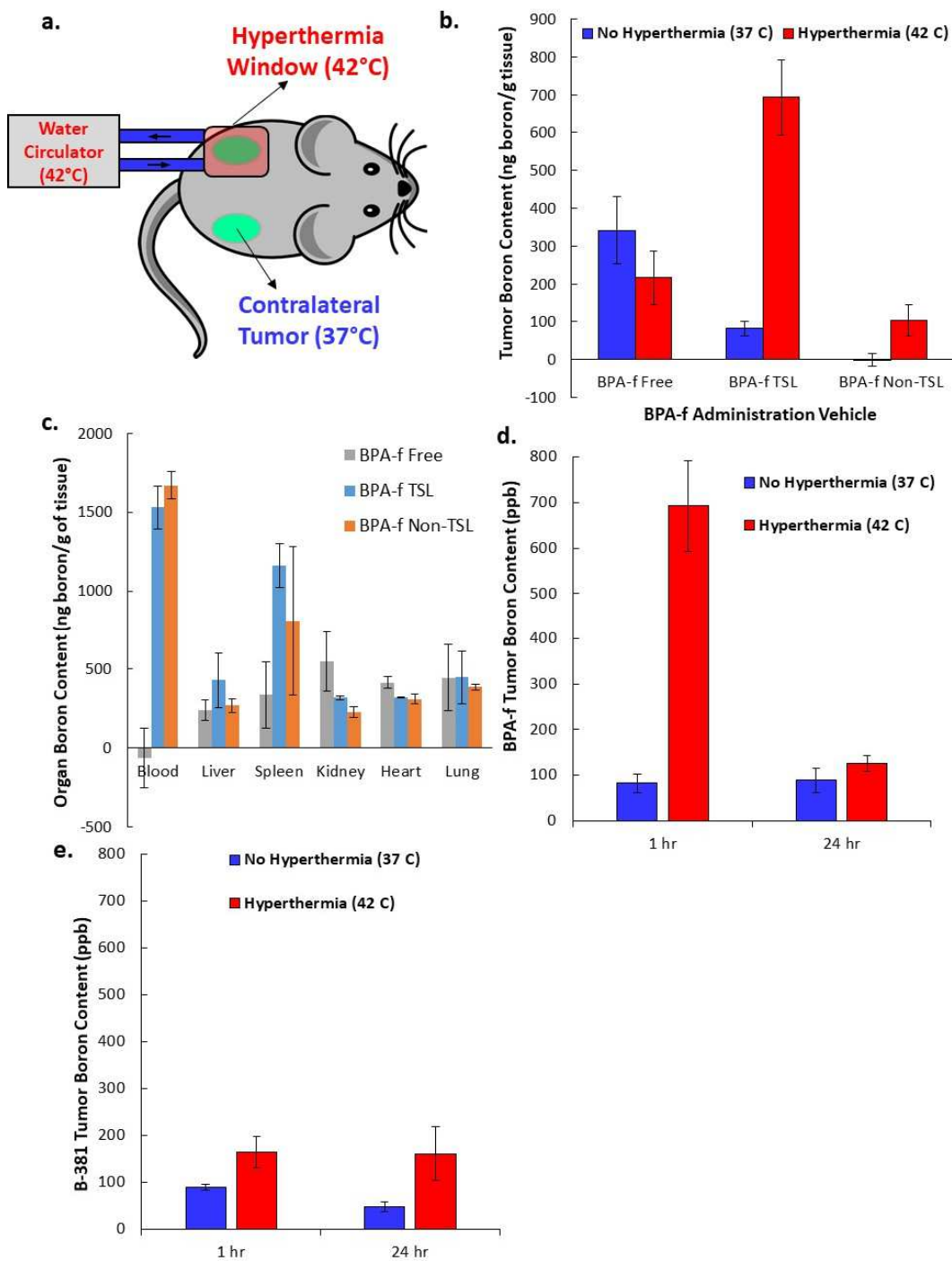


Figure 36. *In Vivo* Comparison of BPA-f, BPA-f TSL and BPA-f Non-TSL with or without hyperthermia. a.) Experimental setup for achieving local tumor hyperthermia; **b.)** Tumor boron content after 30 minute hyperthermia (43°C) treatment following *i.v.* injection of BPA-f free drug, BPA-f TSL or BPA-f non-TSL compared to contralateral control tumor (37°C) **c.)** Biodistribution of BPA-f free drug, BPA-f TSL or BPA-f non-TSL after 30 minute hyperthermia treatment. **d.)** Average tumor boron content 1 or 24 h post-hyperthermia treatment with BPA-f TSL. **e.)** Average tumor boron content 1 or 24 h post-hyperthermia treatment with B-381 TSL.

since both liposome formulations have approximately a blood concentration of 1500 ppb at $t = 30$ minutes. There is no significant difference between the 3 conditions in whole body distribution among the other organs evaluated.

For the final *in vivo* experiment, we hypothesized whether B-381 TSL would have a long-term retention compared to BPA-f. Since BPA-f is an amino acid analog, it does not have a mechanism for long term retention. However, 2-nitroimidazole derivatives such as B-381 can form intracellular protein conjugates in hypoxic cells. Therefore, groups of 3 mice were administered BPA-f-TSL or B-381-TSL and sacrificed at 1 or 24 h post-injection. Mice were subjected to equivalent hyperthermia conditions as the previous *in vivo* experiment and contained 2 tumors each. While BPA-f-TSL administration at 1 hour had a high signal in the hyperthermia treated tumor (692 ppb), this level dramatically decreased at 24 hours to 126 ppb (a near 80% decrease) (**Figure 36 D**). In contrast, hyperthermia treated tumors in the B-381 TSL treatment group had a signal of 160 ppb at 1 h, and had an equivalent signal 24 h post-injection (**Figure 36 E**). Therefore, this near 100% retention of B-381 supports the formation of intracellular protein conjugates. This is favorable for BNCT treatment by possibly allowing a later time point for neutron irradiation. This will provide time for nonspecific boron to clear from the blood and other organs while still remaining in the tumor at a later time point.

3.5 Conclusions

Two novel thermal sensitive liposome formulations have been prepared and show promise for future BNCT studies. Both B-381 and BPA-f have been passively loaded into TSLs formulation. Each formulation exhibits a nice temperature dependent release: each TSL releases ~90% of the drug payload at 42°C with only 10-20% release at 37°C. Furthermore, *in vivo* studies have

confirmed that local hyperthermia treatment of a tumor result in improved delivery of BPA-f compared to physiologic 37°C controls. Delivery of B-381 TSLs demonstrate a long-term retention at 24 hours compared to BPA-f TSLs. This is likely a result of the hypoxic tumor microenvironment, and is consistent with our mechanistic understanding of B-381 accumulation as outlined in Chapter 2. Future studies with B-381 and BPA-f are clearly warranted. Perhaps the greatest potential is administration of a liposome containing both B-381 and BPA-f. This should adequately target both normoxic and hypoxic tumor cells and sensitize them to neutron irradiation. Most importantly, it is the hope that this translates into improved tumor cytotoxicity and prolonged survival for the patient.

Chapter 4: Dissertation Conclusion

The therapeutic potential of boron neutron capture therapy was long-recognized in 1936 by Locher. During the decades to follow, the progression of BNCT would be hampered by non-tumor specific agents and inadequate thermal neutron sources. With the advent of the epithermal neutron beam and its generation using modern day linear accelerators, the need for tumor specific BNCT agents has never been greater. The work presented in this dissertation has provided several strategies to meet this need.

First, a novel boronated 2-nitroimidazole derivative (B-381) has been synthesized capable of targeting the hypoxic tumor microenvironment. B-381 is minimally cytotoxic and represents a new class of BNCT agents in which their selectivity to tumors is based on a hypoxic tumor metabolism. *In vivo*, B-381 has demonstrated a 9.5-fold higher long-term tumor retention compared to BPA. Additionally, several multi-boronated derivatives B-346 and B-403 have been prepared for future investigation.

Second, thermal sensitive liposomes have demonstrated to be an efficacious delivery system of either B-381 or BPA-f. Thermal sensitive liposomes boast a higher boron content and a localized tumor delivery triggered by hyperthermia. Compared to administration of the free agent *in vivo*, BPA-f-TSLs deliver a 3.2-fold higher boron content when comparing hyperthermia treated tumors. Furthermore, drug delivery to the hyperthermic region is highly localized. Mice that contained bilateral tumors and received BPA-f TSLs showed an 8.4-fold higher accumulation at the hyperthermic treated tumor (42 °C) compared to unheated controls (37 °C).

Further studies are warranted to evaluate boronated 2-nitroimidazoles as well as boron-containing thermal sensitive liposomes for future BNCT clinical trials. Boronated agents like B-381 offer a distinct therapeutic advantage because of their long-term tumor retention and their

ability sensitize the hypoxic (and often therapy resistant) cell population to BNCT. Further advances in BNCT can help combat the progression of cancer.

References

1. Hawthorne MF, Lee M. A critical assessment of boron target compounds for boron neutron capture therapy. *J Neurooncol.* 2003;62(1-2):33-45.
2. Hosmane NS. *Boron and Gadolinium Neutron Capture Therapy for Cancer Treatment.* Singapore, SGP: World Scientific Publishing Co.; 2012.
3. Hosmane NS. *Boron science : new technologies and applications.* Boca Raton. FL: CRC Press; 2012.
4. Azab AK, Abu Ali H, Srebnik M. Chapter 5 Boron neutron capture therapy. In: Hijazi Abu Ali VMD, Morris S, editors. *Studies in Inorganic Chemistry: Elsevier;* 2006. p. 337-66.
5. Wittig A, Collette L, Moss R, Sauerwein WA. Early clinical trial concept for boron neutron capture therapy: a critical assessment of the EORTC trial 11001. *Applied radiation and isotopes : including data, instrumentation and methods for use in agriculture, industry and medicine.* 2009;67(7-8 Suppl):S59-62. Epub 2009/04/18.
6. Barth RF, Coderre JA, Vicente MGH, Blue TE. Boron Neutron Capture Therapy of Cancer: Current Status and Future Prospects. *Clinical Cancer Research.* 2005;11(11):3987-4002.
7. AGENCY IAE. *Current Status of Neutron Capture Therapy.* Vienna: INTERNATIONAL ATOMIC ENERGY AGENCY; 2001.
8. Pisarev MA, Dagrosa MA, Juvenal GJ. Boron neutron capture therapy in cancer: past, present and future. *Arq Bras Endocrinol Metabol.* 2007;51(5):852-6.
9. Barth RF, Vicente MG, Harling OK, Kiger WS, 3rd, Riley KJ, Binns PJ, et al. Current status of boron neutron capture therapy of high grade gliomas and recurrent head and neck cancer. *Radiat Oncol.* 2012;7(146):7-146.
10. Soloway AH, Tjarks W, Barnum BA, Rong F-G, Barth RF, Codogni IM, et al. The Chemistry of Neutron Capture Therapy. *Chemical Reviews.* 1998;98(4):1515-62.
11. Liberman SJ, Dagrosa A, Jimenez Rebagliati RA, Bonomi MR, Roth BM, Turjanski L, et al. Biodistribution studies of boronophenylalanine-fructose in melanoma and brain tumor patients in Argentina. *Applied radiation and isotopes : including data, instrumentation and methods for use in agriculture, industry and medicine.* 2004;61(5):1095-100. Epub 2004/08/17.
12. Bergenheim AT, Capala J, Roslin M, Henriksson R. Distribution of BPA and metabolic assessment in glioblastoma patients during BNCT treatment: a microdialysis study. *J Neurooncol.* 2005;71(3):287-93.
13. Kankaanranta L, Seppala T, Koivunoro H, Valimaki P, Beule A, Collan J, et al. L-boronophenylalanine-mediated boron neutron capture therapy for malignant glioma progressing after external beam radiation therapy: a Phase I study. *International journal of radiation oncology, biology, physics.* 2011;80(2):369-76. Epub 2011/01/18.
14. Pellettieri L, H-Stenstam B, Rezaei A, Giusti V, Sköld K. An investigation of boron neutron capture therapy for recurrent glioblastoma multiforme. *Acta Neurologica Scandinavica.* 2008;117(3):191-7.

15. Stupp R, Mason WP, van den Bent MJ, Weller M, Fisher B, Taphoorn MJB, et al. Radiotherapy plus Concomitant and Adjuvant Temozolomide for Glioblastoma. *New England Journal of Medicine*. 2005;352(10):987-96.
16. Henriksson R, Capala J, Michanek A, Lindahl SA, Salford LG, Franzen L, et al. Boron neutron capture therapy (BNCT) for glioblastoma multiforme: a phase II study evaluating a prolonged high-dose of boronophenylalanine (BPA). *Radiother Oncol*. 2008;88(2):183-91. Epub 2008/03/14.
17. Skold K, B HS, Diaz AZ, Giusti V, Pellettieri L, Hopewell JW. Boron Neutron Capture Therapy for glioblastoma multiforme: advantage of prolonged infusion of BPA-f. *Acta Neurol Scand*. 2010;122(1):58-62. Epub 2009/12/03.
18. Diaz A. Assessment of the results from the phase I/II boron neutron capture therapy trials at the Brookhaven National Laboratory from a clinician's point of view. *J Neurooncol*. 2003;62(1-2):101-9.
19. Neumann M, Bergmann M, Gabel D. Cell type selective accumulation of mercaptoundecahydro- closo-dodecaborate (BSH) in glioblastoma multiforme. *Acta neurochirurgica*. 2003;145(11):971-5. Epub 2003/11/25.
20. Yamamoto T, Matsumura A, Nakai K, Shibata Y, Endo K, Sakurai F, et al. Current clinical results of the Tsukuba BNCT trial. *Applied radiation and isotopes : including data, instrumentation and methods for use in agriculture, industry and medicine*. 2004;61(5):1089-93. Epub 2004/08/17.
21. Miyatake S, Kawabata S, Yokoyama K, Kuroiwa T, Michiue H, Sakurai Y, et al. Survival benefit of boron neutron capture therapy for recurrent malignant gliomas. *Applied radiation and isotopes : including data, instrumentation and methods for use in agriculture, industry and medicine*. 2009;67(7-8 Suppl):S22-4. Epub 2009/04/28.
22. Kawabata S, Miyatake S, Nonoguchi N, Hiramatsu R, Iida K, Miyata S, et al. Survival benefit from boron neutron capture therapy for the newly diagnosed glioblastoma patients. *Applied radiation and isotopes : including data, instrumentation and methods for use in agriculture, industry and medicine*. 2009;67(7-8 Suppl):S15-8. Epub 2009/04/29.
23. Gonzalez SJ, Bonomi MR, Santa Cruz GA, Blaumann HR, Calzetta Larrieu OA, Menendez P, et al. First BNCT treatment of a skin melanoma in Argentina: dosimetric analysis and clinical outcome. *Applied radiation and isotopes : including data, instrumentation and methods for use in agriculture, industry and medicine*. 2004;61(5):1101-5. Epub 2004/08/17.
24. Pozzi EC, Cardoso JE, Colombo LL, Thorp S, Monti Hughes A, Molinari AJ, et al. Boron neutron capture therapy (BNCT) for liver metastasis: therapeutic efficacy in an experimental model. *Radiation and environmental biophysics*. 2012;51(3):331-9. Epub 2012/05/01.
25. Garabalino M, Monti Hughes A, Molinari A, Heber E, Pozzi EC, Cardoso J, et al. Boron neutron capture therapy (BNCT) for the treatment of liver metastases: biodistribution studies of boron compounds in an experimental model. *Radiation and environmental biophysics*. 2011;50(1):199-207.
26. Pozzi EC, Trivillin VA, Colombo LL, Monti Hughes A, Thorp SI, Cardoso JE, et al. Boron neutron capture therapy (BNCT) for liver metastasis in an experimental model: dose-

- response at five-week follow-up based on retrospective dose assessment in individual rats. *Radiation and environmental biophysics*. 2013;52(4):481-91. Epub 2013/10/01.
27. Wittig A, Malago M, Collette L, Huiskamp R, Buhrmann S, Nievaart V, et al. Uptake of two ¹⁰B-compounds in liver metastases of colorectal adenocarcinoma for extracorporeal irradiation with boron neutron capture therapy (EORTC Trial 11001). *International journal of cancer*. 2008;122(5):1164-71. Epub 2007/11/07.
 28. Schmitz T, Appelman K, Kudejova P, Schutz C, Kratz JV, Moss R, et al. Determination of boron concentration in blood and tissue samples from patients with liver metastases of colorectal carcinoma using Prompt Gamma Ray Activation Analysis (PGAA). *Applied radiation and isotopes : including data, instrumentation and methods for use in agriculture, industry and medicine*. 2011;69(7):936-41. Epub 2011/03/01.
 29. Zonta A, Pinelli T, Prati U, Roveda L, Ferrari C, Clerici AM, et al. Extra-corporeal liver BNCT for the treatment of diffuse metastases: what was learned and what is still to be learned. *Applied radiation and isotopes : including data, instrumentation and methods for use in agriculture, industry and medicine*. 2009;67(7-8 Suppl):S67-75. Epub 2009/04/28.
 30. Chou FI, Chung HP, Liu HM, Chi CW, Lui WY. Suitability of boron carriers for BNCT: accumulation of boron in malignant and normal liver cells after treatment with BPA, BSH and BA. *Applied radiation and isotopes : including data, instrumentation and methods for use in agriculture, industry and medicine*. 2009;67(7-8 Suppl):S105-8. Epub 2009/04/21.
 31. Wittig A, Collette L, Appelman K, Buhrmann S, Jackel MC, Jockel KH, et al. EORTC trial 11001: distribution of two ¹⁰B-compounds in patients with squamous cell carcinoma of head and neck, a translational research/phase 1 trial. *Journal of cellular and molecular medicine*. 2009;13(8B):1653-65. Epub 2009/07/16.
 32. Wang LW, Chen YW, Ho CY, Hsueh Liu YW, Chou FI, Liu YH, et al. Fractionated BNCT for locally recurrent head and neck cancer: experience from a phase I/II clinical trial at Tsing Hua Open-Pool Reactor. *Applied radiation and isotopes : including data, instrumentation and methods for use in agriculture, industry and medicine*. 2014;88:23-7. Epub 2013/12/29.
 33. Wang LW, Wang SJ, Chu PY, Ho CY, Jiang SH, Liu YW, et al. BNCT for locally recurrent head and neck cancer: preliminary clinical experience from a phase I/II trial at Tsing Hua Open-Pool Reactor. *Applied radiation and isotopes : including data, instrumentation and methods for use in agriculture, industry and medicine*. 2011;69(12):1803-6. Epub 2011/04/12.
 34. Kankaanranta L, Seppala T, Koivunoro H, Saarilahti K, Atula T, Collan J, et al. Boron neutron capture therapy in the treatment of locally recurred head-and-neck cancer: final analysis of a phase I/II trial. *International journal of radiation oncology, biology, physics*. 2012;82(1):e67-75. Epub 2011/02/09.
 35. Aihara T, Hiratsuka J, Morita N, Uno M, Sakurai Y, Maruhashi A, et al. First clinical case of boron neutron capture therapy for head and neck malignancies using ¹⁸F-BPA PET. *Head & neck*. 2006;28(9):850-5. Epub 2006/05/25.
 36. Rij Cv, Wilhelm A, Sauerwein WG, Loenen Av. Boron neutron capture therapy for glioblastoma multiforme. *Pharm World Sci*. 2005;27(2):92-5.

37. Chandra S, Barth RF, Haider SA, Yang W, Huo T, Shaikh AL, et al. Biodistribution and subcellular localization of an unnatural boron-containing amino acid (cis-ABCPC) by imaging secondary ion mass spectrometry for neutron capture therapy of melanomas and gliomas. *PLoS ONE*. 2013;8(9).
38. Sauerwein WAG, Wittig A, Moss R, Nakagawa Y. *Neutron Capture Therapy: Principles and Applications*: Springer Berlin Heidelberg; 2012.
39. Goorley T, Zamenhof R, Nikjoo H. Calculated DNA damage from gadolinium Auger electrons and relation to dose distributions in a head phantom. *International journal of radiation biology*. 2004;80(11-12):933-40. Epub 2005/03/15.
40. Mitin VN, Kulakov VN, Khokhlov VF, Sheino IN, Arnopolskaya AM, Kozlovskaya NG, et al. Comparison of BNCT and GdNCT efficacy in treatment of canine cancer. *Applied radiation and isotopes : including data, instrumentation and methods for use in agriculture, industry and medicine*. 2009;67(7-8 Suppl):S299-301. Epub 2009/05/12.
41. Bavarnegin E, Kasesaz Y, Wagner FM. Neutron beams implemented at nuclear research reactors for BNCT. *Journal of Instrumentation*. 2017;12(05):P05005.
42. Packer S, Coderre J, Saraf S, Fairchild R, Hansrote J, Perry H. Boron neutron capture therapy of anterior chamber melanoma with p-boronophenylalanine. *Investigative Ophthalmology & Visual Science*. 1992;33(2):395-403.
43. Gregoire V, Begg AC, Huiskamp R, Verrijk R, Bartelink H. Selectivity of boron carriers for boron neutron capture therapy: pharmacological studies with borocaptate sodium, L-boronophenylalanine and boric acid in murine tumors. *Radiotherapy and oncology : journal of the European Society for Therapeutic Radiology and Oncology*. 1993;27(1):46-54.
44. Malan C, Morin C. A Concise Preparation of 4-Borono-l-phenylalanine (l-BPA) from l-Phenylalanine. *The Journal of Organic Chemistry*. 1998;63(22):8019-20.
45. Nemoto H, Cai J, Iwamoto S, Yamamoto Y. Synthesis and Biological Properties of Water-Soluble p-Boronophenylalanine Derivatives. Relationship between Water Solubility, Cytotoxicity, and Cellular Uptake. *Journal of Medicinal Chemistry*. 1995;38(10):1673-8.
46. Heikkinen S, Savolainen S, Melkko P. In Vitro Studies on Stability of L-p-boronophenylalanine-fructose Complex (BPA-F). *Journal of Radiation Research*. 2011;52(3):360-4.
47. Wittig A, Sauerwein WA, Coderre JA, Coderre JA. Mechanisms of Transport of p-Borono-Phenylalanine through the Cell Membrane In Vitro. *Radiation Research*. 2000;153(2):173-80.
48. Capuani S, Gili T, Bozzali M, Russo S, Porcari P, Cametti C, et al. Boronophenylalanine uptake in C6 glioma model is dramatically increased by l-DOPA preloading. *Applied Radiation and Isotopes*. 2009;67(7-8, Supplement):S34-S6.
49. Yoshimoto M, Kurihara H, Honda N, Kawai K, Ohe K, Fujii H, et al. Predominant contribution of L-type amino acid transporter to 4-borono-2-(18)F-fluoro-phenylalanine uptake in human glioblastoma cells. *Nuclear medicine and biology*. 2013;40(5):625-9. Epub 2013/04/06.

50. Fuchs BC, Bode BP. Amino acid transporters ASCT2 and LAT1 in cancer: partners in crime? *Seminars in cancer biology*. 2005;15(4):254-66. Epub 2005/05/27.
51. Yokoyama K, Miyatake S, Kajimoto Y, Kawabata S, Doi A, Yoshida T, et al. Pharmacokinetic study of BSH and BPA in simultaneous use for BNCT. *J Neurooncol*. 2006;78(3):227-32. Epub 2006/03/25.
52. Wittig A, Stecher-Rasmussen F, Hilger RA, Rassow J, Mauri P, Sauerwein W. Sodium mercaptoundecahydro-closo-dodecaborate (BSH), a boron carrier that merits more attention. *Applied Radiation and Isotopes*. 2011;69(12):1760-4.
53. Soloway AH, Hatanaka H, Davis MA. Penetration of Brain and Brain Tumor. VII. Tumor-Binding Sulfhydryl Boron Compounds. *Journal of Medicinal Chemistry*. 1967;10(4):714-7.
54. Tietze LF, Griesbach U, Bothe U, Nakamura H, Yamamoto Y. Novel Carboranes with a DNA Binding Unit for the Treatment of Cancer by Boron Neutron Capture Therapy. *ChemBioChem*. 2002;3(2-3):219-25.
55. Barth RF, Yang W, Rotaru JH, Moeschberger ML, Joel DD, Nawrocky MM, et al. Boron Neutron Capture Therapy of Brain Tumors: Enhanced Survival following Intracarotid Injection of either Sodium Borocaptate or Boronophenylalanine with or without Blood-Brain Barrier Disruption. *Cancer Research*. 1997;57(6):1129-36.
56. Barth RF, Yang W, Rotaru JH, Moeschberger ML, Boesel CP, Soloway AH, et al. Boron neutron capture therapy of brain tumors: enhanced survival and cure following blood-brain barrier disruption and intracarotid injection of sodium borocaptate and boronophenylalanine. *International Journal of Radiation Oncology*Biophysics*Physics*. 2000;47(1):209-18.
57. Barth RF, Yang W, Huo T, Riley KJ, Binns PJ, Grecula JC, et al. Comparison of intracerebral delivery of carboplatin and photon irradiation with an optimized regimen for boron neutron capture therapy of the F98 rat glioma. *Applied radiation and isotopes : including data, instrumentation and methods for use in agriculture, industry and medicine*. 2011;69(12):1813-6.
58. Yang F-Y, Chen Y-W, Chou F-I, Yen S-H, Lin Y-L, Wong T-T. Boron neutron capture therapy for glioblastoma multiforme: enhanced drug delivery and antitumor effect following blood-brain barrier disruption induced by focused ultrasound. *Future Oncology*. 2012;8(10):1361-9.
59. Tani H, Kurihara H, Hiroi K, Honda N, Yoshimoto M, Kono Y, et al. Correlation of (18)F-BPA and (18)F-FDG uptake in head and neck cancers. *Radiother Oncol*. 2014;113(2):193-7. Epub 2014/12/04.
60. Evangelista L, Jori G, Martini D, Sotti G. Boron neutron capture therapy and 18F-labelled borophenylalanine positron emission tomography: a critical and clinical overview of the literature. *Applied radiation and isotopes : including data, instrumentation and methods for use in agriculture, industry and medicine*. 2013;74:91-101.
61. Snajdr I, Janousek Z, Takagaki M, Cisarova I, Hosmane NS, Kotora M. Alpha (alpha-) and beta (beta-carboranyl-C-deoxyribosides: syntheses, structures and biological evaluation. *European journal of medicinal chemistry*. 2014;83:389-97. Epub 2014/07/02.

62. Khalil A, Ishita K, Ali T, Tjarks W. N3-substituted thymidine bioconjugates for cancer therapy and imaging. *Future medicinal chemistry*. 2013;5(6):677-92. Epub 2013/04/27.
63. Barth RF, Yang W, Al-Madhoun AS, Johnsamuel J, Byun Y, Chandra S, et al. Boron-Containing Nucleosides as Potential Delivery Agents for Neutron Capture Therapy of Brain Tumors. *Cancer Research*. 2004;64(17):6287-95.
64. Satapathy R, Dash BP, Bode BP, Byczynski EA, Hosmane SN, Bux S, et al. New classes of carborane-appended 5-thio-D-glucopyranose derivatives. *Dalton transactions*. 2012;41(29):8982-8. Epub 2012/06/23.
65. Patel H, Takagaki M, Bode BP, Snajdr I, Patel D, Sharman C, et al. Carborane-Appended Saccharides: Prime Candidates for Boron Neutron Capture Therapy (BNCT) Clinical Trials. *Biochemical and Biophysical Journal of Neutron Therapy & Cancer Treatments*. 2013;1(1):15-21.
66. Kabalka GW, Yao ML, Marepally SR, Chandra S. Biological evaluation of boronated unnatural amino acids as new boron carriers. *Applied Radiation and Isotopes*. 2009;67(7-8, Supplement):S374-S9.
67. Washburn LC, Sun TT, Anon JB, Hayes RL. Effect of Structure on Tumor Specificity of Alicyclic α -Amino Acids. *Cancer Research*. 1978;38(8):2271-3.
68. Maderna A, Huertas R, Hawthorne MF, Luguaya R, Vicente MGaH. Synthesis of a porphyrin-labelled carboranyl phosphate diester: a potential new drug for boron neutron capture therapy of cancer. *Chemical Communications*. 2002(16):1784-5.
69. Vicente MGH, Nurco DJ, Shetty SJ, Osterloh J, Ventre E, Hegde V, et al. Synthesis, dark toxicity and induction of in vitro DNA photodamage by a tetra(4-nido-carboranylphenyl)porphyrin. *Journal of Photochemistry and Photobiology B: Biology*. 2002;68(2-3):123-32.
70. Dougherty TJ, Gomer CJ, Henderson BW, Jori G, Kessel D, Korbelik M, et al. Photodynamic Therapy. *Journal of the National Cancer Institute*. 1998;90(12):889-905.
71. Fabris C, Vicente MG, Hao E, Friso E, Borsetto L, Jori G, et al. Tumour-localizing and -photosensitising properties of meso-tetra(4-nido-carboranylphenyl)porphyrin (H2TCP). *Journal of photochemistry and photobiology B, Biology*. 2007;89(2-3):131-8. Epub 2007/11/06.
72. Jori G, Soncin M, Friso E, Vicente MG, Hao E, Miotto G, et al. A novel boronated-porphyrin as a radio-sensitizing agent for boron neutron capture therapy of tumours: in vitro and in vivo studies. *Applied radiation and isotopes : including data, instrumentation and methods for use in agriculture, industry and medicine*. 2009;67(7-8 Suppl):S321-4. Epub 2009/04/21.
73. Yang W, Wu G, Barth RF, Swindall MR, Bandyopadhyaya AK, Tjarks W, et al. Molecular targeting and treatment of composite EGFR and EGFRvIII-positive gliomas using boronated monoclonal antibodies. *Clinical cancer research : an official journal of the American Association for Cancer Research*. 2008;14(3):883-91. Epub 2008/02/05.
74. Wu G, Barth RF, Yang W, Chatterjee M, Tjarks W, Ciesielski MJ, et al. Site-Specific Conjugation of Boron-Containing Dendrimers to Anti-EGF Receptor Monoclonal Antibody

- Cetuximab (IMC-C225) and Its Evaluation as a Potential Delivery Agent for Neutron Capture Therapy. *Bioconjugate Chemistry*. 2003;15(1):185-94.
75. Yang W, Barth RF, Wu G, Tjarks W, Binns P, Riley K. Boron neutron capture therapy of EGFR or EGFRvIII positive gliomas using either boronated monoclonal antibodies or epidermal growth factor as molecular targeting agents. *Applied radiation and isotopes : including data, instrumentation and methods for use in agriculture, industry and medicine*. 2009;67(7-8 Suppl):S328-31. Epub 2009/05/27.
 76. Chacko AM, Li C, Pryma DA, Brem S, Coukos G, Muzykantov V. Targeted delivery of antibody-based therapeutic and imaging agents to CNS tumors: crossing the blood-brain barrier divide. *Expert opinion on drug delivery*. 2013;10(7):907-26. Epub 2013/06/12.
 77. Azab AK, Srebnik M, Doviner V, Rubinstein A. Targeting normal and neoplastic tissues in the rat jejunum and colon with boronated, cationic acrylamide copolymers. *Journal of controlled release : official journal of the Controlled Release Society*. 2005;106(1-2):14-25. Epub 2005/07/12.
 78. Michiue H, Sakurai Y, Kondo N, Kitamatsu M, Bin F, Nakajima K, et al. The acceleration of boron neutron capture therapy using multi-linked mercaptoundecahydrododecaborate (BSH) fused cell-penetrating peptide. *Biomaterials*. 2014. Epub 2014/01/24.
 79. Wicki A, Witzigmann D, Balasubramanian V, Huwyler J. Nanomedicine in cancer therapy: Challenges, opportunities, and clinical applications. *Journal of controlled release : official journal of the Controlled Release Society*. 2015;200C:138-57. Epub 2014/12/30.
 80. Fang J, Nakamura H, Maeda H. The EPR effect: Unique features of tumor blood vessels for drug delivery, factors involved, and limitations and augmentation of the effect. *Advanced drug delivery reviews*. 2011;63(3):136-51. Epub 2010/05/06.
 81. Maeda H. Toward a full understanding of the EPR effect in primary and metastatic tumors as well as issues related to its heterogeneity. *Advanced drug delivery reviews*. 2015. Epub 2015/01/13.
 82. Theodoropoulos D, Rova A, Smith JR, Barbu E, Calabrese G, Vizirianakis IS, et al. Towards boron neutron capture therapy: The formulation and preliminary in vitro evaluation of liposomal vehicles for the therapeutic delivery of the dequalinium salt of bis-nido-carborane. *Bioorganic & Medicinal Chemistry Letters*. 2013;23(22):6161-6.
 83. Altieri S, Balzi M, Bortolussi S, Bruschi P, Ciani L, Clerici AM, et al. Carborane derivatives loaded into liposomes as efficient delivery systems for boron neutron capture therapy. *J Med Chem*. 2009;52(23):7829-35. Epub 2009/12/04.
 84. Kueffer PJ, Maitz CA, Khan AA, Schuster SA, Shlyakhtina NI, Jalisatgi SS, et al. Boron neutron capture therapy demonstrated in mice bearing EMT6 tumors following selective delivery of boron by rationally designed liposomes. *Proceedings of the National Academy of Sciences of the United States of America*. 2013;110(16):6512-7. Epub 2013/03/29.
 85. Heber EM, Hawthorne MF, Kueffer PJ, Garabalino MA, Thorp SI, Pozzi EC, et al. Therapeutic efficacy of boron neutron capture therapy mediated by boron-rich liposomes for oral cancer in the hamster cheek pouch model. *Proceedings of the National Academy of Sciences of the United States of America*. 2014;111(45):16077-81. Epub 2014/10/29.

86. Pardridge WM. Drug Delivery to the Brain. *Journal of Cerebral Blood Flow and Metabolism*. 1997;17(7):713-31.
87. Achilli C, Grandi S, Ciana A, Guidetti GF, Malara A, Abbonante V, et al. Biocompatibility of functionalized boron phosphate (BPO₄) nanoparticles for boron neutron capture therapy (BNCT) application. *Nanomedicine : nanotechnology, biology, and medicine*. 2014;10(3):589-97. Epub 2013/10/29.
88. Caruso G, Caffo M, Alafaci C, Raudino G, Cafarella D, Lucerna S, et al. Could nanoparticle systems have a role in the treatment of cerebral gliomas? *Nanomedicine : nanotechnology, biology, and medicine*. 2011;7(6):744-52. Epub 2011/03/23.
89. Li N, Zhao P, Salmon L, Ruiz J, Zabawa M, Hosmane NS, et al. "Click" star-shaped and dendritic PEGylated gold nanoparticle-carborane assemblies. *Inorganic chemistry*. 2013;52(19):11146-55. Epub 2013/10/08.
90. Oliveira MF, Guimaraes PP, Gomes AD, Suarez D, Sinisterra RD. Strategies to target tumors using nanodelivery systems based on biodegradable polymers, aspects of intellectual property, and market. *Journal of chemical biology*. 2012;6(1):7-23. Epub 2012/01/01.
91. Brannon-Peppas L, Blanchette JO. Nanoparticle and targeted systems for cancer therapy. *Advanced drug delivery reviews*. 2004;56(11):1649-59. Epub 2004/09/08.
92. Brigger I, Dubernet C, Couvreur P. Nanoparticles in cancer therapy and diagnosis. *Advanced drug delivery reviews*. 2002;54(5):631-51. Epub 2002/09/03.
93. Luderer M, de la Puente P, Azab A. Advancements in Tumor Targeting Strategies for Boron Neutron Capture Therapy. *Pharm Res*. 2015:1-13.
94. Statistics NCfH. Health, United States, 2016: With Chartbook on Long-term Trends in Health. 2016.
95. Franceschi E, Minichillo S, Brandes AA. Pharmacotherapy of Glioblastoma: Established Treatments and Emerging Concepts. *CNS Drugs*. 2017;31(8):675-84.
96. Schwartzbaum JA, Fisher JL, Aldape KD, Wrensch M. Epidemiology and molecular pathology of glioma. *Nature clinical practice Neurology*. 2006;2(9):494-503; quiz 1 p following 16. Epub 2006/08/26.
97. <http://www.mayoclinic.org/diseases-conditions/glioma/home/ovc-20129412>.
98. Stupp R, Hegi ME, Mason WP, van den Bent MJ, Taphoorn MJB, Janzer RC, et al. Effects of radiotherapy with concomitant and adjuvant temozolomide versus radiotherapy alone on survival in glioblastoma in a randomised phase III study: 5-year analysis of the EORTC-NCIC trial. *The Lancet Oncology*. 2009;10(5):459-66.
99. Weller M, Cloughesy T, Perry JR, Wick W. Standards of care for treatment of recurrent glioblastoma—are we there yet? *Neuro-Oncology*. 2012.
100. Hanahan D, Weinberg Robert A. Hallmarks of Cancer: The Next Generation. *Cell*. 144(5):646-74.
101. Alexiou GA, Tsiouris S, Kyritsis AP, Argyropoulou MI, Voulgaris S, Fotopoulos AD. Assessment of glioma proliferation using imaging modalities. *Journal of clinical*

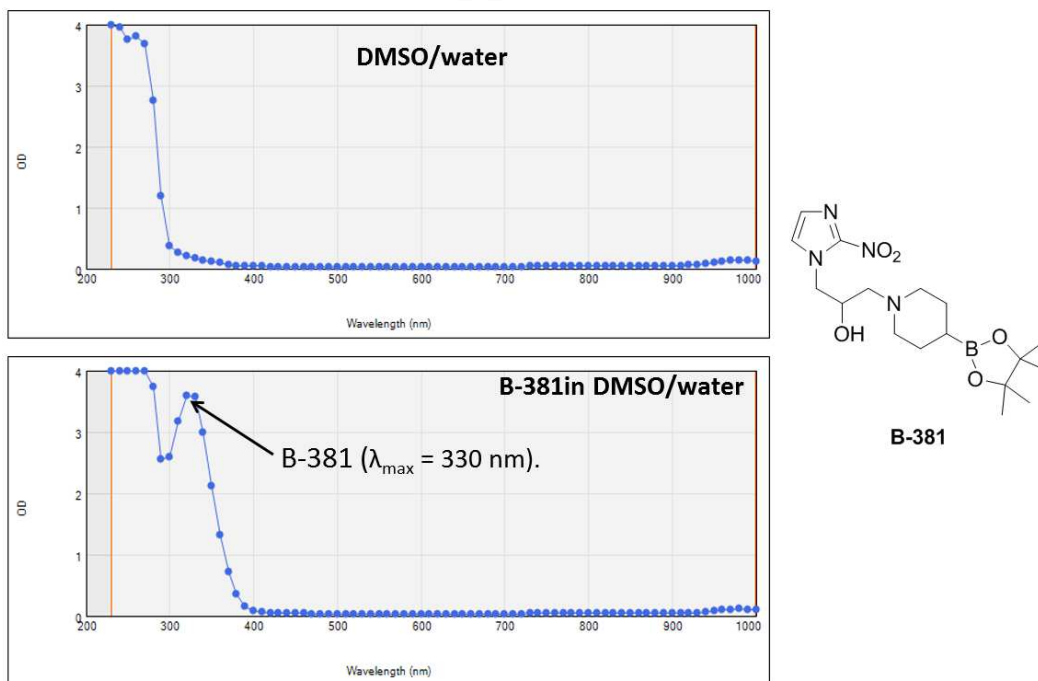
- neuroscience : official journal of the Neurosurgical Society of Australasia. 2010;17(10):1233-8. Epub 2010/07/20.
102. Collins VP. Progression as exemplified by human astrocytic tumors. *Seminars in cancer biology*. 1999;9(4):267-76. Epub 1999/08/17.
 103. Brat DJ, Mapstone TB. Malignant glioma physiology: cellular response to hypoxia and its role in tumor progression. *Annals of internal medicine*. 2003;138(8):659-68. Epub 2003/04/16.
 104. Muz B, de la Puente P, Azab F, Luderer M, Azab AK. The role of hypoxia and exploitation of the hypoxic environment in hematologic malignancies. *Molecular cancer research : MCR*. 2014;12(10):1347-54. Epub 2014/08/28.
 105. Oliver L, Olivier C, Marhuenda FB, Campone M, Vallette FM. Hypoxia and the malignant glioma microenvironment: regulation and implications for therapy. *Current molecular pharmacology*. 2009;2(3):263-84. Epub 2009/12/22.
 106. Fu Y, Zheng S, Zheng Y, Huang R, An N, Liang A, et al. Glioma derived isocitrate dehydrogenase-2 mutations induced up-regulation of HIF-1alpha and beta-catenin signaling: possible impact on glioma cell metastasis and chemo-resistance. *The international journal of biochemistry & cell biology*. 2012;44(5):770-5. Epub 2012/02/09.
 107. Greenfield JP, Cobb WS, Lyden D. Resisting arrest: a switch from angiogenesis to vasculogenesis in recurrent malignant gliomas. *The Journal of clinical investigation*. 2010;120(3):663-7. Epub 2010/02/25.
 108. Haar CP, Hebbar P, Wallace GC, Das A, Vandergrift WA, 3rd, Smith JA, et al. Drug resistance in glioblastoma: a mini review. *Neurochemical research*. 2012;37(6):1192-200. Epub 2012/01/10.
 109. Amberger-Murphy V. Hypoxia helps glioma to fight therapy. *Current cancer drug targets*. 2009;9(3):381-90. Epub 2009/05/16.
 110. Rycaj K, Tang DG. Cancer stem cells and radioresistance. *International journal of radiation biology*. 2014;90(8):615-21. Epub 2014/02/18.
 111. Bell C, Dowson N, Fay M, Thomas P, Puttick S, Gal Y, et al. Hypoxia Imaging in Gliomas With F-Fluoromisonidazole PET: Toward Clinical Translation. *Seminars in nuclear medicine*. 2015;45(2):136-50. Epub 2015/02/24.
 112. Parker NR, Khong P, Parkinson JF, Howell VM, Wheeler HR. Molecular heterogeneity in glioblastoma: potential clinical implications. *Frontiers in oncology*. 2015;5:55. Epub 2015/03/19.
 113. Muz B, de la Puente P, Azab F, Azab AK. The role of hypoxia in cancer progression, angiogenesis, metastasis, and resistance to therapy. *Hypoxia*. 2015;3:83-92.
 114. Mickaël Bourgeois HR, François Guerar, Marie Mougin-Degraef, Jacques Barbet, Nathalie Michel, Michel Cherel, Alain Faivre-Chauvet, Jean-François Gestin. Contribution of [64Cu]-ATSM PET in molecular imaging of tumour hypoxia compared to classical [18F]-MISO — a selected review. *Nucl Med Rev*. 2011;14(2):90-5.

115. Hockel M, Vaupel P. Tumor hypoxia: definitions and current clinical, biologic, and molecular aspects. *Journal of the National Cancer Institute*. 2001;93(4):266-76. Epub 2001/02/22.
116. Siemann DW. The Unique Characteristics of Tumor Vasculature and Preclinical Evidence for its Selective Disruption by Tumor-Vascular Disrupting Agents. *Cancer treatment reviews*. 2011;37(1):63-74.
117. Vordermark D, Brown JM. Endogenous markers of tumor hypoxia predictors of clinical radiation resistance? *Strahlentherapie und Onkologie : Organ der Deutschen Röntgengesellschaft [et al]*. 2003;179(12):801-11. Epub 2003/12/04.
118. Benej M, Pastorekova S, Pastorek J. Carbonic anhydrase IX: regulation and role in cancer. *Sub-cellular biochemistry*. 2014;75:199-219. Epub 2013/10/23.
119. Varghese AJ, Gulyas S, Mohindra JK. Hypoxia-dependent Reduction of 1-(2-Nitro-1-imidazolyl)-3-methoxy-2-propanol by Chinese Hamster Ovary Cells and KHT Tumor Cells in Vitro and in Vivo. *Cancer Research*. 1976;36(10):3761-5.
120. Carlin S, Zhang H, Reese M, Ramos NN, Chen Q, Ricketts S-A. A Comparison of the Imaging Characteristics and Microregional Distribution of 4 Hypoxia PET Tracers. *Journal of Nuclear Medicine*. 2014;55(3):515-21.
121. Anderson CJ, Ferdani R. Copper-64 radiopharmaceuticals for PET imaging of cancer: advances in preclinical and clinical research. *Cancer biotherapy & radiopharmaceuticals*. 2009;24(4):379-93. Epub 2009/08/22.
122. Dehdashti F, Mintun MA, Lewis JS, Bradley J, Govindan R, Laforest R, et al. In vivo assessment of tumor hypoxia in lung cancer with ⁶⁰Cu-ATSM. *European Journal of Nuclear Medicine and Molecular Imaging*. 2003;30(6):844-50.
123. Chao KS, Bosch WR, Mutic S, Lewis JS, Dehdashti F, Mintun MA, et al. A novel approach to overcome hypoxic tumor resistance: Cu-ATSM-guided intensity-modulated radiation therapy. *International journal of radiation oncology, biology, physics*. 2001;49(4):1171-82. Epub 2001/03/10.
124. Bernsen HJ, Rijken PF, Peters H, Raleigh JA, Jeuken JW, Wesseling P, et al. Hypoxia in a human intracerebral glioma model. *Journal of neurosurgery*. 2000;93(3):449-54. Epub 2000/09/02.
125. Olive PL, Durand RE, Raleigh JA, Luo C, Aquino-Parsons C. Comparison between the comet assay and pimonidazole binding for measuring tumour hypoxia. *Br J Cancer*. 2000;83(11):1525-31. Epub 2000/11/15.
126. de la Puente P, Azab F, Muz B, Luderer M, Arbiser J, Azab AK. Tris DBA palladium overcomes hypoxia-mediated drug resistance in multiple myeloma. *Leukemia & Lymphoma*. 2015:1-10.
127. William T. Golde PG, Luis L. Rodriguez. A rapid, simple, and humane method for submandibular bleeding of mice using a lancet. *Lab Animal*. 2005;34(9):4.

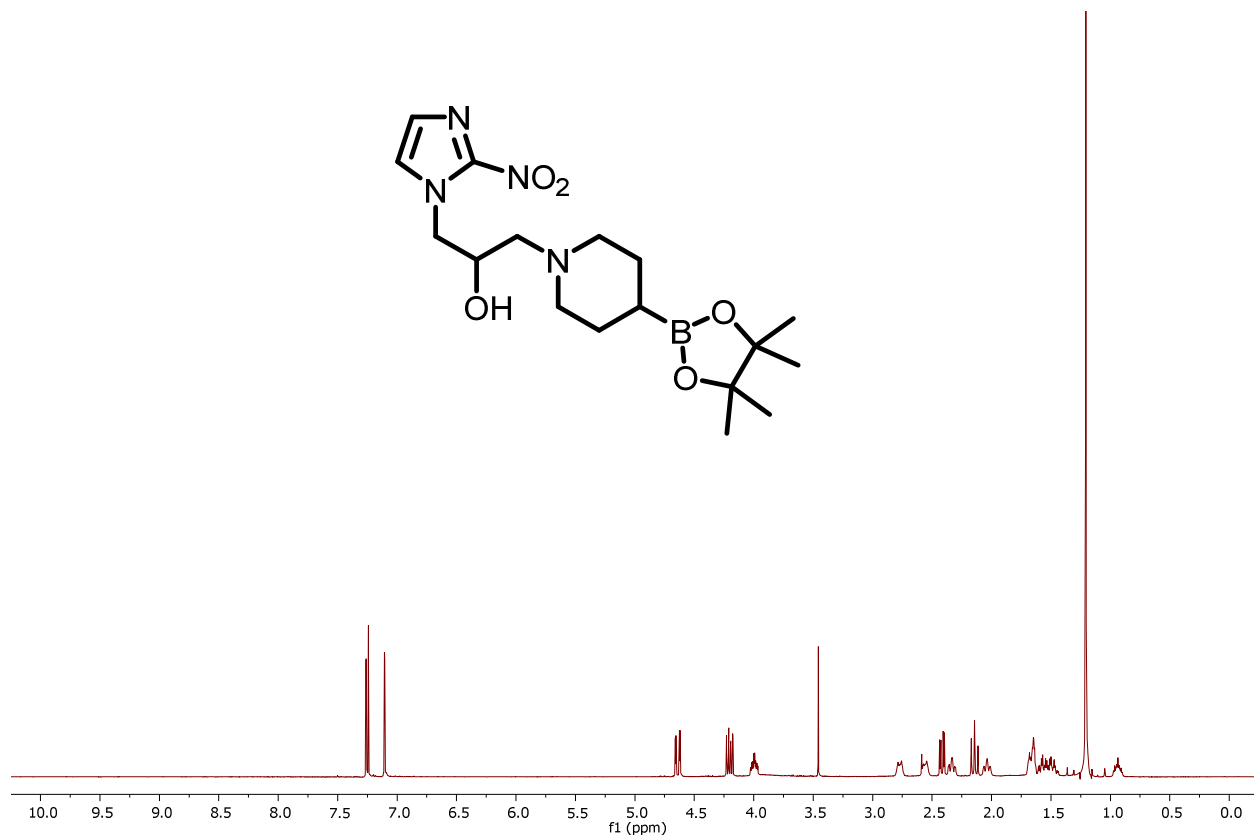
128. Varia MA, Calkins-Adams DP, Rinker LH, Kennedy AS, Novotny DB, Fowler WC, et al. Pimonidazole: A Novel Hypoxia Marker for Complementary Study of Tumor Hypoxia and Cell Proliferation in Cervical Carcinoma. *Gynecologic Oncology*. 1998;71(2):270-7.
129. Bell C, Dowson N, Fay M, Thomas P, Puttick S, Gal Y, et al. Hypoxia Imaging in Gliomas With 18F-Fluoromisonidazole PET: Toward Clinical Translation. *Seminars in Nuclear Medicine*. 2015;45(2):136-50.
130. Genady AR, Ioppolo JA, Azaam MM, El-Zaria ME. New functionalized mercaptoundecahydrododecaborate derivatives for potential application in boron neutron capture therapy: Synthesis, characterization and dynamic visualization in cells. *European Journal of Medicinal Chemistry*. 2015;93:574-83.
131. Frazier N, Ghandehari H. Hyperthermia approaches for enhanced delivery of nanomedicines to solid tumors. *Biotechnology and Bioengineering*. 2015;112(10):1967-83.
132. Staruch RM, Hynynen K, Chopra R. Hyperthermia-mediated doxorubicin release from thermosensitive liposomes using MR-HIFU: therapeutic effect in rabbit Vx2 tumours. *International journal of hyperthermia : the official journal of European Society for Hyperthermic Oncology, North American Hyperthermia Group*. 2015;31(2):118-33. Epub 2015/01/15.
133. Issels RD, Lindner LH, Verweij J, Wust P, Reichardt P, Schem B-C, et al. Neo-adjuvant chemotherapy alone or with regional hyperthermia for localised high-risk soft-tissue sarcoma: a randomised phase 3 multicentre study. *The Lancet Oncology*. 2010;11(6):561-70.
134. Kothapalli S, Altman MB, Partanen A, Wan L, Gach HM, Straube W, et al. Acoustic field characterization of a clinical magnetic resonance-guided high-intensity focused ultrasound system inside the magnet bore. *Medical physics*. 2017. Epub 2017/06/20.
135. Li L, ten Hagen TLM, Hossann M, Süss R, van Rhoon GC, Eggermont AMM, et al. Mild hyperthermia triggered doxorubicin release from optimized stealth thermosensitive liposomes improves intratumoral drug delivery and efficacy. *Journal of Controlled Release*. 2013;168(2):142-50.
136. Kneidl B, Peller M, Winter G, Lindner LH, Hossann M. Thermosensitive liposomal drug delivery systems: state of the art review. *International Journal of Nanomedicine*. 2014;9:4387-98.
137. Kueffer PJ, Maitz CA, Khan AA, Schuster SA, Shlyakhtina NI, Jalisatgi SS, et al. Boron neutron capture therapy demonstrated in mice bearing EMT6 tumors following selective delivery of boron by rationally designed liposomes. *Proceedings of the National Academy of Sciences*. 2013;110(16):6512-7.
138. Luderer MJ, de la Puente P, Azab AK. Advancements in Tumor Targeting Strategies for Boron Neutron Capture Therapy. *Pharmaceutical Research*. 2015;32(9):2824-36.
139. Luderer MJ, Muz B, de la Puente P, Chavalmane S, Kapoor V, Marcelo R, et al. A Hypoxia-Targeted Boron Neutron Capture Therapy Agent for the Treatment of Glioma. *Pharmaceutical Research*. 2016;33(10):2530-9.

140. Sauerwein W. Neutron capture therapy : principles and applications. Heidelberg ; New York: Springer; 2012. ix, 553 p. p.

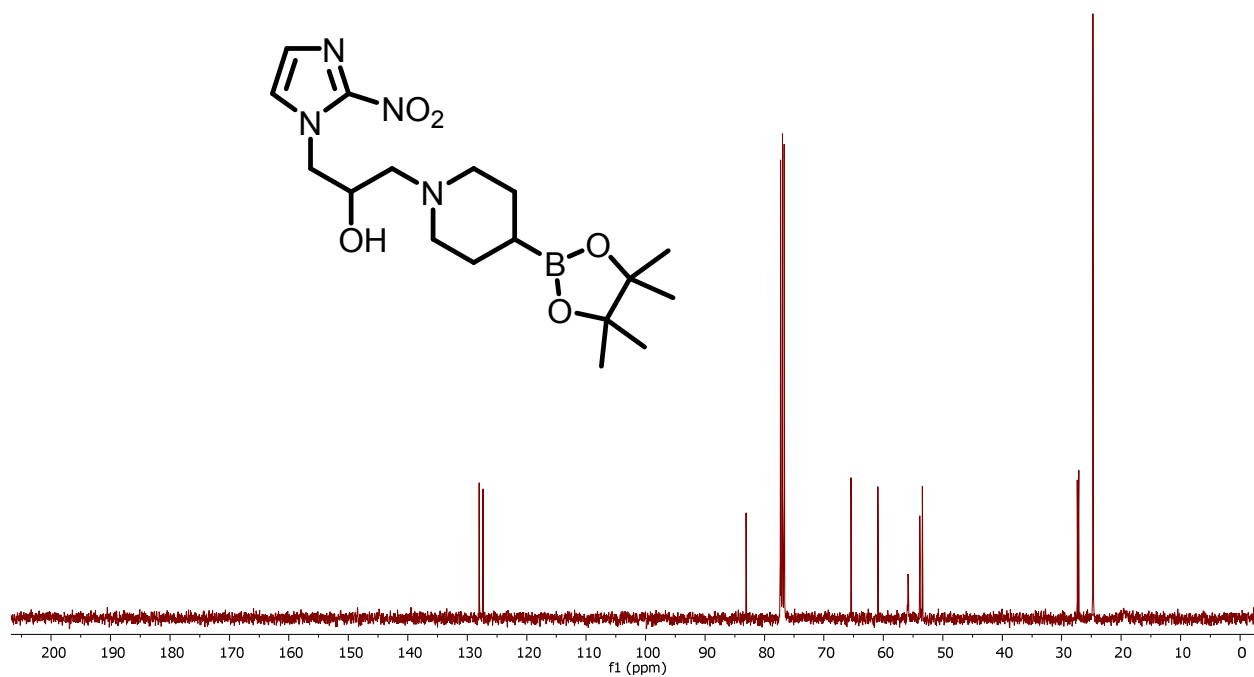
Appendix



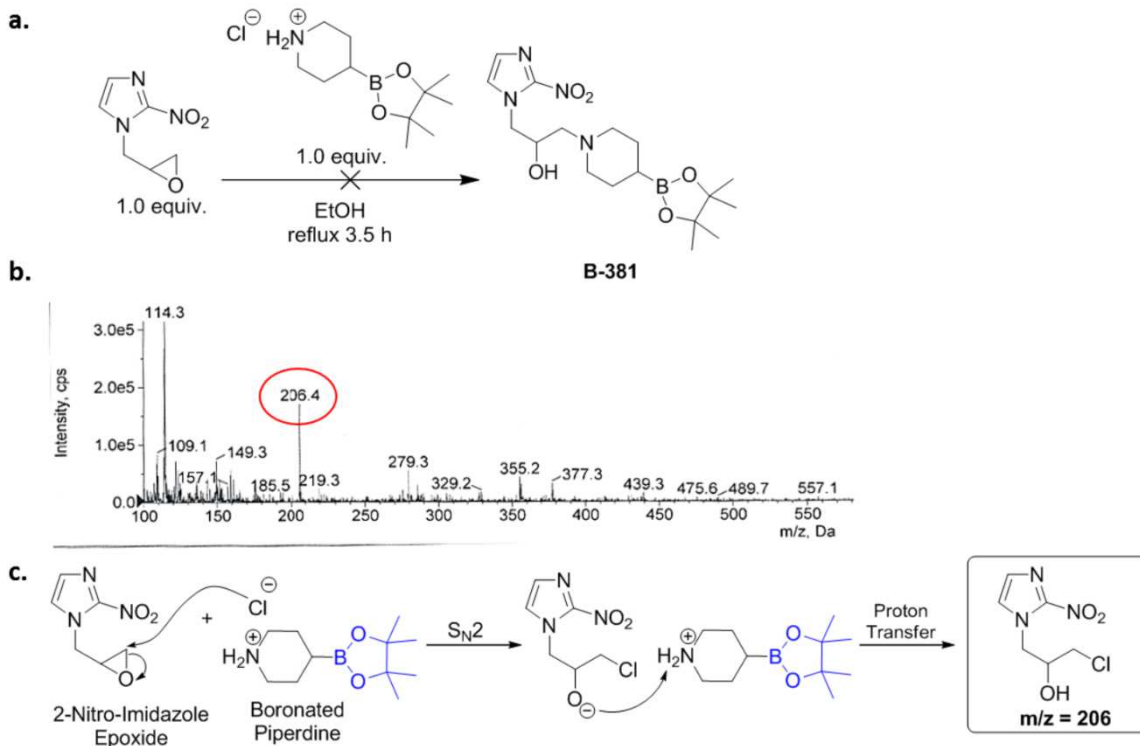
Supplementary Figure 1. Determining the wavelength of maximum absorbance for B-381 ($\lambda_{\max} = 330 \text{ nm}$). Non-specific absorbance below 300 nm is attributed to the 96-well plate.



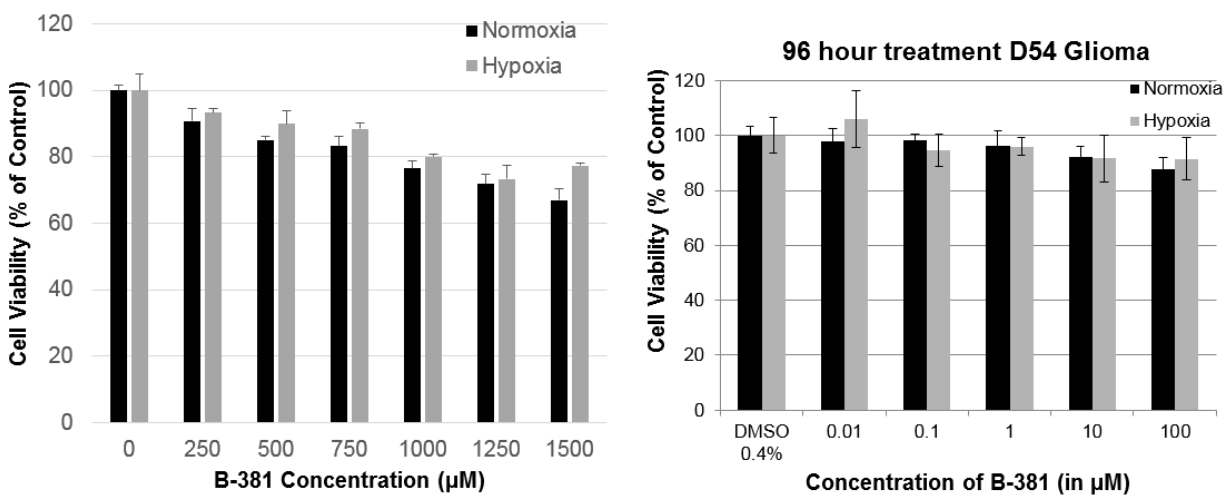
Supplementary Figure 2: $^1\text{H-NMR}$ of 2-nitroimidazole derivative B-381 in deuterated chloroform. B-381 was purified as a precipitate from methanol.



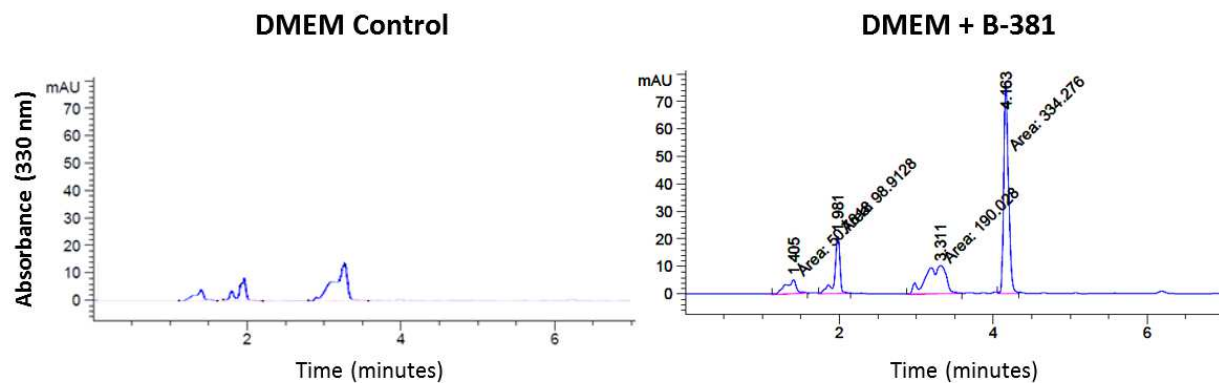
Supplementary Figure 3. $^{13}\text{C-NMR}$ of 2-nitroimidazole derivative B-381 in deuterated chloroform. B-381 was purified as a precipitate from methanol.



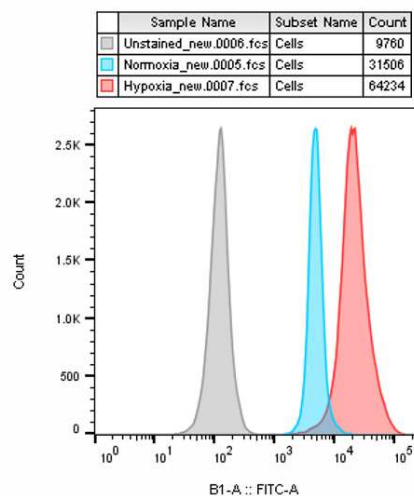
Supplementary Figure 4. **a.)** Initial epoxide ring opening with piperidine-4-boronic acid pinacol ester HCl and 1-(2,3-Epoxypropyl)-2-nitroimidazole **b.)** LC-MS does not contain desired product m/z of 381 but shows a predominate peak at m/z 206.4. **c.)** $m/z = 206$ peak can be attributed to the chloride ion rapidly opening the epoxide ring which was introduced inadvertently since piperidine-4-boronic acid is sold as an HCl salt.



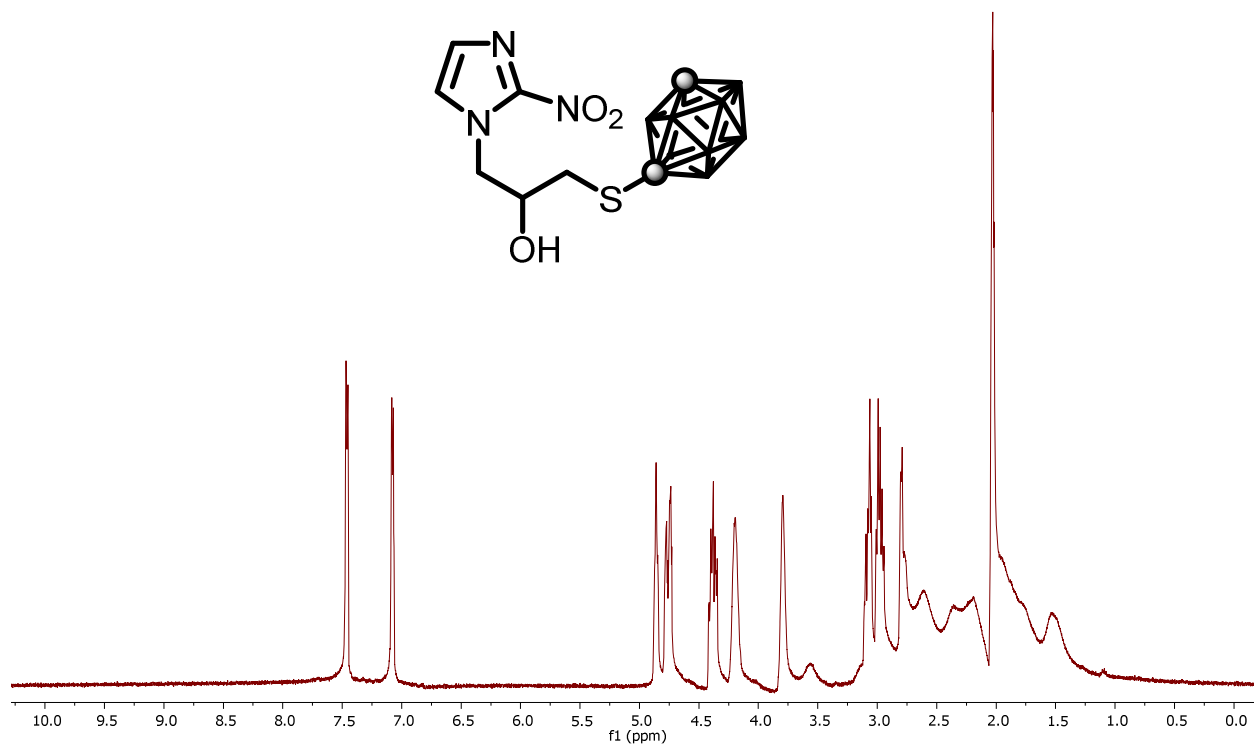
Supplementary Figure 5. D54 Glioma cells treated with millimolar B-381 concentrations for 24 hours (left) or for 96 hours at micromolar concentrations (right).



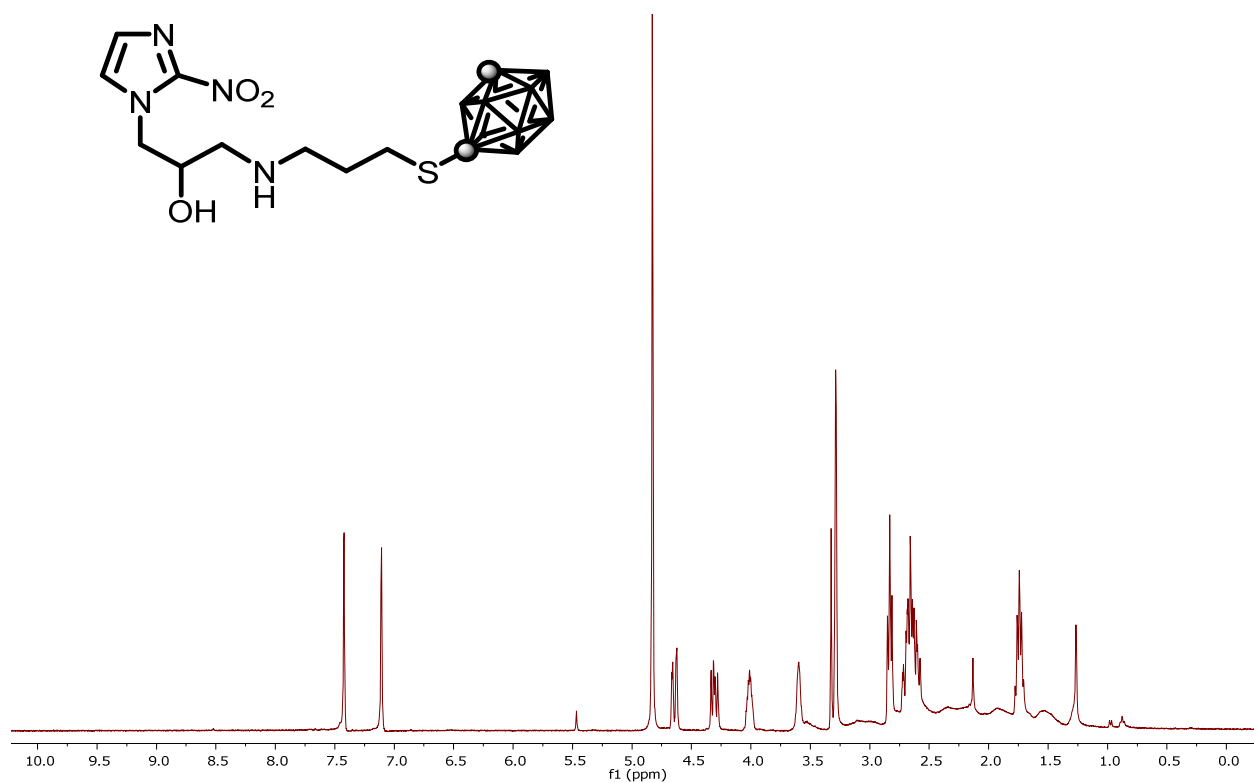
Supplementary Figure 6. Representative chromatogram of serum free DMEM without (left) and with B-381 (right). B-381 has a characteristic retention time at 4.1 minutes with a strong absorbance at 330 nm.



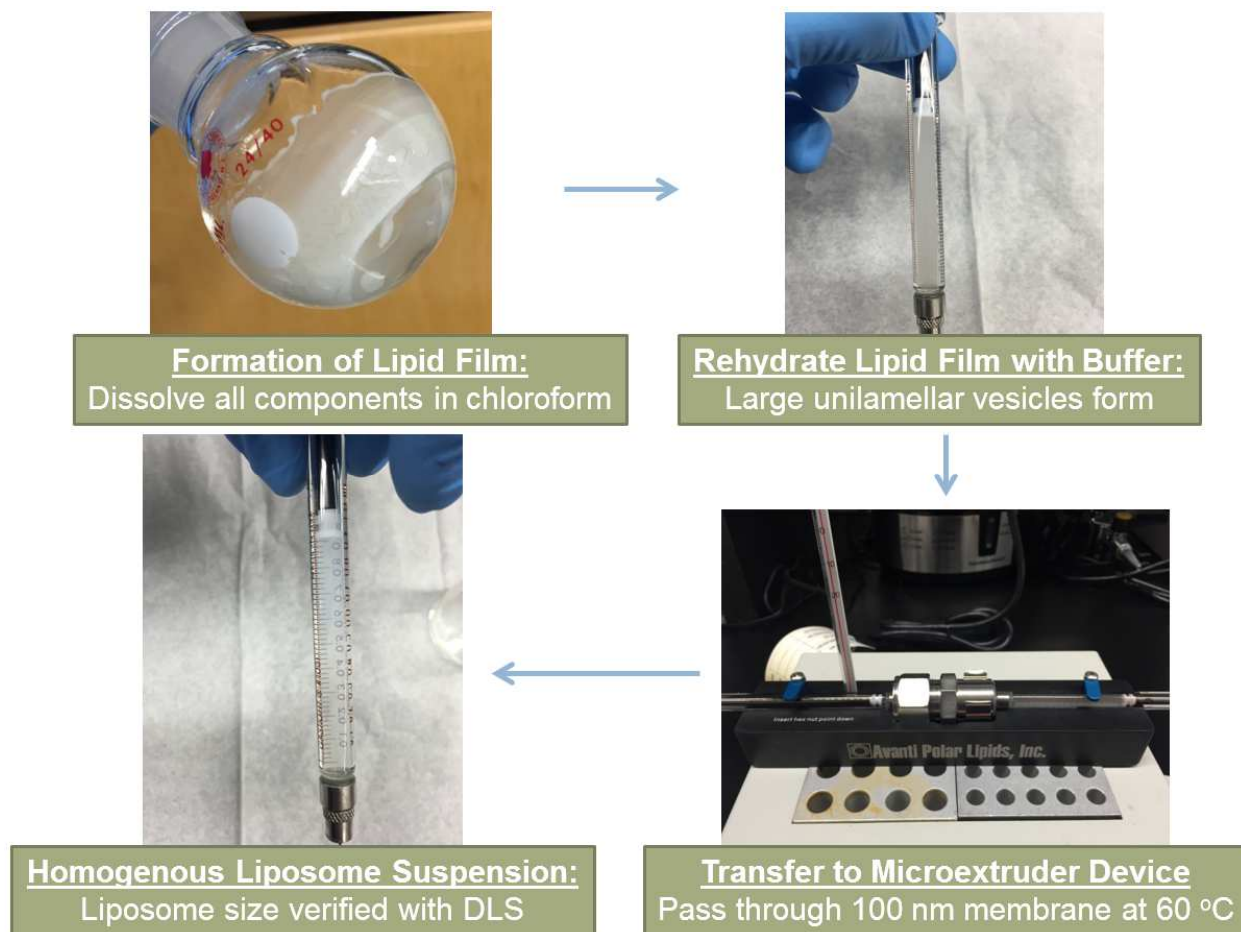
Supplementary Figure 7: D54 cells were cultured in normoxia (21% O₂) or hypoxia (1% O₂) and treated with pimonidazole. Normoxic and hypoxic cells were fixed with 70% ethanol and stained with FITC-anti-pimonidazole monoclonal antibody. Some normoxic cells were utilized as unstained control.



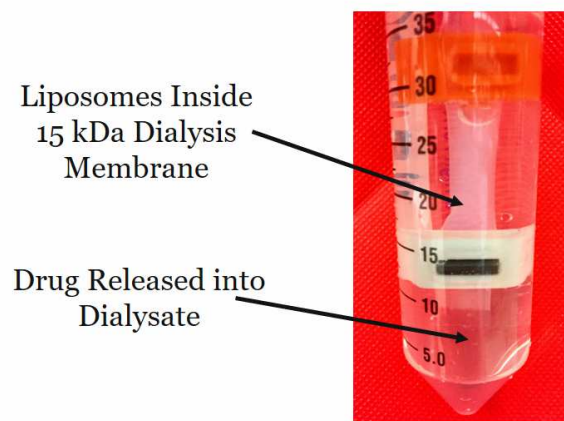
Supplementary Figure 8: ¹H-NMR of 2-nitroimidazole derivative B-346 in deuterated acetone. B-346 was purified as a precipitate from ethanol.



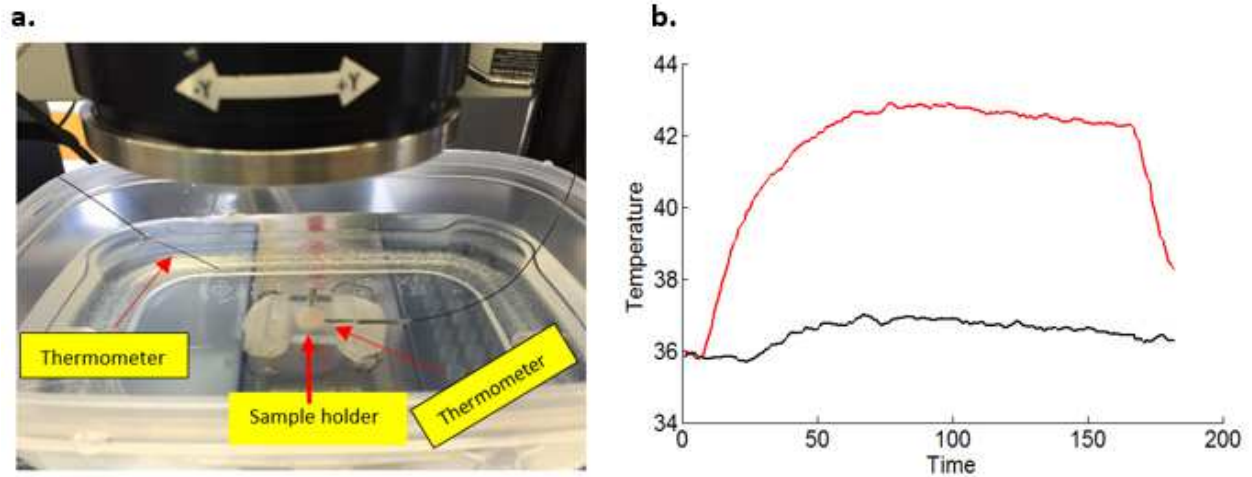
Supplementary Figure 9: ¹H-NMR of 2-nitroimidazole derivative B-403 in deuterated methanol. B-403 was purified by normal phase flash chromatography (10% methanol/90% dichloromethane).



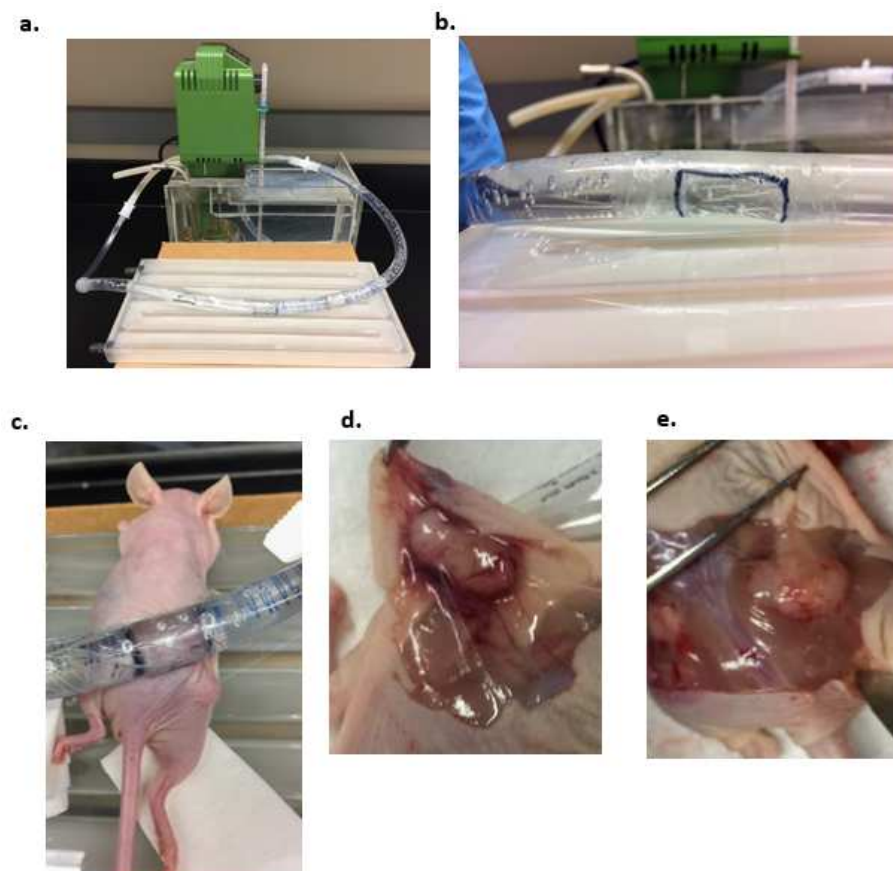
Supplementary Figure 10: Schematic diagram for thermosensitive liposome synthesis in a microextruder.



Supplementary Figure 11. Water bath release studies with thermal sensitive liposomes at 37°C or 42°C.



Supplementary Figure 12. Experimental setup for HIFU Release Studies. a.) Sample chamber holder for HIFU TSL release experiments b.) Real-time thermocouple measurement indicating HIFU treatment could maintain stable hyperthermia temperatures (42°C).



Supplementary Figure 13. Mild Hyperthermia Treatment Device for Mice. a.) Water circulator was used to maintain water temperature of 43°C b.) Illustration of hyperthermia window – a thin layer of Tegaderm allows heat transfer to tumor. c.) Left tumor is receiving hyperthermia treatment while right contralateral tumor is at physiologic temperature. d.) Illustration of left tumor that was exposed to 30 minute hyperthermia treatment. e.) Illustration of right tumor that did not receive hyperthermia treatment.

Curriculum Vitae

Micah Luderer

4105 Olive Street | St. Louis, MO 63108 | 269-352-2535 | mluderer@wustl.edu

Professional Summary:

MD/PhD student enrolled in Medical Scientist Training Program at Washington University in St. Louis School of medicine. Anticipated degrees will be awarded in May 2019, followed by continuation into an oncology residency program. I hope to have the opportunity during residency/fellowship training to have dedicated research time to continue my preparation for a physician-scientist research track. From Master's and Doctoral research, I am proficient with the following laboratory techniques: cell culture (normoxia and hypoxia), *in vivo* mouse models, Inductively Coupled Plasma Optical Emission Spectrometry (ICP-OES), Inductively Coupled Plasma Mass Spectrometry (ICP-MS), flow cytometry, organic synthesis, NMR spectroscopy (^1H and ^{13}C), column chromatography, HRMS, IR spectroscopy HPLC.

Education

Washington Univ. in St. Louis School of Medicine

Aug 2011 – May 2019

[MD/PhD Candidate, Molecular Cell Biology]

- Anticipated MD and PhD (Molecular Cell Biology) Degrees May 2019
- USMLE Step 1 examination (score = 230).
- PhD Courses completed: Chemistry and Physics of Biomolecules (Bio 5357); Contrast Agents for Biological Imaging (Bio 5147), Cancer Biology Journal Club (Bio 5192), Molecular Cell and Organ Systems (Bio 5224), Ethics and Research Science (Bio 5011).

Dissertation Research Summary: Under the guidance of Dr. Kareem Azab, my research includes the synthesis and biological evaluation of novel compounds for Boron Neutron Capture Therapy (BNCT). BNCT has the capability to provide the regional selectivity of radiation therapy with significantly less destruction to healthy tissues because of its utilization of a lower energy neutron beam compared to traditional higher energy x-ray or gamma particles. When ^{10}B atoms absorb a neutron, the unstable ^{11}B isotope undergoes nuclear fission to release an alpha particle (^4He), lithium-7 (^7Li) ion and gamma radiation. The resulting cell destruction is limited to approximately the diameter of a single cell. The focus of my research is to synthesize and evaluate boronated compounds that selectively accumulate in cancerous tissue compared to normal tissue. These compounds utilized with BNCT would have therapeutic potential for the treatment of glioblastoma, astrocytoma and many others.

Research Rotation Summary: During the summer of 2012 I worked in the lab of Drs. Dipanjan Pan and Gregory Lanza. During this time, I worked on the synthesis of novel optically active carbon nanoparticles (OCNs). These OCNs can be utilized for optical imaging in the near

infrared range. By coating these OCNs with a hyperbranched polymer, I was able to create a nanoparticle with superior optical properties compared to first generation OCNs which were coated with linear polyethylene glycol. Additionally, my work also included synthesis of a manganese oleate nanoparticle with a copper core which exemplified MRI enhancement of fibrin rich clots.

Michigan State University
[MS, Chemistry]

Aug. 2009 – Aug. 2011

- GPA: 3.91
- Master's Thesis: Synthesis and Evaluation of Novel Checkpoint Kinase II Inhibitors.
- Laboratory skills: ^1H and ^{13}C NMR spectroscopy, column chromatography, HRMS, IR spectroscopy and HPLC.
- Graduate classes completed: CEM 845 (Structure and Spectroscopy of Organic Compounds), CEM 850 (Intermediate Organic Chemistry), CEM 851 (Advanced Organic Chemistry), CEM 852 (Methods of Organic Synthesis), and CEM 956 (Heterocyclic Chemistry).

Thesis Summary: In the laboratory of Dr. Jetze Tepe, I worked on two organic synthesis projects for my MS degree. My first project included synthesizing novel inhibitors of checkpoint kinase II that were investigated as radioprotectors during ionizing radiation treatments. The second project included resolving racemic imidazolines into their perspective enantiomers. These compounds were then evaluated as proteasome inhibitors.

Michigan State University
[BS, Chemistry]

Aug. 2006 – Dec. 2009

- GPA: 4.0
- Received Honors College Chemistry BS degree (Dec 2009) as part of BS/MS 5 year program.
- Undergraduate research in Jetze Tepe's Laboratory (2007-2009)

Publications

1. **Luderer MJ**, Muz B, de la Puente P, Chavalmane S, Kapoor V, Marcelo R, *et al.* A Hypoxia-Targeted Boron Neutron Capture Therapy Agent for the Treatment of Glioma. *Pharmaceutical research*. 2016;33(10):2530-9.
2. **Luderer MJ**, de la Puente P, Azab AK. Advancements in Tumor Targeting Strategies for Boron Neutron Capture Therapy. *Pharmaceutical research*. 2015;32(9):2824-36.
3. Wu L, **Luderer M***, Yang X, Swain C, Zhang H, Nelson K, *et al.* Surface passivation of carbon nanoparticles with branched macromolecules influences near infrared bioimaging. *Theranostics*. 2013;3(9):677-86. ***Co-first author**
4. de la Puente P, Quan N, Hoo RS, Muz B, Gilson RC, **Luderer M**, *et al.* Newly established myeloma-derived stromal cell line MSP-1 supports multiple myeloma proliferation, migration, and adhesion and induces drug resistance more than normal-derived stroma. *Haematologica*. 2016;101(7):e307-11.
5. de la Puente P, Muz B, Jin A, Azab F, **Luderer M**, Salama NN, *et al.* MEK inhibitor, TAK-733 reduces proliferation, affects cell cycle and apoptosis, and synergizes with other targeted therapies in multiple myeloma. *Blood cancer journal*. 2016;6:e399.

6. Muz B, Ghazarian RN, Ou M, **Luderer MJ**, Kusdono HD, Azab AK. Spotlight on ixazomib: potential in the treatment of multiple myeloma. *Drug design, development and therapy*. 2016;10:217-26.
7. Muz B, de la Puente P, Azab F, **Luderer MJ**, King J, Vij R, et al. A CD138-independent strategy to detect minimal residual disease and circulating tumour cells in multiple myeloma. *British journal of haematology*. 2016;173(1):70-81.
8. de la Puente P, Azab F, Muz B, **Luderer M**, Arbiser J, Azab AK. Tris DBA palladium overcomes hypoxia-mediated drug resistance in multiple myeloma. *Leukemia & lymphoma*. 2016;57(7):1677-86.
9. de la Puente P, Weisberg E, Muz B, Nonami A, **Luderer M**, Stone RM, et al. Identification of ILK as a novel therapeutic target for acute and chronic myeloid leukemia. *Leukemia research*. 2015.
10. de la Puente P, Muz B, Gilson RC, Azab F, **Luderer M**, King J, et al. 3D tissue-engineered bone marrow as a novel model to study pathophysiology and drug resistance in multiple myeloma. *Biomaterials*. 2015;73:70-84.
11. Muz B, de la Puente P, Azab F, **Luderer M**, Azab AK. Hypoxia promotes stem cell-like phenotype in multiple myeloma cells. *Blood cancer journal*. 2014;4:e262.
12. Muz B, de la Puente P, Azab F, **Luderer M**, Azab AK. The role of hypoxia and exploitation of the hypoxic environment in hematologic malignancies. *Molecular cancer research : MCR*. 2014;12(10):1347-54.
13. de la Puente P, Muz B, Azab F, **Luderer M**, Azab AK. Molecularly targeted therapies in multiple myeloma. *Leukemia research and treatment*. 2014;2014:976567.
14. Wu L, Cai X, Nelson K, Xing W, Xia J, Zhang R, **Luderer M**, et al. A Green Synthesis of Carbon Nanoparticle from Honey for Real-Time Photoacoustic Imaging. *Nano research*. 2013;6(5):312-25.
15. Nguyen TN, Saleem RS, **Luderer MJ**, Hovde S, Henry RW, Tepe JJ. Radioprotection by hymenialdisine-derived checkpoint kinase 2 inhibitors. *ACS chemical biology*. 2012;7(1):172-84.

Honors & Awards

Graduate of Michigan State University Honors College (2009)

Distinguished Award in Chemistry (MSU Chemistry Department, Spring 2009)

Hershal Goren Scholarship Award in Chemistry (MSU Chemistry Department, Spring 2008)

American Chemical Society Award for Outstanding Performance in Physical Chemistry (CEM 391/392) in the Department of Chemistry (MSU Chemistry Department, Spring 2008)

Dean's Honor List, College of Natural Science at Michigan State University (Fall 2006-Spring 2009)

Teaching Experience

Graduate Teaching Assistant

Aug. 2013-Dec. 2013

- Taught neurophysiology lab (Bio 404) at Washington University in St. Louis. This was an upper level lab taught to a select number of junior/senior students (must apply for the course). Teaching responsibilities included pre-lab discussions, assisting students perform neurological recordings from live species, and grading lab reports.

Graduate Teaching Assistant

Aug. 2009 – Aug. 2011

- Taught recitation at Michigan State University for general chemistry I & II. Also was a lab instructor for junior/senior level labs CEM 395 (Analytical/Physical Chemistry Lab) and CEM 495 (Molecular Spectroscopy Lab).

Scientific Presentations

17th International Congress on Neutron Capture Therapy (Columbia, Missouri) **plenary oral presentation** entitled “Targeting the Glioma Hypoxic Tumor Microenvironment with a novel Boron Neutron Capture Therapy Agent” (October 2016).

Radiation Research Society Annual Meeting (Waikoloa Village, Hawaii) **poster presentation** titled “Towards sensitizing the hypoxic and therapy resistant glioma tumor microenvironment with boron neutron capture therapy (October 2016).

Washington University in St. Louis School of Medicine, Division of Cancer Biology, Research Forum, **oral presentation** entitled “Targeting the Glioma Hypoxic Tumor Microenvironment with Novel Boron Neutron Capture Therapy Agents” (Nov 2014, Nov 2016).

56th American Society of Hematology Annual Meeting and Exposition. San Francisco, CA. (December 2014) *Attendee.*

20th Annual Biochemistry and Computational & Molecular Biophysics Retreat. Washington University in St. Louis (October 2013). *Attendee.*

Medical Scientist Training Program Retreat. Washington University in St. Louis (April 2012). *Attendee.*

Volunteer Activities

- Site leader for a community Nutrition Class: A 5-week program that is offered to members of the community to learn about nutrition followed by helping them cook a healthy meal (2012, St. Louis, MO).
- “Having a Ball with Chemistry”: ACS sponsored science presentation geared toward an elementary audience (2008, East Lansing, MI).

References: References available upon request.